Analiza i implementacija metode harmoničke ravnoteže u proračunskoj mehanici fluida

Cvijetić, Gregor

UNIVERSITY OF ZAGREB
Faculty of Mechanical Engineering and Naval Architecture

MASTER'S THESIS

Gregor Cvijetić

Zagreb, 2015

UNIVERSITY OF ZAGREB
Faculty of Mechanical Engineering and Naval Architecture

ANALYSIS AND IMPLEMENTATION OF THE HARMONIC BALANCE METHOD IN COMPUTATIONAL FLUID DYNAMICS

Supervisor:
Prof. Hrvoje Jasak, PhD

Student:
Gregor Cvijetić

Zagreb, 2015

I would like to express my gratitude to all those whose comments, insights and advices were a great help to me while working on the thesis.

I am truly thankful to *Professor Hrvoje Jasak* for being my supervisor, suggesting me a remarkably challenging topic for my thesis and giving me a plenty of constructive comments and encouragement whenever needed. Without his support, and what is more important, without his guidance in extending my knowledge in the area of CFD and programming, this thesis would not have been possible.

My friends and colleagues also deserve my sincere *thank you*, and my special thanks goes to *Vuko Vukčević* whose valuable comments pointed me always in the right direction; *Tessa Uroić* for providing mesh for majority of test cases and for her willingness to modify it regardless of how difficult it was; and *Inno Gatin* who was always ready for meaningful discussions.

Finally, I am deeply grateful for the patience, understanding and love I have received from my *mean value*[*], *Tamara*.

Thank you,
Gregor Cvijetić

[*] See chapter 3.2.

I hereby declare that this thesis is entirely the result of my own work except where otherwise indicated. I have fully cited all used sources and I have only used the ones given in the list of references.

Gregor Cvijetić

SVEUČILIŠTE U ZAGREBU
FAKULTET STROJARSTVA I BRODOGRADNJE
Središnje povjerenstvo za završne i diplomske ispite
Povjerenstvo za diplomske ispite studija strojarstva za smjerove:
procesno-energetski, konstrukcijski, brodostrojarski i inženjersko modeliranje i računalne simulacije

Sveučilište u Zagrebu Fakultet strojarstva i brodogradnje	
Datum	Prilog
Klasa:	
Ur.broj:	

DIPLOMSKI ZADATAK

Student: Gregor Cvijetić Mat. br.: 0035177345

Naslov rada na hrvatskom jeziku: **Analiza i implementacija metode harmoničke ravnoteže u proračunskoj mehanici fluida**

Naslov rada na engleskom jeziku: **Analysis and implementation of the Harmonic Balance Method in Computational Fluid Dynamics**

Opis zadatka:

Proračunska mehanika fluida redovno se koristi u simulacijama strujanja u turbostrojevima. Strujanje u trodimenzionalnim statorskim i rotorskim rešetkama donosi posebne izazove, od kojih se ističe problem opisa tranzijentosti toka. Radi geometrijske periodičnosti, strujanje sadrži jasno harmoničku komponentu, dok je za potrebe analize i optimizacije toka potrebno ostvariti kvazi-stacionarni prikaz strujanja.
Ovo je moguće postići primjenom metode harmoničke ravnoteže (*engl. harmonic balance*), gdje se tranzijentost pojave opisuje kroz spektralnu dekompoziciju u dominantne frekvencijske komponente.
Kandidat treba izvršiti sljedeće zadatke tokom izrade rada:

- izvršiti pregled literature vezane uz izvod i formulaciju matematičkog modela harmoničke ravnoteže u proračunskoj mehanici fluida, uz detaljnu analizu postupka dekompozicije vremenskog signala za slučaj frekvencijskih rješenja s više frekvencija;
- opisati implementaciju metode harmoničke ravnoteže u vremenu, na način koji dozvoljava korištenje postojećih komponenti diskretizacije u prostornoj domeni;
- implementirati metodu harmoničke ravnoteže u softverskom paketu OpenFOAM;
- validirati implementaciju na odgovarajućim primjerima skalarne transportne jednadzbe;
- po završenoj validaciji metode harmoničke ravnoteže na skalarnoj transportnoj jednadžbi, predložiti formulaciju harmoničke ravnoteže na sustavu Navier-Stokesovih jednadžbi za tranzijentna harmonička strujanja. Posvetiti posebnu pažnju spregnutim algoritmima jednadžbe kontinuiteta i jednadžbe količine gibanja;
- validirati implementirane metode harmoničke ravnoteže na sustavu Navier-Stokesovih jednadžbi na primjerima viskoznog strujanja fluida s poznatom dominantnom frekvencijom;
- prikazati ponašanje modela na primjerima sa slabo definiranim dominantnim frekvencijama, npr. von Karmanovih vrtloga u strujanju oko cilindra ili laminarnog strujanja oko klina;
- opisati implementaciju i ostvarene rezultate u diplomskom radu.

U radu je potrebno navesti korištenu literaturu i eventualnu pomoć.

Zadatak zadan:	Rok predaje rada:	Predviđeni datumi obrane:
7. svibnja 2015.	9. srpnja 2015.	15., 16. i 17. srpnja 2015.

Zadatak zadao: Predsjednica Povjerenstva:

Prof. dr. sc. Hrvoje Jasak Prof. dr. sc. Tanja Jurčević Lulić

Table of Contents

Nomenclature

Greek letters

γ	Diffusion coefficient	m^2/s
ν	Kinematic viscosity	m^2/s
ω	Angular frequency	$1/s$

Latin letters

$\hat{\boldsymbol{\mathcal{R}}}$	Discrete time domain residual field	m/s
$\hat{\boldsymbol{\mathcal{U}}}$	Discrete time domain velocity field	m/s
$\mathcal{Q}$	Scalar field in time domain	-
$\boldsymbol{\mathcal{Q}}$	Matrix of variable Q in discrete time instants	-
$\mathcal{R}$	Scalar transport equation residual in time domain	-
$\boldsymbol{\mathcal{R}}$	Matrix of variable R in discrete time instants	-
$\boldsymbol{\mathcal{R}}$	Time domain residual field	m/s
$\boldsymbol{\mathcal{U}}$	Time domain velocity field	m/s
$\boldsymbol{\mathcal{U}}^o$	Time domain velocity field from previous iteration	m/s
$\mathbf{A}$	Coefficient matrix	-
$\mathbf{E}$	Transformation matrix from time to frequency domain	-
$\mathbf{E}^{-1}$	Transformation matrix from frequency to time domain	-
$\mathbf{Q}$	Fourier coefficient matrix	-
$\mathbf{R}$	Fourier coefficient matrix	-
$\mathbf{u}$	Velocity vector	m/s
$\mathbf{u}^o$	Velocity field from the previous iteration	m/s
$\mathbf{u}_0$	Mean value Fourier coefficient for velocity expansion	m/s
$\mathbf{u}_N$	Neighbouring cell velocity	m/s

$\mathbf{u}_P$	Cell velocity	m/s
$\mathbf{u}_{C_n}$	Fourier coefficient for velocity expansion multiplying cosine term	m/s
$\mathbf{u}_{S_n}$	Fourier coefficient for velocity expansion multiplying sine term	m/s
$\mathbf{u}_{t_j}$	Velocity field in time instant t_j	m/s
$\mathrm{P_i}$	Coefficient substituting the summation term	-
Q_0	Scalar field, zeroth harmonic of Fourier series	-
$\mathrm{Q}_{\mathrm{C}_n}$	Scalar field, Fourier coefficient of nth harmonic multiplying the cosine term	-
$\mathrm{Q}_{\mathrm{S}_n}$	Scalar field, Fourier coefficient of nth harmonic multiplying the sine term	-
R_0	Residual, zeroth harmonic of Fourier series	-
$\mathrm{R}_{\mathrm{C}_n}$	Residual, Fourier coefficient of nth harmonic multiplying the cosine term	-
$\mathrm{R}_{\mathrm{S}_n}$	Residual, Fourier coefficient of nth harmonic multiplying the sine term	-
A	Scalar coefficient, sine wave amplitude	-
a_0	First term of Fourier series, mean value	-
a_N	Matrix coefficient corresponding to the neighbour N	-
a_n	Fourier coefficient of nth harmonic multiplying cosine term	-
A_n^2	Energy of the nth harmonic	-
a_P	Central coefficient	-
B	Scalar coefficient, cosine wave amplitude	-
b_n	Fourier coefficient of nth harmonic multiplying sine term	-
F	Mass flux through the face	m^3/s
f	Frequency of the period	Hz
f_{cos}	Cosine wave frequency	Hz
f_{sin}	Sine wave frequency	Hz
k	Summation index	-

n	Number of harmonic in Fourier series	-
P	Period in Fourier series	-
p	Kinematic pressure	m^2/s^2
q_v	Sources and sinks of scalar field	-
Q_{t_n}	Discrete variable Q in the nth time step within a period	-
S	Face area	-
T	Scalar field	-
t	Time	s
T_j	Scalar field corresponding to time instant t_j	-
t_n	nth time step within a period	s
x	Argument of the function decomposed in Fourier series	-
x_0	Initial point of the period	-

List of Figures

List of Tables

Abstract

Gregor Cvijetić

ANALYSIS AND IMPLEMENTATION OF THE HARMONIC BALANCE METHOD IN COMPUTATIONAL FLUID DYNAMICS

In this thesis the Harmonic Balance Method for non-linear periodic flows is presented. Assumption of a time-periodic flow allows us to formulate $2n+1$ coupled steady state problems. By solving $2n+1$ steady state problems, a transient flow field is obtained. Fourier series expansion is the core of the Harmonic Balance Method, therefore the accuracy of the method depends on the number of harmonics specified, n. Accuracy of the method also depends on the periodic nature of the problem.

The method was first derived for a passive scalar transport and implemented in OpenFOAM. Validation has been carried out on 4 test cases concerning forced periodic behaviour at the inlet of the rectangular 2D domain. The first test case was a sine wave, which was fully resolved with 1 harmonic. The second case was a linear combination of sine and cosine waves with different frequencies, resolved with 2 harmonics. After successful validation of harmonic waves, robustness and accuracy test was carried out on two square waves. Square waves are numerically more difficult and more demanding, which was also shown in the convergence study carried out using 3, 5, 7 and 10 harmonics. Harmonic Balance Method results were compared to transient simulation for all of the test cases.

After validation of the passive scalar transport, pressure-velocity system for the Harmonic Balance Method was derived and implemented. Validation of NACA2412 pitching airfoil was presented together with performance comparison of transient solver and harmonic balance.

Keywords: Harmonic Balance, CFD, OpenFOAM, Fourier series, harmonic, periodic, non-linear, NACA, airfoil pitching

Sažetak

(ABSTRACT IN CROATIAN)

Gregor Cvijetić

ANALIZA I IMPLEMENTACIJA METODE HARMONIČKE RAVNOTEŽE U PRORAČUNSKOJ MEHANICI FLUIDA

U ovom radu predstavljena je metoda harmoničke ravnoteže za nelinearna periodična strujanja. Pretpostavka o periodičnosti strujanja omogućuje dobivanje $2n+1$ spregnutih stacionarnih problema iz jedne tranzijentne transportne jednadžbe. Rješavanjem $2n+1$ stacionarnih problema dobiva se tranzijentno polje strujanja. Metoda harmoničke ravnoteže temelji se na Fourierovom razvoju funkcije u red što znači da točnost metode ovisi o broju korištenih harmonika n. Osim broja harmonika, točnost metode također ovisi i o prirodi periodičnog problema.

Metoda je prvo izvedena za pasivni prijenos skalara i implementirana u OpenFOAM. Validacija je izvedena koristeći 4 slučaja u kojima su mijenjani rubni uvjeti na ulazu domene. Korištena je 2D pravokutna domena. U prvom slučaju nametnut je ulazni signal u obliku sinusnog vala, za čije je rješavanje potreban 1 harmonik. Drugi slučaj validacije pasivnog prijenosa skalara pokazao je Fourierovu prirodu metode: nametnut je signal u obliku linearne kombinacije dva harmonijska vala različitih frekvencija. Pokazano je da su za rješavanje takvog složenog vala potrebna dva harmonika. Posljednja dva slučaja izvedena su kako bi se pokazala otpornost i preciznost metode te su nametnuti pravokutni valovi. Budući da pravokutni val predstavlja izazov u numeričkom smislu, prikazana je konvergencija s porastom broja harmonika i to za slučajeve s 3, 5, 7 i 10 harmonika. Rezultati svih slučajeva dobiveni metodom harmoničke ravnoteže uspoređeni su s rezultatima konvencionalne tranzijentne simulacije.

Nakon uspješne validacije metode za pasivni prijenos skalara, metoda harmoničke ravnoteže proširena je na rješavanje sustava jednadžbi za tlak i brzinu. Validacija metode harmoničke ravnoteže za Navier-Stokesove jednadžbe napravljena je na slučaju NACA 2412 aeroprofila koji mijenja napadni kut. Naposljetku, napravljena je usporedba učinkovitosti između tranzijentnog rješavača i rješavača za metodu harmoničke ravnoteže.

Ključne riječi: metoda harmoničke ravnoteže, računalna dinamika fluida, Fourierov razvoj, harmonik, periodično strujanje, NACA, CFD

Prošireni sažetak

(EXTENDED ABSTRACT IN CROATIAN)

U ovom radu predstavljena je metoda harmoničke ravnoteže za nelinearna periodična strujanja. Pretpostavka o periodičnosti strujanja omogućuje dobivanje $2n+1$ spregnutih stacionarnih problema iz jedne tranzijentne transportne jednadžbe. Rješavanjem $2n+1$ stacionarnih problema dobivaju se rješenja u diskretnim vremenskim trenucima tijekom reprezentativnog perioda. Metoda je implementirana u OpenFOAM, koristeći metodu konačnih volumena drugog reda točnosti.

Matematički model

Matematički model metode harmoničke ravnoteže dan je u nastavku, te primijenjen na skalarnu transportnu jednadžbu. Nakon validacije, metoda je proširena na Navier-Stokesove jednadžbe.

Skalarna transportna jednadžba

Pasivni prijenos skalara Q određen je brzinom $\mathbf{u}$ i koeficijentom difuzije γ, a definiran je konvekcijsko-difuzijskom jednadžbom:

$$\frac{\partial Q}{\partial t} + \mathcal{R} = 0\,, \tag{1}$$

gdje $\mathcal{R}$ predstavlja konvekcijski i difuzijski transport te izvorne članove:

$$\mathcal{R} = \nabla\bullet(\mathbf{u}Q) - \nabla\bullet(\gamma\nabla Q) - S_Q\,. \tag{2}$$

Za nastavak potrebno je prikazati varijablu Q u obliku konačnog Fourierovog reda s n harmonika:

$$Q(t) = Q_0 + \sum_{k=1}^{n} Q_{S_k}\sin(k\omega t) + Q_{C_k}\cos(k\omega t)\,. \tag{3}$$

Treba primijetiti da se za varijablu u vremenskoj domeni koristi notacija Q, dok se varijabla Q nalazi u frekvencijskoj domeni. Fourierov razvoj od $\mathcal{R}$ jednak je razvoju danom u jednadžbi (3), pri čemu je Q zamijenjen s R. Ako vremenski član u jednadžbi (1) zamijenimo derivacijom razvoja Q iz jednadžbe (3) i Fourierovim razvojem varijable $\mathcal{R}$ u izvornu transportnu jednadžbu (1), dobivamo:

$$\sum_{k=1}^{n} i\omega \left(Q_{S_k} \cos(k\omega t) - Q_{C_k} \sin(k\omega t) \right) + \sum_{k=1}^{n} \left(R_{C_k} \cos(k\omega t) + R_{S_k} \sin(k\omega t) \right) = R_0 \,. \tag{4}$$

Jednadžba (4) predstavlja skalarnu transportnu jednadžbu u frekvencijskoj domeni, gdje su Fourierovi koeficijenti Q_{S_k} i Q_{C_k} nepoznati. Svaki od navedenih Q i R je polje varijable, točnije, nezavisan Fourierov razvoj za svaku točku u prostoru, uz pretpostavku jednake osnovne frekvencije. Prema tome, rješenje je harmonijsko u svakoj točki neovisno o koeficijentima ostalih točaka. Grupiramo li koeficijente s istim harmonijskim članovima u jednadžbi (4), dobivamo $2n+1$ jednadžbi:

$$\begin{aligned} -k\omega Q_{C_k} + R_{S_k} = 0 &\rightarrow n \text{ jednadžbi uz sinus, za } k = 1 \ldots n \,, \\ R_0 = 0 &\rightarrow 1 \text{ jednadžba za srednju vrijednost} \\ k\omega Q_{S_k} + R_{C_k} = 0 &\rightarrow n \text{ jednadžbi uz kosinus, za } k = 1 \ldots n \,. \end{aligned} \tag{5}$$

Jednadžba (5) može se napisati u sažetom matričnom obliku:

$$\omega \mathbf{A}\,\mathbf{Q} + \mathbf{R} = \mathbf{0} \,, \tag{6}$$

gdje:

$$\mathbf{A} = \begin{bmatrix} & & & & & 0 & -1 & & & & & \\ & & & & & 0 & & -2 & & & & \\ & & 0 & & & . & & & -3 & & & \\ & & & & & . & & & & \ddots & & \\ & & & & & . & & & & & -n & \\ 0 & 0 & 0 & \cdots & 0 & 0 & 0 & \cdots & 0 & 0 & 0 & \\ 1 & & & & & . & & & & & & \\ & 2 & & & & . & & & & & & \\ & & 3 & & & . & & & 0 & & & \\ & & & \ddots & & 0 & & & & & & \\ & & & & n & 0 & & & & & & \end{bmatrix}, \quad \mathbf{Q} = \begin{bmatrix} Q_{S_1} \\ Q_{S_2} \\ Q_{S_3} \\ \vdots \\ Q_{S_n} \\ Q_0 \\ Q_{C_1} \\ Q_{C_2} \\ Q_{C_3} \\ \vdots \\ Q_{C_n} \end{bmatrix}, \quad \mathbf{R} = \begin{bmatrix} R_{S_1} \\ R_{S_2} \\ R_{S_3} \\ \vdots \\ R_{Sn} \\ R_0 \\ R_{C_1} \\ R_{C_2} \\ R_{C_3} \\ \vdots \\ R_{C_n} \end{bmatrix}. \tag{7}$$

Rješavanjem (6) dobili bi se Fourierovi koeficijenti za varijablu Q, no takav postupak nije poželjan budući da $\mathbf{R}$ sadrži diferencijalne operatore koje bi trebalo prilagoditi za frekvencijsku domenu.

Stoga, nastavlja se u smjeru definiranja matrice koja ima ulogu direktne Fourierove

transformacije (DFT) kako bi se omogućio jednostavan prelazak iz vremenske u frekvencijsku domenu i obrnuto. Da bismo imali jednoznačno jedan–na–jedan mapiranje, diskretni vektor varijable $\boldsymbol{Q}$ u vremenskoj domeni definiramo kao:

$$\boldsymbol{Q}^T = \begin{bmatrix} Q_{t_1} & Q_{t_2} & Q_{t_3} & \cdots & Q_{t_{2n+1}} \end{bmatrix}, \tag{8}$$

gdje t_n označava:

$$t_i = \frac{iT}{2n+1}\,, \text{ za } i = 1 \ldots 2n+1\,. \tag{9}$$

DFT koji služi za transformaciju iz vremenske domene varijable $\boldsymbol{Q}$ u frekvencijsku domenu $\mathbf{Q}$ može se zapisati:

$$\mathbf{Q} = \mathbf{E}\boldsymbol{Q}\,, \tag{10}$$

matrica $\mathbf{E}$ ima oblik:

$$\mathbf{E} = \frac{2}{2n+1} \begin{bmatrix} \sin(\omega t_1) & \sin(\omega t_2) & \ldots & \sin(\omega t_{2n+1}) \\ \sin(2\omega t_1) & \sin(2\omega t_2) & \ldots & \sin(2\omega t_{2n+1}) \\ \vdots & \vdots & & \vdots \\ \sin(n\omega t_1) & \sin(n\omega t_2) & \ldots & \sin(n\omega t_{2n+1}) \\ \frac{1}{2} & \frac{1}{2} & \ldots & \frac{1}{2} \\ \cos(\omega t_1) & \cos(\omega t_2) & \ldots & \cos(\omega t_{2n+1}) \\ \cos(2\omega t_1) & \cos(2\omega t_2) & \ldots & \cos(2\omega t_{2n+1}) \\ \vdots & \vdots & & \vdots \\ \cos(n\omega t_1) & \cos(n\omega t_2) & \ldots & \cos(n\omega t_{2n+1}) \end{bmatrix}. \tag{11}$$

Množenjem jednadžbe (10) matricom $\mathbf{E}^{-1}$ s lijeva, dobiva se transformacija iz frekvencijske u vremensku domenu:

$$\boldsymbol{Q} = \mathbf{E}^{-1}\mathbf{Q}\,, \tag{12}$$

pri čemu je inverzna matrica jednaka:

$$\mathbf{E}^{-1} = \begin{bmatrix} \sin(\omega t_1) & \ldots & \sin(n\omega t_1) & 1 & \cos(\omega t_1) & \ldots & \cos(n\omega t_1) \\ \sin(\omega t_2) & \ldots & \sin(n\omega t_2) & 1 & \cos(\omega t_2) & \ldots & \cos(n\omega t_2) \\ & & & & \vdots & & \\ & & & & \vdots & & \\ \sin(\omega t_{2n+1}) & \ldots & \sin(n\omega t_{2n+1}) & 1 & \cos(\omega t_{2n+1}) & \ldots & \cos(n\omega t_{2n+1}) \end{bmatrix}. \tag{13}$$

Korištenjem matrica transformacije $\mathbf{E}$ i $\mathbf{E}^{-1}$, nastavit će se oblikovanje skalarne transportne jednadžbe u frekvencijskoj domeni, jednadžba (6). Ako zamijenimo izraz u jednadžbi (6) izrazom (10), dobivamo jednadžbu u frekvencijskoj domeni izraženu preko varijable $\boldsymbol{\mathcal{Q}}$ u vremenskoj domeni:

$$\omega \mathbf{A}\,\mathbf{E}\boldsymbol{\mathcal{Q}} + \mathbf{E}\boldsymbol{\mathcal{R}} = \mathbf{0}\,, \tag{14}$$

Ista transformacija je primijenjena na $\boldsymbol{\mathcal{R}}$ i $\boldsymbol{\mathcal{Q}}$. Iako bi rješavanje (linearnih) jednadžbi u ovom obliku bilo moguće, dobivanje izvornih članova i protoka kroz stranicu kontrolnih volumena bilo bi skupo u pogledu računalnih resursa. U skladu s navedenim, jednadžbu (14) transformiramo natrag u vremensku domenu. Jednadžbu (14) množimo s lijeva matricom $\mathbf{E}^{-1}$ iz čega slijedi:

$$\omega \mathbf{E}^{-1}\,\mathbf{A}\,\mathbf{E}\boldsymbol{\mathcal{Q}} + \boldsymbol{\mathcal{R}} = \mathbf{0}\,. \tag{15}$$

Dobivena jednadžba predstavlja spregnuti sustav $2n+1$ stacionarnih problema. Uspoređujući jednadžbu (15) s originalnom skalarnom transportnom jednadžbom (1), mogu se uočiti dvije bitne karakteristike:

- $\mathcal{R}$ je zamijenjen diskretnom varijablom $\boldsymbol{\mathcal{R}}$, pri čemu upućuje da su rješenja dobivena u određenom broju diskretnih vremenskih trenutaka. Broj vremenskih trenutaka određen je korištenim brojem harmonika n, prema izrazu (8).
- Vremenski član zamijenjen je spregnutim izvornim članovima koji međusobno povezuju različite vremenske trenutke. Takav pristup istovjetan je računanju derivacije harmonijskog signala po vremenu u $2n+1$ ekvidistantnih vremenskih trenutaka, uključujući i rješenje srednje vrijednosti.

Matrica $\mathbf{E}^{-1}\,\mathbf{A}\,\mathbf{E}$ koja množi $\boldsymbol{\mathcal{Q}}$ u jednadžbi (15) ima slijedeći oblik:

$$\mathbf{E}^{-1}\,\mathbf{A}\,\mathbf{E} = \frac{2}{2n+1}\begin{bmatrix} 0 & P_1 & P_2 & P_3 & \dots & \dots & P_{2n} \\ -P_1 & 0 & P_1 & P_2 & P_3 & & \vdots \\ -P_2 & -P_1 & 0 & P_1 & P_2 & & \vdots \\ -P_3 & -P_2 & -P_1 & 0 & P_1 & & \vdots \\ \vdots & & & & \ddots & & P_2 \\ \vdots & & & & & \ddots & P_1 \\ -P_{2n} & \dots & \dots & -P_3 & -P_2 & -P_1 & 0 \end{bmatrix}, \tag{16}$$

gdje je P_i definiran kao:

$$P_i = \sum_{k=1}^{n} k \sin(ik\omega t_1)\,, \text{ za } i = 1 \ldots 2n\,. \tag{17}$$

Koeficijenti P_i ovise samo o osnovnoj frekvenciji i korištenom broju harmonika, a oboje se određuje unaprijed. Prema tome, budući da su koeficijenti P_i konstantni, dovoljno ih je izračunati i spremiti samo jednom, uz zanemariv trošak računalnih resursa u odnosu na trošak simulacije.

Koristeći (16) zajedno s jednadžbom (15), prošireni oblik spregnutih jednadžbi za skalarni transport u formi metode harmoničke ravnoteže moguće je zapisati:

$$\nabla\bullet(\mathbf{u}Q_{t_j}) - \nabla\bullet\left(\gamma\nabla Q_{t_j}\right) - S_{Q_{t_j}} = -\frac{2\omega}{2n+1}\left(\sum_{i=1}^{2n} P_{i-j}Q_{t_i}\right)\,, \text{ za } j = 1 \ldots 2n+1\,, \tag{18}$$

pri čemu je sprega rješenja u različitim vremenskim trenucima t_j postignuta matricom P_{i-j} kojom se modelira član vremenske derivacije kao dodatni izvorni član. Dakle, jedna tranzijentna jednadžba dana izrazom (1) pretvorena je u sustav od $2n+1$ spregnutih stacionarnih jednadžbi, izraz (18).

Navier-Stokesove jednadžbe

U nastavku je dan izvod metode harmoničke ravnoteže za Navier-Stokesove jednadžbe. Nestlačivo, laminarno, jednofazno strujanje opisano je jednadžbom kontinuiteta te momentnom jednadžbom:

$$\nabla\bullet\mathbf{u} = 0\,, \tag{19}$$

$$\frac{\partial\mathbf{u}}{\partial t} + \nabla\bullet(\mathbf{u}\mathbf{u}) - \nabla\bullet(\nu\nabla\mathbf{u}) = -\frac{\nabla p}{\rho}\,, \tag{20}$$

gdje ν označava kinematičku viskoznost, ρ je gustoća, a p polje tlaka.

Analizirajući metodu harmoničke ravnoteže za skalarnu transportnu jednadžbu, moguće

je zaključiti da se član vremenske derivacije u transportnoj jednadžbi zamjenjuje spregnutim izvornim članovima: konvekcijski, difuzijski i drugi izvorni članovi ostaju nepromijenjeni. Prema tome, može se pokazati da jednadžba kontinuiteta zadržava svoj oblik, uz zamjenu brzine $\mathbf{u}$ svojim diskretnim oblikom $\mathbf{u}_{t_j}$:

$$\nabla\bullet\mathbf{u}_{t_j} = 0\,. \tag{21}$$

Jednadžba (21) pokazuje da jednadžba kontinuiteta mora biti zadovoljena u svakom diskretnom vremenskom trenutku t_j. Momentna jednadžba u formi metode harmoničke ravnoteže dobiva

se analogno derivaciji skalarne transportne jednadžbe, te glasi:

$$\nabla\bullet(\mathbf{u}_{t_j}\mathbf{u}_{t_j}) - \nabla\bullet\left(\nu\nabla\mathbf{u}_{t_j}\right) = -\nabla p_{t_j} - \frac{2\omega}{2n+1}\left(\sum_{i=1}^{2n} P_{i-j}\mathbf{u}_{t_i}\right), \text{ za } j = 1\ldots 2n+1\,. \qquad (22)$$

Jednadžbe (21) i (22) predstavljaju $2n+1$ spregnutih sustava tlak–brzina uz nametnuto periodično ponašanje određenom osnovnom frekvencijom ω i brojem harmonika n.

Validacija

U nastavku su dani rezultati dobiveni metodom harmoničke ravnoteže. Metoda je prvo validirana za pasivni prijenos skalara. Dobiveni rezultati uspoređeni su s rezultatima tranzijentne simulacije, a nakon validacije metode harmoničke ravnoteže za skalarni transport, validirana je metoda za Navier-Stokesove jednadžbe.

Za validaciju pasivnog transporta skalara metodom harmoničke ravnoteže, korištena je 2D pravokutna domena. Domena je dimenzija 10 m$\times$7 m, diskretizirana sa 6 633 heksaedarskih ćelija. Pretpostavljeno je uniformno polje brzine, $\mathbf{u} = 10$ m/s, a koeficijent difuzije jednak je $\gamma = 1{,}5\cdot 10^{-5}$ m^2/s.
Kako bi usporedba rezultata metode harmoničke ravnoteže i tranzijentne simulacije bila moguća, dijagrami prikazuju vrijednosti skalara Q_{t_j} po uzdužnoj sredini domene ($x \in [0\text{ m}, 10\text{ m}]$, $y = 0$) za sve slučajeve.

Jedan sinusni val

Prvi slučaj validacije odnosi se na jedan sinusni val. Rubni uvjeti su modelirani tako da se vrijednost skalara na ulazu mijenja po sinusnom zakonu kroz vrijeme:

$$Q(t) = A\sin(2\pi f t)\,, \qquad (23)$$

gdje je $A = 5$ amplituda vala, a $f = 2$ Hz frekvencija vala. Za tranzijentnu simulaciju koristi se promjenjivi rubni uvjet, dok je za metodu harmoničke ravnoteže korišten rubni uvjet konstantne vrijednosti koja odgovara izrazu $Q_{t_j} = A\sin(2\pi f t_j)$ za svaki vremenski trenutak t_j. Na ostalim granicama kao rubni uvjet postavljen je iznos gradijenta na nula. Budući da je nametnuti val sinusnog oblika, samo jedan harmonik je dovoljan, $n = 1$. Slika 1 prikazuje usporedbu rezultata metode harmoničke ravnoteže s rezultatima tranzijentne simulacije. Na slici 1a prikazana je vizualizacija domene kroz koju propagiraju dva vala. Slike 1b do 1d daju usporedbu rezultata

u različitim vremenskim trenucima.

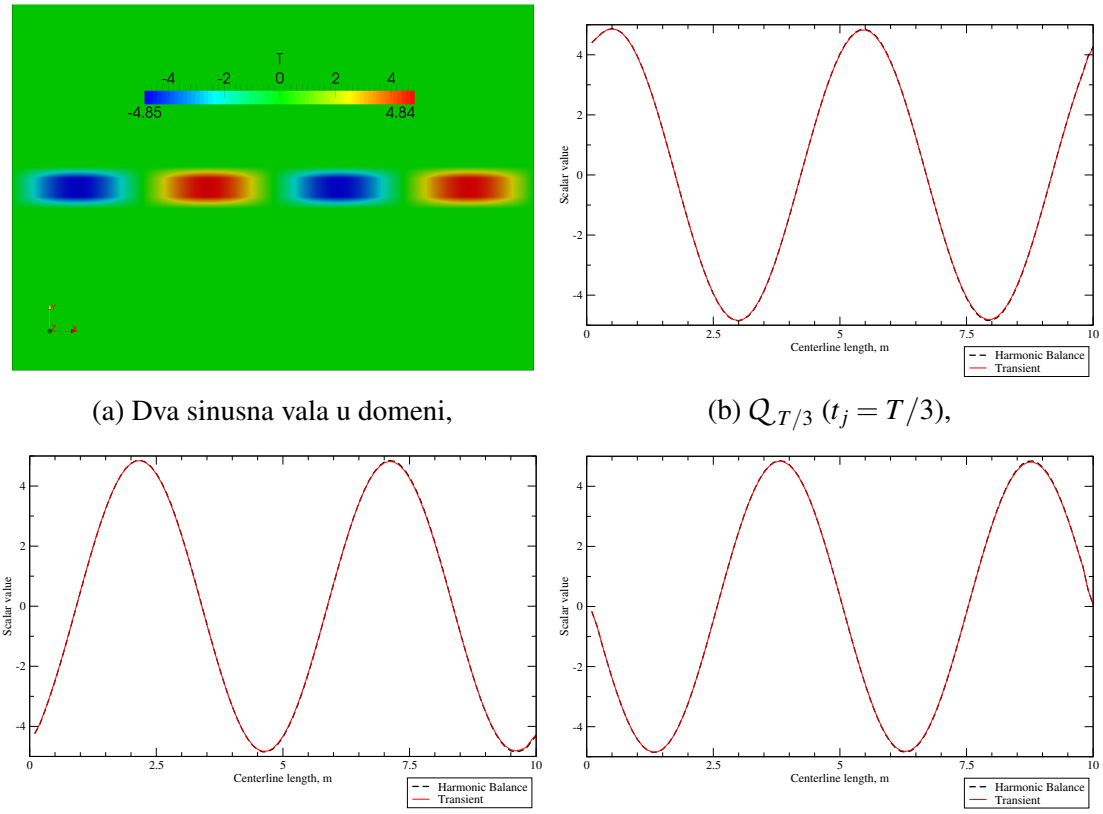

(a) Dva sinusna vala u domeni, (b) $Q_{T/3}$ $(t_j = T/3)$,

(c) $Q_{2T/3}$ $(t_j = 2T/3)$, (d) Q_T, $(t_j = T)$.

Slika 1: Vizualizacija domene te usporedba metode harmoničke ravnoteže i konvencionalnog tranzijentnog rješavača.

Linearna kombinacija sinusnog i kosinusnog vala

Drugi validacijski slučaj modelira rubne uvjete tako da odgovaraju zbroju sinusnog i kosinusnog vala:

$$Q(t) = A\sin(2\pi f(t-\phi)) + B\cos(2\pi 2 f(t-\phi)) \,, \tag{24}$$

pri čemu je $A = 3$ amplituda sinusnog vala, $B = 5$ amplituda kosinusnog vala, a $f = 1$ Hz osnovna frekvencija. Za pozicioniranje vala tako da se skalarna vrijednost nule poklopi sa $t = 0$ korišten je fazni pomak $\phi = 0.35$. Frekvencija kosinusnog vala jednaka je dvostrukoj frekvenciji sinusnog vala, zbog čega su potrebna $n = 2$ harmonika. Ostali rubni uvjeti definirani su jednako kao i u prethodnom slučaju. Slika 2 prikazuje usporedbu rezultata dobivenih metodom harmoničke ravnoteže s rezultatima tranzijentne simulacije u različitim vremenskim trenucima.

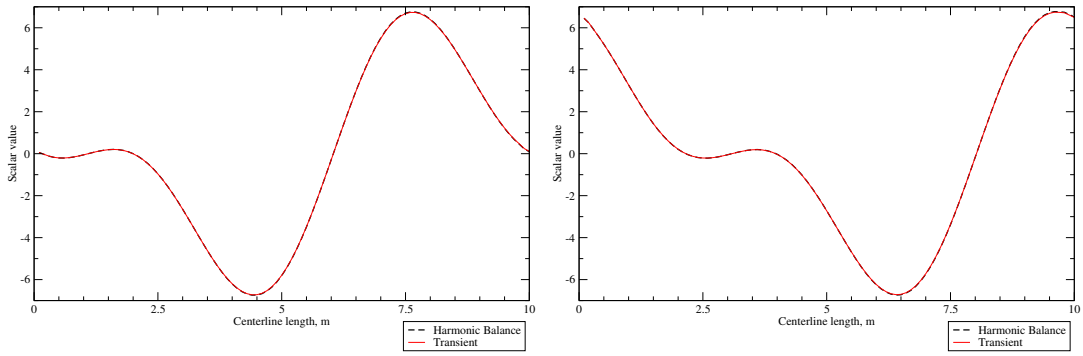

(a) $Q_{T/5}$ $(t_j = T/5)$, (b) $Q_{2T/5}$ $(t_j = 2T/5)$,

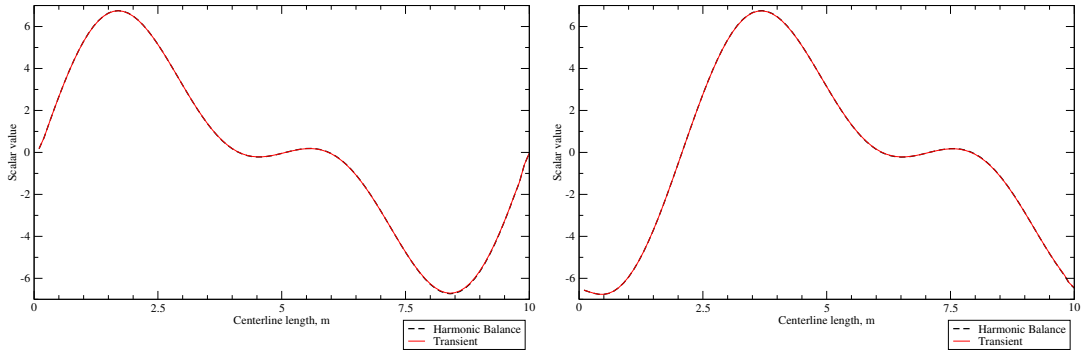

(c) $Q_{3T/5}$ $(t_j = 3T/5)$, (d) $Q_{4T/5}$, $(t_j = 4T/5)$.

Slika 2: Usporedba metode harmoničke ravnoteže s tranzijentnom simulacijom za kombinaciju sinusnog i kosinusnog vala.

Pravokutni val

Prethodni validacijski slučajevi predstavili su sposobnost metode harmoničke ravnoteže da prikaže harmonijski poremećaj. Kako bi testirali rješavač na zahtjevnijim slučajevima, simuliraju se pravokutni valovi, budući da takvi poremećaji i inače predstavljaju izazov numeričkim algoritmima.

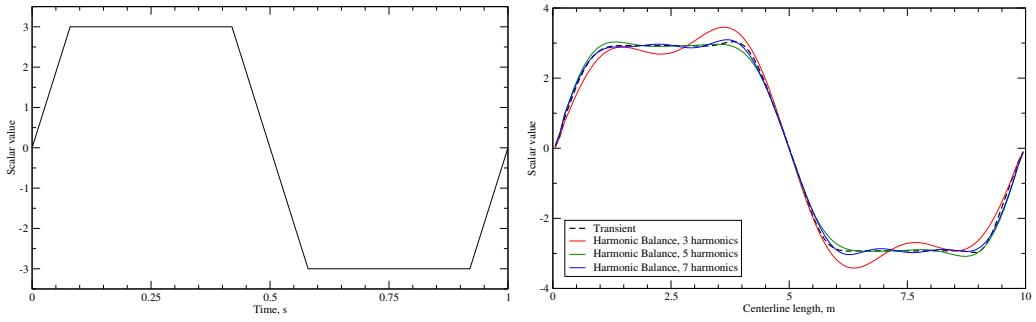

(a) Pravokutni val nametnut na ulazu, (b) Q_T $(t_j = T)$ za različit broj harmonika.

Slika 3: Usporedba metode harmoničke ravnoteže i tranzijentne simulacije za pravokutni val.

Slika 3a prikazuje signal nametnut na ulazu u obliku pravokutnog vala. Umjesto rješenja u različitim vremenskim trenucima, ovdje je dan prikaz konvergencije rezultata s povećanjem

broja harmonika, slika 3b. Može se uočiti da se korištenjem više harmonika rezultat približava rezultatu tranzijentne simulacije.

Složeni pravokutni val

Posljednji validacijski slučaj za pasivni prijenos skalara modelira složeni pravokutni val s $n = 3, 5, 7$ i 10 harmonika. Slika 4a prikazuje složeni pravokutni val nametnut na ulazu u domenu. Usporedba profila vala na kraju perioda za različit broj harmonika prikazana je na slici 4b. Rješenje konvergira rješenju tranzijentne simulacije kako se povećava broj harmonika.

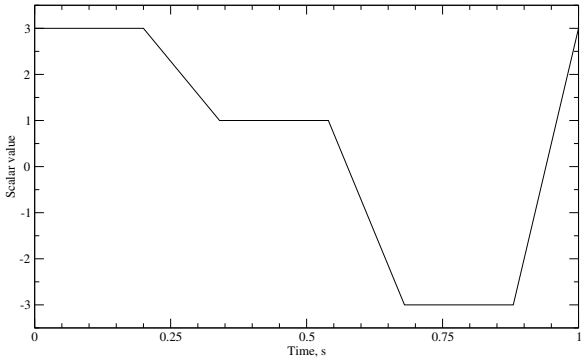

(a) Složeni pravokutni val nametnut na ulazu,

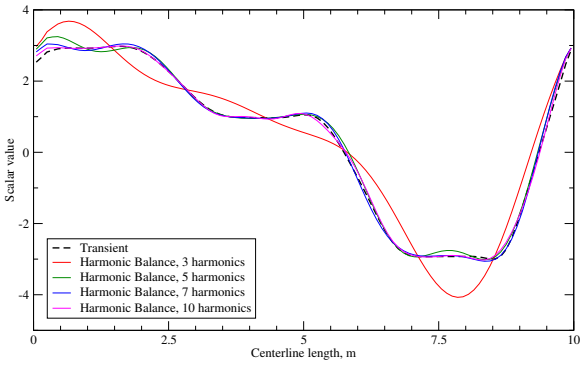

(b) Q_T $(t_j = T)$ za različit broj harmonika.

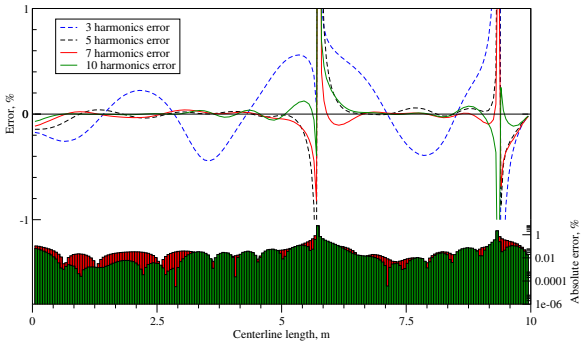

(c) Greška metode harmoničke ravnoteže naspram tranzijentnog rješenja.

Slika 4: Usporedba metode harmoničke ravnoteže i tranzijentne simulacije za složeni pravokutni val.

Na slici 4c prikazano je odstupanje rezultata dobivenih koristeći $n = 3, 5, 7$ i 10 harmonika od rezultata tranzijentne simulacije. Stupci pri dnu dijagrama prikazuju apsolutnu vrijednost odstupanja u logaritamskom mjerilu pri čemu zelena boja označava 10 harmonika, a crvena 7. Stupci su dodani kako bi prikazali male razlike između simulacije sa 7 i 10 harmonika. S druge strane, simulacija sa 7 harmonika uključuje 15 spregnutih jednadžbi, dok se za 10

harmonika rješava 21 spregnuta jednadžba, što je nepotrebni, ali značajni računalni trošak.

Oscilirajući NACA 2412 aeroprofil

U ovom poglavlju predstavljena je validacija nestlačivog, laminarnog strujanja oko NACA 2412 aeroprofila dobivenog metodom harmoničke ravnoteže. Duljina tetive iznosi 1 m, brzina na ulazu je 1 m/s, a napadni kut varira između ± 3 deg. Računalna domena sastoji se od 6 060 heksaedarskih ćelija. Rezultati metode harmoničke ravnoteže uspoređeni su s tranzijentnom simulacijom u kojoj se zakretanjem mreže modelira promjena napadnog kuta aeroprofila. Promjena napadnog kuta kod metode harmoničke ravnoteže modelirana je promjenom rubnih uvjeta, pri čemu svaki vremenski trenutak ima zadanu konstantnu brzinu pri promijenjenom kutu u odnosu na prethodni vremenski trenutak. U nastavku su dani rezultati za jedan korišteni harmonik. Slika 5 prikazuje konture tlaka na površini aeroprofila. Os apscisa predstavlja razmotanu površinu aeroprofila, a vrijednosti označavaju broj ćelije. Vrijednosti 0 i 100 su izlazni bridovi aeroprofila pri čemu od 0-50 označava donju površinu krila dok 50-100 označava gornju površinu krila. Rezultati su dani za 3 vremenska trenutka dobivena korištenjem jednog harmonika.

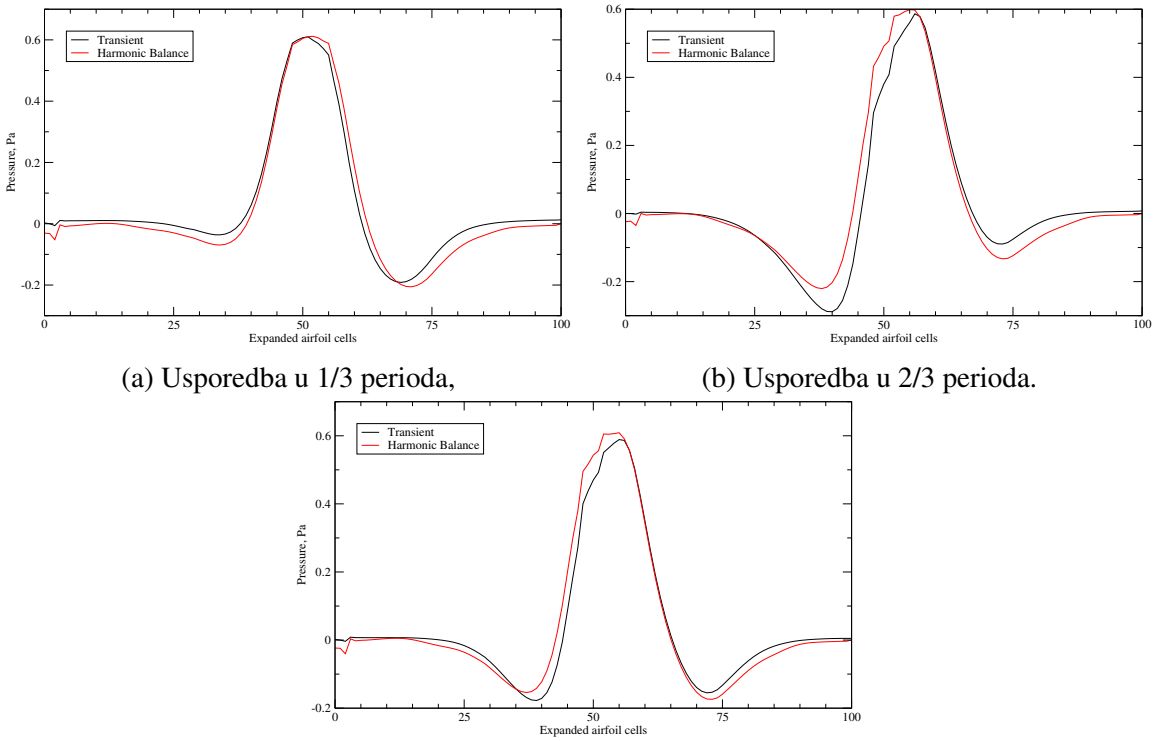

(a) Usporedba u 1/3 perioda, (b) Usporedba u 2/3 perioda.

(c) Usporedba na kraju perioda.

Slika 5: Usporedba rezultata metode harmoničke ravnoteže i tranzijentne simulacije.

1 Introduction

A fascination with the natural world of fluids and flows dates back since the beginning of civilisation. In antiquity, it was approached in a philosophical sense (Heraclitus „Everything flows“), and centuries were needed to give the ideas focused to fluid flow phenomena a scientific character in the form of Newtonian physical equations. In the 19th century, two important scientists, Navier and Stokes emerged and developed the famous Navier-Stokes equation, the first requirement for the development of computational fluid dynamics. It was not until the evolution of high-speed computers that the modern day computational fluid dynamics (CFD) developed and became an indispensable part of the design process for indeed any craft or manufacturing process that mankind has devised.

Over the several past decades, computational fluid dynamics has brought a major break-through in the development of technology and industry. It is a highly interdisciplinary research area that provides a qualitative and sometimes even quantitative prediction of fluid flows based on mathematical modelling, numerical methods and software tools. It enables scientists and engineers perform computer simulations of fluid flow that are used as a reliable tool in commercial research and development centres. In modern industry applications it is becoming a common part of the design process and is routinely used in a wide variety of industries, such as automotive, aerospace, marine, power generation manufacturing, etc. In many of these fields, CFD is associated with the occurrence of periodic phenomena, and in order to analyse and predict them the Harmonic Balance Method [1] has been developed. Its deployment in computational fluid dynamics is on the continuous increase and it is an efficient tool for tackling periodic problems where base frequency is known.

Compared to the Harmonic balance Method, conventional transient simulations are long and computationally expensive, especially for periodic problems: there are cases where up to 100 periods have to be simulated to obtain accurate results. Steady-state simulations as a significantly cheaper option, offer insight into the flow field but cannot resolve the transient effects. In order to avoid long transient simulations and maintain the CPU efficiency of steady-state simulations, a new method has been proposed. The main goal is to offer savings in time while concurrently reproduce transient effects. Hence, Harmonic Balance Method is a quasi steady-state method developed for simulating non-linear temporally periodic flows. The Harmonic Balance Method is based on the assumption that primitive variables can be accurately represented by a Fourier series in time. Additional source terms are introduced by replacing a time derivative term in transport equations with Fourier series derivative. Therefore, instead of time derivative term, all the time instants are coupled in source terms, resulting in a set of steady-state equations for a set of time instants within a period. Such approach offers both the temporal accuracy by calculating more than one time instant within a period, and the spatial

accuracy by resolving transient effects. Additionally, it offers CPU time reduction.

In this thesis, the Harmonic Balance Method is introduced, derived and validated. The work covered by the thesis can be briefly summarised by sections, as follows: Section 2, Mathematical Model, introduces the scalar transport equation and Navier-Stokes equations that are later modelled in terms of Harmonic Balance Method. During its development, Harmonic Balance Method was first tested to solve scalar transport equation only, which explains the reason for introduction of scalar transport. Afterwards, Harmonic Balance Method was expanded for calculations of both pressure and velocity, which resulted in solving Navier-Stokes equations.

Section 3 deals with the derivation of the Harmonic Balance Method and introduces the Fourier series expansion on which harmonic balance is based. The Section ends with an example for one harmonic, explaining the algorithm and presenting the equations in its expanded form. The derived mathematical model is implemented in foam-extend, a fork of the open source software OpenFOAM [2].

Sections 4 and 5 describe the process of validation. Section 4 deals with the validation of scalar transport equation using four test cases. First test case demonstrates the ability of the Harmonic Balance Method using one harmonic. Signal imposed at inlet resembles the sine wave, varying the scalar value in time and it is successfully resolved using one harmonic. Second test case imposes a signal consisting of two harmonic waves for which two harmonics are used. Ramped square wave and a complex square wave are imposed at inlet in test cases 3 and 4. Third and fourth test case present the convergence of solution for higher number of harmonics used. Section 5 presents validation of Harmonic Balance for Navier-Stokes equations. First test case is a NACA 2412 pitching airfoil. The pitch angle is periodically changed in time for two inlet velocities: one yielding high Re number and the other yielding low Re number. For both velocities results obtained using 1, 3 and 6 harmonics are compared with transient solution. The last subsection deals with the test cases for phenomena in which the base frequency is not known in advance: laminar vortex shedding behind a cylinder [3] and the edge tone noise [4]. The two cases are used to show the problems that may occur in Harmonic Balance approach for non-typical phenomena. All the results are compared to transient simulation.

2 Mathematical Model

2.1 Introduction

In this thesis two models of transport equations are presented. First model describes passive scalar transport, while the second deals with Navier–Stokes equations. Scalar transport equation is presented in the first subsection. Equations for incompressible laminar flow of a viscous fluid is given in the second subsection. Last subsections explains boundary conditions.

2.2 Scalar Transport Equation

Scalar transport equation Eq. (1) models a combination of the diffusion and convection transport for passive scalar [5]:

$$\frac{\partial Q}{\partial t} + \nabla\cdot(\mathbf{u}Q) - \nabla\cdot(\gamma\nabla Q) = q_v, \tag{1}$$

where Q is a passive scalar being transported (e.g. species concentration), γ is a diffusion coefficient, q_v represents sources or sinks of the quantity Q and $\mathbf{u}$ is the convective velocity field. Sources and sinks account for non-transport effects (not described by convection or diffusion) such as local volume production or destruction of Q.

In order of appearance, terms in Eq. (1) are:

- Temporal derivative describing inertia of the system;
- Convection term, representing transport with the fluid velocity field;
- Diffusion term, representing transport due to the gradient of a passive scalar;
- Sources and sinks.

The convection term is of hyperbolic nature: information comes from the vicinity and it is defined by the direction of velocity. The diffusion term is an elliptic term: every point in the domain feels the influence of every other point instantaneously.

2.3 Navier–Stokes Equations

Incompressible flow of a fluid is described by a set of partial differential equations [6]: continuity equation Eq. (2) and Navier–Stokes equations Eq. (3):

$$\nabla \bullet \mathbf{u} = 0, \tag{2}$$

$$\frac{\partial \mathbf{u}}{\partial t} + \nabla \bullet (\mathbf{u}\mathbf{u}) - \nabla \bullet (\nu \nabla \mathbf{u}) = -\nabla p, \tag{3}$$

where $\mathbf{u}$ is the velocity, ν is the kinematic viscosity and p is the kinematic pressure. In Navier-Stokes equations velocity is both the transported property and the transporting quantity. Transient and convective terms are also called inertial terms, while diffusion and pressure gradient terms represent the divergence of the stress tensor field.

The Navier–Stokes equations contain four independent variables: the x, y and z spatial coordinates and time t. There are four dependent variables: the kinematic pressure p and three components of the velocity vector field, where all four of dependent variables are functions of the remaining three variables. Therefore, the system of equations is closed and coupled. Solution will be shown in section 3.4.

2.4 Boundary Conditions

A unique solution for a set of partial differential equations is obtained by specifying boundary conditions. Boundary conditions are prescribed on the boundary of the domain for each dependent variable.

There are two main types of boundary conditions: Dirichlet boundary condition and generalised von Neumman boundary condition. Dirichlet boundary condition specifies the value of the variable at the boundary of a domain. Generalised von Neumman boundary condition specifies the surface normal gradient of a variable at the boundary. There are also many other types of boundary conditions: they represent a combination of the two mentioned here.

The types of boundaries used most often in computational fluid dynamics are: inlet, outlet, wall and symmetry plane. Depending on the problem, the Dirichlet and generalised von Neumman boundary conditions are generally used in pair when solving Navier–Stokes equations. For example, inlet boundary is usually specified with Dirichlet boundary condition for velocity, and von Neumman boundary condition for pressure. Outlet boundary is usually modelled with von Neumman boundary condition for velocity and Dirichlet boundary condition for pressure. Wall is a boundary where velocity is equal to zero: there is no flux

through the wall. Consequently, von Neumman boundary condition is specified for pressure. Symmetry plane is used to reduce computational efforts as it allows smaller domain provided that symmetry of the solution can be guaranteed. It is necessary that the imposed boundary conditions are physically correct and reflect the real situation as much as possible.

2.5 Closure

In this section an overview of the scalar transport equation and Navier–Stokes equations for incompressible laminar flow of a viscous fluid was given. The next section deals with the derivation of the mathematical model for the Harmonic Balance Method. The method will be explained thoroughly and derived for both scalar transport equation and Navier–Stokes equations.

3 Harmonic Balance Method

A wide area of Computational Fluid Dynamics (CFD) problems where periodic behaviour occurs, explain the extensive effort towards developing a method that utilizes both the features of transient and steady-state simulations. Transient simulations offer temporal accuracy and give insight into transient flow behaviour, but require increased CPU time compared to steady-state simulations. Steady-state simulations offer savings in time, but they are not able to reproduce transient effects. The Harmonic Balance Method consists of a coupled set of steady-state equations, where the temporal term is modelled as additional source terms. Hence, it offers savings in CPU time compared to transient simulation and gives better temporal accuracy in comparison to steady-state simulation. The assumption of temporal periodic flow makes it valid for periodic problems only.

3.1 Introduction

Harmonic balance is a quasi steady-state method developed for simulation of non–linear temporally periodic flows. The main assumption on which harmonic balance is based concerns the primitive variables. We assume that each primitive variable can be accurately represented by a Fourier series in time, using first n harmonics and the mean value. Such assumption allows replacing the time derivative term in transport equations with additional source terms, thus transforming the transient equations into a coupled set of steady-state equations. When compared to other steady-state methods, the improvement is that harmonic balance is able to describe the transient effects of the periodic flow. Because of the nature of Fourier expansion, in Harmonic Balance Method the snapshots of a flow field in certain time steps within one period are obtained. Other time steps can be reconstructed as a post processing step. In most of the cases, the Harmonic Balance Method should reduce the computational time, but the method is bound to use more memory.

Applications of harmonic balance are widely used in turbomachinery [7], [8] and [9] where the influence of rotor wakes passing on to the stator can be resolved without the need of conventional transient simulation; for solving problems such as vortex shedding and edge tone noise; for reproducing waves in marine engineering, etc. Hydrodynamic problems with prescribed wave motion are a perfect example of a periodic case. Practically, any temporally periodic problem can be simulated.

Turbomachinery, pitching airfoil [10], [11], [13] and all the problems with well-defined base frequency are significantly simpler than problems where the non–linear nature of the flow field is causing periodic instabilities (such as cylinder vortex shedding). The base frequency must be prescribed as an input parameter for harmonic balance. In an unsteady problem such

as cylinder vortex shedding, frequency can also be calculated using the Strouhal and Reynolds number, but it is only the approximate rather than the exact value. So far, there exists only a limited number of examples in literature other than pitching airfoils and turbomachinery, which means that other areas of application have not been explored. Therefore, Harmonic Balance Method is not yet deployed in practical simulations for these purposes .

The scalar transport equation and Navier–Stokes equations presented in the previous section will be extended to harmonic balance form in this section. Before getting to the derivation of the Harmonic Balance Method, Fourier series expansion will be presented to facilitate understanding of the method as it is the core of the Harmonic Balance Method.

3.2 Fourier Series Expansion

The Harmonic Balance Method is based on Fourier series expansion of a periodic function. Fourier series expansion [12] is a decomposition of any periodic function into an infinite series of sine and cosine functions. Sine and cosine terms vary in amplitude and frequency, allowing their sum to closely approximate the original function.

If $f(x)$ is a function of the real variable x and it is integrable on an interval $[x_0, x_0+P]$, where P is the repeating period of $f(x)$, then the Fourier expansion reads:

$$f(x) = a_0 + \sum_{n=1}^{\infty} \left(a_n \cos\left(\frac{2\pi n x}{P}\right) + b_n \sin\left(\frac{2\pi n x}{P}\right) \right), \qquad x \in [x_0, x_0+P]. \tag{4}$$

Because of periodicity of the function, the function repeats with period P before and after the interval $[x_0, x_0+P]$, consequently the expansion is invariant of the interval chosen.
Coefficients a_n and b_n are called Fourier coefficients and can be calculated if $f(x)$ is known:

$$\begin{aligned} a_n &= \frac{2}{P} \int_{x_0}^{x_0+P} f(x) \cdot \cos\left(\frac{2\pi n x}{P}\right) \mathrm{d}x, \\ b_n &= \frac{2}{P} \int_{x_0}^{x_0+P} f(x) \cdot \sin\left(\frac{2\pi n x}{P}\right) \mathrm{d}x. \end{aligned} \tag{5}$$

Expression in Eq. (4) shows that the sum is infinite which is inconvenient for practical use: we are able to calculate only a finite series with N sine and cosine terms. This implies that we are introducing an error to our approximation and by reducing the number of sine and cosine terms in Fourier expansion, our result is approximating more and more loosely the original function $f(x)$. Also, if the function $f(x)$ is not continuous on the interval $[x_0, x_0+P]$, then Fourier expansion will not converge at the discontinuities.

To obtain satisfactory results, a suitable number of terms should be chosen so that both the

calculation time and error introduced are small enough depending on the purpose:

$$f(x) \approx a_0 + \sum_{n=1}^{N} \left(a_n \cos\left(\frac{2\pi n x}{P}\right) + b_n \sin\left(\frac{2\pi n x}{P}\right) \right), \qquad x \in [x_0, x_0 + P]. \tag{6}$$

The upper limit of the summation, N, is also called the number of harmonics, while the nth term of the Fourier series is called the nth harmonic:

$$f_n(x) = a_n \cos\left(\frac{2\pi n x}{P}\right) + b_n \sin\left(\frac{2\pi n x}{P}\right). \tag{7}$$

For $N = 0$, only the zeroth harmonic (the a_0 term) is accounted for and it represents the mean value. In general, expansion with N harmonics will have $2N + 1$ terms: N sine terms, N cosine and the mean value.

The amplitude of the nth harmonic is:

$$A_n = \sqrt{a_n^2 + b_n^2}, \tag{8}$$

and its square A_n^2 is called the energy of the nth harmonic.

A graphical example of a Fourier expansion is given in Figure 1. The function represents a square-wave. It is used to demonstrate convergence of approximation with an increase in the number of harmonics, and also to show how discontinuities affect the Fourier expansion. The example is given for approximations with 1, 3, 5, 7 ,11 and 15 harmonics.

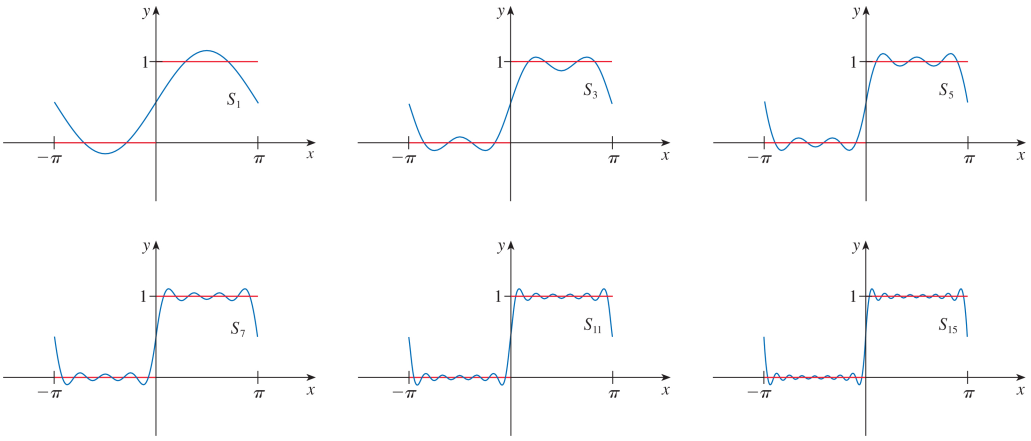

Figure 1: Step function approximated with different number of harmonics [12].

3.3 Harmonic Balance for Scalar Transport

After introducing the Fourier series expansion that will be used in harmonic balance derivation, several points should still be noted. By assuming that each primitive variable can be accurately represented by a Fourier series in time, using first n harmonics and mean value, a certain error is introduced. As it was stated in the previous section, the more harmonics we use, the greater accuracy of the solution. If we use n harmonics, perturbations occurring with frequency order higher than nth harmonic will not be resolved. On the other hand, the more harmonics we use, the longer the calculation time: we will show in the sequel that harmonic balance method solves $2n+1$ steady-state problems rather than just one transient problem. The computational time between two harmonics can vary greatly with results being very close. It should also be noted that in the Harmonic Balance Method, Fourier coefficients vary in space and are calculated for each cell (a numerical approximation for a field).

The derivation of the Harmonic Balance Method for scalar transport will be given here. It starts from the scalar transport equation presented in Eq. (1) written in following form:

$$\frac{\partial \mathcal{Q}}{\partial t} + \mathcal{R} = 0. \tag{9}$$

Here, $\mathcal{R}$ stands for the convection and diffusion transport and source/sink terms of the transport equation:

$$\mathcal{R} = \nabla\bullet(\mathbf{u}\mathcal{Q}) - \nabla\bullet(\gamma\nabla\mathcal{Q}) - q_v \tag{10}$$

Time domain variables will be caligraphic: $\mathcal{Q}$ and frequency domain will be latin Q. The discrete variables will also be denoted by the hat symbol, eg. $\hat{\mathcal{Q}}$.

Fourier series expansion of variable $\mathcal{Q}$ with n harmonics reads:

$$\begin{aligned}\mathcal{Q}(t) = \mathrm{Q}_0 + \mathrm{Q}_{\mathrm{S}_1}\sin(\omega t) + \mathrm{Q}_{\mathrm{C}_1}\cos(\omega t) + \mathrm{Q}_{\mathrm{S}_2}\sin(2\omega t) + \mathrm{Q}_{\mathrm{C}_2}\cos(2\omega t) + \ldots + \\ \mathrm{Q}_{\mathrm{S}_n}\sin(n\omega t) + \mathrm{Q}_{\mathrm{C}_n}\cos(n\omega t),\end{aligned} \tag{11}$$

and expansion of $\mathcal{R}$ reads:

$$\begin{aligned}\mathcal{R}(t) = \mathrm{R}_0 + \mathrm{R}_{\mathrm{S}_1}\sin(\omega t) + \mathrm{R}_{\mathrm{C}_1}\cos(\omega t) + \mathrm{R}_{\mathrm{S}_2}\sin(2\omega t) + \mathrm{R}_{\mathrm{C}_2}\cos(2\omega t) + \ldots + \\ \mathrm{R}_{\mathrm{S}_n}\sin(n\omega t) + \mathrm{R}_{\mathrm{C}_n}\cos(n\omega t).\end{aligned} \tag{12}$$

Inserting the $\mathcal{R}$ expansion from Eq. (12) and time derivative of $\mathcal{Q}$ expansion from Eq. (11)

into the transport equation, yields:

$$\begin{gathered}
\omega \mathrm{Q}_{\mathrm{S}_1} \cos(\omega t) - \omega \mathrm{Q}_{\mathrm{C}_1} \sin(\omega t) \\
+2\mathrm{Q}_{\mathrm{S}_2} \cos(2\omega t) - 2\mathrm{Q}_{\mathrm{C}_2} \sin(2\omega t) \\
+...+ \\
n\mathrm{Q}_{\mathrm{S}_n} \cos(n\omega t) - n\mathrm{Q}_{\mathrm{C}_n} \sin(n\omega t) \\
+\mathrm{R}_{\mathrm{C}_1} \cos(\omega t) + \mathrm{R}_{\mathrm{S}_1} \sin(\omega t) \\
+2\mathrm{R}_{\mathrm{S}_2} \sin(2\omega t) + 2\mathrm{R}_{\mathrm{C}_2} \cos(2\omega t) \\
+...+ \\
n\mathrm{R}_{\mathrm{S}_n} \sin(n\omega t) + n\mathrm{R}_{\mathrm{C}_n} \cos(n\omega t) = -\mathrm{R}_0.
\end{gathered} \tag{13}$$

In Eq. (13), Q and R are the Fourier coefficients coming from Eq. (11) and Eq. (12). Q represents Fourier coefficients related to the $\mathcal{Q}$ expansion, where subscripts S and C denote the sine or cosine term. The index number denotes the harmonic. R represents Fourier coefficients related to the $\mathcal{R}$ expansion, while the rest of the notation remains the same.
Grouping together the sine and cosine parts, we get $2n+1$ equations:

$$\begin{aligned}
&\text{n for sine} \begin{cases} -\omega \mathrm{Q}_{C_1} + R_{S_1} = 0, \\ -2\omega \mathrm{Q}_{C_2} + R_{S_2} = 0, \\ \quad ... \\ -n\omega \mathrm{Q}_{C_n} + R_{S_n} = 0, \end{cases} \\
&\text{mean} - \qquad\qquad R_0 = 0
\end{aligned} \tag{14}$$

$$\text{n for cosine} \begin{cases} \omega \mathrm{Q}_{S_1} + R_{C_1} = 0, \\ 2\omega \mathrm{Q}_{S_2} + R_{C_2} = 0, \\ \quad ... \\ n\omega \mathrm{Q}_{S_n} + R_{C_n} = 0, \end{cases}$$

or, written in a compact, matrix form:

$$\omega \mathbf{A}\mathbf{Q} + \mathbf{R} = 0. \tag{15}$$

Matrices **A, Q** and **R** are coefficient matrices:

$$\mathbf{A}=\begin{bmatrix} & & & & & 0 & -1 & & & & \\ & & & & & 0 & & -2 & & & \\ & & 0 & & & . & & & -3 & & \\ & & & & & . & & & & \ddots & \\ & & & & & . & & & & & -n \\ 0 & 0 & 0 & \cdots & 0 & 0 & 0 & \cdots & 0 & 0 & 0 \\ 1 & & & & & . & & & & & \\ & 2 & & & & . & & & & & \\ & & 3 & & & . & & & 0 & & \\ & & & \ddots & & 0 & & & & & \\ & & & & n & 0 & & & & & \end{bmatrix}, \quad \mathbf{Q}=\begin{bmatrix} \mathrm{Q}_{S_1} \\ \mathrm{Q}_{S_2} \\ \mathrm{Q}_{S_3} \\ \vdots \\ \mathrm{Q}_{S_n} \\ \mathrm{Q}_0 \\ \mathrm{Q}_{C_1} \\ \mathrm{Q}_{C_2} \\ \mathrm{Q}_{C_3} \\ \vdots \\ \mathrm{Q}_{C_n} \end{bmatrix}, \quad \mathbf{R}=\begin{bmatrix} \mathrm{R}_{S_1} \\ \mathrm{R}_{S_2} \\ \mathrm{R}_{S_3} \\ \vdots \\ \mathrm{R}_{Sn} \\ \mathrm{R}_0 \\ \mathrm{R}_{C_1} \\ \mathrm{R}_{C_2} \\ \mathrm{R}_{C_3} \\ \vdots \\ \mathrm{R}_{C_n} \end{bmatrix}. \tag{16}$$

A new matrix that will be used for switching between the time domain and the frequency domain needs to be introduced. This matrix is called the time-to-frequency domain transformation matrix **E** and it is a matrix representation of Direct Fourier Transform (DFT). The derivation of matrix **E** for only one harmonic will be shown below and then generalised for n harmonics. The transformation matrix **E** connects the time and the frequency domain:

$$\mathbf{Q}=\mathbf{E}\hat{\boldsymbol{Q}}(t) \qquad \text{and} \qquad \mathbf{R}=\mathbf{E}\hat{\boldsymbol{\mathcal{R}}}(t). \tag{17}$$

Matrix **E** is obtained from discrete Fourier expansion for $2n+1$ time steps within one period. If the simulation period is T and only one harmonic is used, variables will be calculated at time instants t_1, t_2 and t_3 where:

$$t_1=\frac{T}{3}, \qquad t_2=2t_1=\frac{2T}{3} \qquad \text{and} \qquad t_3=3t_1=\frac{3T}{3}=T. \tag{18}$$

This is necessary in order to obtain the inverse matrix **E** that will be needed later. n harmonics will have $2n+1$ terms and to create a square matrix (instead of a column matrix) $2n+1$ equally spaced time steps need to be calculated.

Discrete Fourier expansions in t_1, t_2 and t_3 read:

$$\begin{aligned} \mathrm{Q}_{t_1} &= \mathrm{Q}_0 + \mathrm{Q}_S \sin(\omega t_1) + \mathrm{Q}_C \cos(\omega t_1) \\ \mathrm{Q}_{t_2} &= \mathrm{Q}_0 + \mathrm{Q}_S \sin(\omega t_2) + \mathrm{Q}_C \cos(\omega t_2) \\ \mathrm{Q}_{t_3} &= \mathrm{Q}_0 + \mathrm{Q}_S \sin(\omega t_3) + \mathrm{Q}_C \cos(\omega t_3). \end{aligned} \tag{19}$$

Once Q_0, Q_S and Q_C coefficients have been calculated, one can evaluate the variable Q in any time by changing t. Set of equation give in Eq. (19) can be written in matrix form:

$$\begin{bmatrix} \mathrm{Q}_{t_1} \\ \mathrm{Q}_{t_2} \\ \mathrm{Q}_{t_3} \end{bmatrix} = \begin{bmatrix} \sin(\omega t_1) & 1 & \cos(\omega t_1) \\ \sin(\omega t_2) & 1 & \cos(\omega t_2) \\ \sin(\omega t_3) & 1 & \cos(\omega t_3) \end{bmatrix} \begin{bmatrix} \mathrm{Q}_S \\ \mathrm{Q}_0 \\ \mathrm{Q}_C \end{bmatrix}, \tag{20}$$

or:

$$\hat{\boldsymbol{Q}} = \mathbf{E}^{-1}\mathbf{Q}, \tag{21}$$

where $\mathbf{E}$ stands for:

$$\mathbf{E} = \frac{2}{3} \begin{bmatrix} \sin(\omega t_1) & \sin(\omega t_2) & \sin(\omega t_3) \\ \frac{1}{2} & \frac{1}{2} & \frac{1}{2} \\ \cos(\omega t_1) & \cos(\omega t_2) & \cos(\omega t_3) \end{bmatrix}. \tag{22}$$

$\mathbf{E}^{-1}$ is the inverse matrix of $\mathbf{E}$. Matrix $\mathbf{E}$ is the transformation matrix from the frequency domain to the time domain, while matrix $\mathbf{E}^{-1}$ is the transformation matrix from the time domain to the frequency domain.

Generalised for n harmonics, matrix $\mathbf{E}$ has the following form:

$$\mathbf{E} = \frac{2}{2n+1}\begin{bmatrix} \sin(\omega t_1) & \sin(\omega t_2) & \sin(\omega t_3) & \dots & \sin(\omega t_{2n+1}) \\ \sin(2\omega t_1) & \sin(2\omega t_2) & \sin(2\omega t_3) & \dots & \sin(2\omega t_{2n+1}) \\ \sin(3\omega t_1) & \sin(3\omega t_2) & \sin(3\omega t_3) & \dots & \sin(3\omega t_{2n+1}) \\ \vdots & \vdots & \vdots & & \vdots \\ \sin(n\omega t_1) & \sin(n\omega t_2) & \sin(n\omega t_3) & \dots & \sin(n\omega t_{2n+1}) \\ \frac{1}{2} & \frac{1}{2} & \frac{1}{2} & \dots & \frac{1}{2} \\ \cos(\omega t_1) & \cos(\omega t_2) & \cos(\omega t_3) & \dots & \cos(\omega t_{2n+1}) \\ \cos(2\omega t_1) & \cos(2\omega t_2) & \cos(2\omega t_3) & \dots & \cos(2\omega t_{2n+1}) \\ \cos(3\omega t_1) & \cos(3\omega t_2) & \cos(3\omega t_3) & \dots & \cos(3\omega t_{2n+1}) \\ \vdots & \vdots & \vdots & & \vdots \\ \cos(n\omega t_1) & \cos(n\omega t_2) & \cos(n\omega t_3) & \dots & \cos(n\omega t_{2n+1}) \end{bmatrix}, \tag{23}$$

and matrix $\mathbf{E}^{-1}$ can analytically be expressed as:

$$\mathbf{E}^{-1} = \begin{bmatrix} \sin(\omega t_1) & \sin(2\omega t_1) & \dots & \sin(n\omega t_1) & 1 & \cos(\omega t_1) & \cos(2\omega t_1) & \dots & \cos(n\omega t_1) \\ \sin(\omega t_2) & \sin(2\omega t_2) & \dots & \sin(n\omega t_2) & 1 & \cos(\omega t_2) & \cos(2\omega t_2) & \dots & \cos(n\omega t_2) \\ \sin(\omega t_3) & \sin(2\omega t_3) & \dots & \sin(n\omega t_3) & 1 & \cos(\omega t_3) & \cos(2\omega t_3) & \dots & \cos(n\omega t_3) \\ & & & & \vdots & & & & \\ & & & & \vdots & & & & \\ \sin(\omega t_{2n+1}) & \sin(2\omega t_{2n+1}) & \dots & \sin(n\omega t_{2n+1}) & 1 & \cos(\omega t_{2n+1}) & \cos(2\omega t_{2n+1}) & \dots & \cos(n\omega t_{2n+1}) \end{bmatrix}. \tag{24}$$

Therefore, by using the matrix $\mathbf{E}$ and its inverse $\mathbf{E}^{-1}$ we can keep the equation in the frequency domain, but use variables in the time domain. Inserting Eq. (17) into Eq. (15) yields:

$$\omega \mathbf{A}\mathbf{E}\hat{\boldsymbol{Q}} + \mathbf{E}\hat{\boldsymbol{\mathcal{R}}} = 0. \tag{25}$$

While the linear equations could be solved in this form, evaluating sources and fluxes in the frequency domain is computationally expensive and inconvenient [1]. Therefore, we shall proceed to transform the equation back to time domain. Multiplying Eq. (25) by the transformation matrix $\mathbf{E}^{-1}$ from the left, the final form of the harmonic balance for transport

equation in time domain is obtained:

$$\omega \mathbf{E}^{-1}\mathbf{A}\mathbf{E}\hat{\boldsymbol{Q}} + \hat{\boldsymbol{\mathcal{R}}} = 0. \tag{26}$$

This is possible because $\mathbf{E}^{-1}$ is a two-sided inverse of $\mathbf{E}$, i.e.:

$$\mathbf{E}\mathbf{E}^{-1} = \mathbf{E}^{-1}\mathbf{E} = \mathbf{I}. \tag{27}$$

In Eq. (26), time-domain matrices $\hat{\boldsymbol{Q}}$ and $\hat{\boldsymbol{\mathcal{R}}}$ contain variables in $2n+1$ time steps:

$$\hat{\boldsymbol{Q}} = \begin{bmatrix} \mathrm{Q}_{t_1} \\ \mathrm{Q}_{t_2} \\ \mathrm{Q}_{t_3} \\ \vdots \\ \mathrm{Q}_{t_{2n+1}} \end{bmatrix}, \quad \hat{\boldsymbol{\mathcal{R}}} = \begin{bmatrix} \mathrm{R}_{t_1} \\ \mathrm{R}_{t_2} \\ \mathrm{R}_{t_3} \\ \vdots \\ \mathrm{R}_{t_{2n+1}} \end{bmatrix}, \tag{28}$$

where t_n stands for:

$$t_1 = \frac{T}{2n+1}, \quad t_2 = \frac{2T}{2n+1}, \quad \ldots, \quad t_n = \frac{nT}{2n+1} \quad \ldots, \quad t_{2n+1} = T. \tag{29}$$

t_n may be expressed in terms of t_1. Because of equally spaced time steps, the following substitution can be applied:

$$t_2 = 2t_1, \quad t_3 = 3t_1, \quad \ldots, \quad t_n = nt_1. \tag{30}$$

Eq. (26) represents a coupled set of $2n+1$ steady-state problems. Comparing Eq. (25) with the original scalar transport equation, Eq. (1), two important features may be observed:

- $\mathcal{R}$ has been replaced with its discrete counterpart $\hat{\boldsymbol{\mathcal{R}}}$, indicating that the solution is sought at fixed number of discrete time instants only. The number of discrete time instants is defined with specified number of harmonics n, as indicated in Eq. (28).
- Time derivative term has been replaced by terms coupling the solutions at different time steps. This is equivalent to evaluating the time derivative of a harmonic signal via $2n+1$ uniformly spaced coupled temporal snapshots, including a mean (steady) solution.

Solving the Eq. (26) in terms of computational cost means solving a coupled set of $2n+1$ steady-state equations. With increase in number of harmonics, the computational time grows for two reasons. The first reason is increase in number of equations to be solved, while the second reason concerns the coupling of a increasingly larger set of equations. In contrast to harmonic balance, transient simulation calculates $2n+1$ times less equations, but calculates the solution in many time instants, which depend on the velocity field. Higher velocities will usually require smaller time steps, thus increasing the calculation time. When simulating periodic phenomena, transient simulations are usually run for at least several periods in order to achieve meaningful, periodically averaged results. This comparison will be discussed more thoroughly in sections 4 and 5 concerning validation.

Using trigonometric sum identity $\sin(\alpha+\beta) = \sin\alpha\cos\beta+\cos\alpha\sin\beta$ to simplify the expression, only the sine functions remain. Finally, Eq. (26) can be written in expanded form for each time instant:

$$\mathrm{Q}_{t_1}: \quad \nabla\bullet(\mathbf{u}\mathrm{Q}_{t_1})-\nabla\bullet(\gamma\nabla\mathrm{Q}_{t_1}) = -\frac{2\omega}{2n+1}\left(\mathrm{Q}_{t_2}\sum_{k=1}^{n}k\sin(k\omega t_1)+ \right. \tag{31}$$
$$\left. +\mathrm{Q}_{t_3}\sum_{k=1}^{n}k\sin(k\omega 2t_1)+ \quad \ldots \quad +\mathrm{Q}_{t_{2n+1}}\sum_{k=1}^{n}k\sin(k\omega 2nt_1)\right),$$

$$\mathrm{Q}_{t_2}: \quad \nabla\bullet(\mathbf{u}\mathrm{Q}_{t_2})-\nabla\bullet(\gamma\nabla\mathrm{Q}_{t_2}) = -\frac{2\omega}{2n+1}\left(\mathrm{Q}_{t_1}\sum_{k=1}^{n}k\sin(-k\omega t_1)\right. \tag{32}$$
$$\left. +\mathrm{Q}_{t_3}\sum_{k=1}^{n}k\sin(k\omega t_1) \quad \ldots \quad +\mathrm{Q}_{t_{2n+1}}\sum_{k=1}^{n}k\sin(k\omega(2n-1)t_1)\right),$$

$$\begin{array}{ll} \mathrm{Q}_{t_3}: & \ldots \\ \vdots & \vdots \\ \mathrm{Q}_{t_n}: & \ldots \end{array}$$

In order to further simplify the obtained expressions, additional substitution is defined.

Because the summation terms in the brackets repeat, coefficients $\mathrm{P}_1 - \mathrm{P}_i$ are introduced:

$$\begin{aligned}
\mathrm{P}_1 &= \sum_{k=1}^{n} k\sin(k\omega t_1);\\
\mathrm{P}_2 &= \sum_{k=1}^{n} k\sin(k\omega 2t_1);\\
\mathrm{P}_3 &= \sum_{k=1}^{n} k\sin(k\omega 3t_1);\\
&\vdots\\
\mathrm{P}_i &= \sum_{k=1}^{n} k\sin(k\omega i t_1), \qquad\qquad \text{for} \quad i=\{1,2n\}.
\end{aligned} \tag{33}$$

The summation terms come from the $\mathbf{E}^{-1}\mathbf{AE}$ matrix multiplication in Eq. (26):

$$\mathbf{E}^{-1}\mathbf{AE} = \frac{2}{2n+1}\begin{bmatrix}
0 & P_1 & P_2 & P_3 & \dots & \dots & P_{2n}\\
-P_1 & 0 & P_1 & P_2 & P_3 & & \vdots\\
-P_2 & -P_1 & 0 & P_1 & P_2 & & \vdots\\
-P_3 & -P_2 & -P_1 & 0 & P_1 & & \vdots\\
\vdots & & & & \ddots & & P_2\\
\vdots & & & & & \ddots & P_1\\
-P_{2n} & \dots & \dots & -P_3 & -P_2 & -P_1 & 0
\end{bmatrix}. \tag{34}$$

Final form of the harmonic balance equations for scalar transport reads:

$$\mathrm{Q}_{t_1}: \qquad \nabla\bullet(\mathbf{u}\mathrm{Q}_{t_1}) - \nabla\bullet(\gamma\nabla\mathrm{Q}_{t_1}) = -\frac{2\omega}{2n+1}\left(\mathrm{Q}_{t_2}\mathrm{P}_1 + \mathrm{Q}_{t_3}\mathrm{P}_2 + \ldots + \mathrm{Q}_{t_{2n+1}}\mathrm{P}_{2n}\right), \tag{35}$$

$$\mathrm{Q}_{t_2}: \qquad \nabla\bullet(\mathbf{u}\mathrm{Q}_{t_2}) - \nabla\bullet(\gamma\nabla\mathrm{Q}_{t_2}) = -\frac{2\omega}{2n+1}\left(-\mathrm{Q}_{t_1}\mathrm{P}_1 + \mathrm{Q}_{t_3}\mathrm{P}_1 + \ldots + \mathrm{Q}_{t_{2n+1}}\mathrm{P}_{2n-1}\right), \tag{36}$$

$$\vdots$$

or written in general form:

$$\nabla\bullet(\mathbf{u}\mathrm{Q}_{t_\mathrm{j}}) - \nabla\bullet(\gamma\nabla\mathrm{Q}_{t_\mathrm{j}}) = -\frac{2\omega}{2n+1}\left(\sum_{i=1}^{2n}\mathrm{P}_{(\mathrm{i-j})}\mathrm{Q}_{t_i}\right), \quad \text{where} \quad P_{-i} = -P_i. \tag{37}$$

Figure 2 shows the difference between temporal resolution obtained using different number of harmonics. Symbol + presents the time instant in which the solution is calculated. For 1 harmonic, 3 equally spaced time instants are calculated, as shown in Figure 2a. Increasing the number of harmonics to $n = 3$, 7 time instants are calculated offering finer temporal resolution. By further increasing the number of harmonics to 6, Figure 2c, more detailed temporal resolution is obtained.

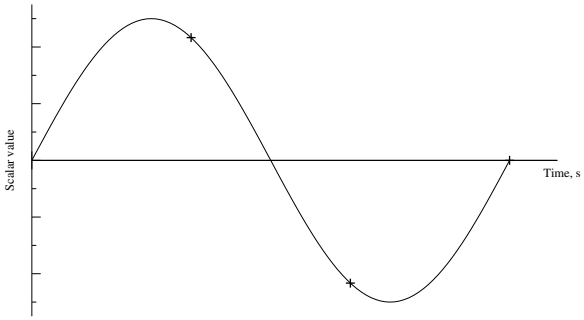

(a) 1 harmonic temporal resolution,

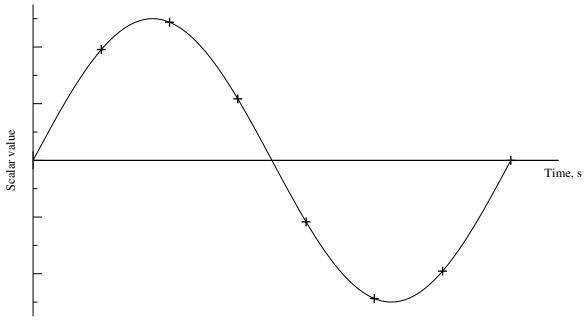

(b) 3 harmonics temporal resolution,

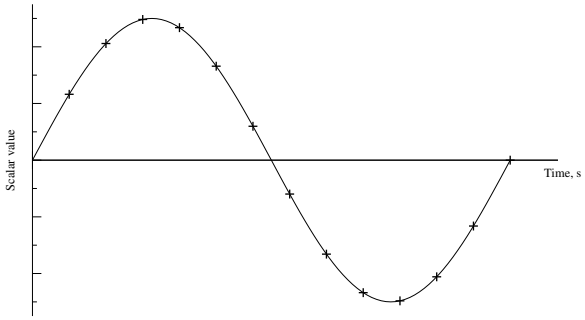

(c) 6 harmonics temporal resolution,

Figure 2: Temporal resolution of a single harmonic signal with 1, 3 and 6 harmonics.

Since the time variation is presented in frequency domain, temporal accuracy is formally spectral. However, the notion of temporal discretisation error is now converted into the fidelity of variation of the temporal signal with a given number of harmonics, as shown in Figure 1. It should be noted that solution in any time step can be obtained in post processing step. Using calculated solution, Fourier coefficients and mean value in matrices **Q** and **R**, Eq. (15), can be evaluated. Fourier coefficients and mean value allow obtaining the solution in any time, as presented in Eq. (19).

3.3.1 Finite Volume Implementation

Following notation by Rusche [14], we use $[\cdot]$ to denote implicit FV discretisation. Details on FV discretisation may be found in Jasak [15] and will not be presented here. Since the convection, diffusion and source terms remain unchanged, the discretised form of the harmonic

balance scalar transport equation, Eq. (37), reads:

$$\left[\nabla\bullet(\mathbf{u}\mathrm{Q}_{t_j})\right]-\left[\nabla\bullet\left(\gamma\nabla\mathrm{Q}_{t_j}\right)\right]=-\frac{2\omega}{2n+1}\left(\sum_{i=1}^{2n}P_{i-j}\mathrm{Q}_{t_i}\right),\ \text{for } j=1\ldots2n+1\,, \tag{38}$$

where the source terms in Eq. (24), arising from the harmonic balance treatment of the time derivative term are treated explicitly. Hence, a segregated, iterative solution algorithm for successive Q_{t_j} is employed. Following analogy with the Gauss–Seidel iterative solution algorithm [16], each Q_{t_j} is solved once per outer iteration during a forward sweep ($j=1\ldots2n+1$). Latest available Q_{t_j} is always used in source terms for other equations ($k>j$), preventing additional memory requirements. Outer iterations are continued until convergence.

3.4 Harmonic Balance for the Navier-Stokes Equations

In previous section, derivation of the Harmonic Balance Method for scalar transport equation was presented. In order to solve the fluid flow equations, the Harmonic Balance Method will be applied to the Navier–Stokes system. Before harmonic balance treatment, discretisation of the Navier-Stokes equations will be presented. The derivation of the pressure equation will be presented as well, in order to examine the coupling between pressure and velocity in the Harmonic Balance Method.

3.4.1 Discretisation of the Navier-Stokes Equations

Compared to scalar transport equation, Navier–Stokes equations have two distinctive features. The first is the non–linearity of convection term in the momentum equation. The second concerns pressure-velocity coupling [15].

Convection term $\nabla\bullet(\mathbf{uu})$ models transport of the velocity field by itself. Therefore, this expression is quadratic in velocity and should be linearised by using the existing velocity field in flux calculation and performing Picard iterations to convergence. The discretised form of the convection term is:

$$\begin{aligned}\nabla\bullet(\mathbf{uu})&=\sum_f S.(\mathbf{u}^o)_f(\mathbf{u})_f\\&=\sum_f F(\mathbf{u})_f\\&=a_P\mathbf{u}_P+\sum_N a_N\mathbf{u}_N,\end{aligned} \tag{39}$$

where a_P and a_N contain the appropriate contributions from flux F and convection interpolation factors. Flux F is evaluated using available $\mathbf{u}^o$, thus linearising the expression:

$$F = \mathbf{S}_f \cdot \mathbf{u}_f^o. \tag{40}$$

3.4.2 Derivation of the Pressure Equation

The derivation of the pressure equation starts from a semi-discretised form of the momentum equation valid for each control volume, as shown in [15]:

$$\frac{\mathbf{u}^o}{\delta t} + a_P \mathbf{u}_P + \sum_N a_N \mathbf{u}_N = -\nabla p \tag{41}$$

Eq. (41) is obtained from the integral form of the momentum equation, Eq. (3). Index P presents the finite volume cell, while index N presents the neighbouring cells. a_P is the diagonal coefficient which multiplies the cell velocity. We shall introduce the $\mathbf{H}(\mathbf{u})$ operator to simplify the expression:

$$\mathbf{H}(\mathbf{u}) = -\sum_N a_N \mathbf{u}_N + \frac{\mathbf{u}^o}{\Delta t}, \tag{42}$$

Hence, Eq. (41) becomes:

$$a_P \mathbf{u}_P = \mathbf{H}(\mathbf{u}) - \nabla p. \tag{43}$$

The $\mathbf{H}(\mathbf{u})$ consists of two parts, the transport part and the source part. The transport part presents all the neighbouring coefficients multiplied by neighbouring velocities, while the source part includes the transient term and all other source terms apart from the pressure gradient. The pressure gradient is not discretised at this stage.

We proceed to express $\mathbf{u}$ from Eq. (43) as:

$$\mathbf{u}_P = \frac{\mathbf{H}(\mathbf{u})}{a_P} - \frac{1}{a_P} \nabla p, \tag{44}$$

and use it for the face interpolate:

$$\mathbf{u}_f = \left(\frac{\mathbf{H}(\mathbf{u})}{a_P} \right)_f - \left(\frac{1}{a_P} \right)_f (\nabla p)_f, \tag{45}$$

which will be needed for calculation of face fluxes.

The discretised form of the continuity equation reads:

$$\nabla \bullet \mathbf{u} = \sum_f \mathrm{S}.\mathbf{u}_f = 0. \tag{46}$$

Inserting Eq. (45) into the discretised incompressible continuity equation Eq. (46), we obtain the pressure equation for incompressible fluid:

$$\nabla \bullet \left(\frac{1}{a_P} \nabla p \right) = \nabla \bullet \left(\frac{\mathbf{H}(\mathbf{u})}{a_P} \right) = \sum_f \mathrm{S}. \left(\frac{\mathbf{H}(\mathbf{u})}{a_P} \right)_f . \tag{47}$$

After the solution of the pressure equation, the conservative face flux F is calculated using Eq. (45):

$$F = \mathrm{S}.\mathbf{u}_f = \left(\frac{\mathbf{H}(\mathbf{u})}{a_P} \right)_f - \left(\frac{1}{a_P} \right)_f (\nabla p)_f . \tag{48}$$

3.4.3 Harmonic Balance for the Navier–Stokes System

The conventional derivation of the pressure equation was presented in the previous section. In order to describe the flow field, both velocity and pressure fields have to be calculated. The derivation of the Harmonic Balance Method for the Navier–Stokes equations will be presented in this section. Because of the similarity with the harmonic balance for a scalar transport equation, this section will often refer to section 3.3.

The momentum equation for the velocity expressed as a Fourier expansion, in condensed form reads:

$$\frac{\partial \boldsymbol{\mathcal{U}}}{\partial t} + \boldsymbol{\mathcal{R}} = 0, \tag{49}$$

where $\boldsymbol{\mathcal{R}}$ stands for the convection and diffusion transport and source/sink terms of the transport equation:

$$\boldsymbol{\mathcal{R}} = \nabla \bullet (\boldsymbol{\mathcal{U}}^o \boldsymbol{\mathcal{U}}) - \nabla \bullet (\gamma \nabla \boldsymbol{\mathcal{U}}) + \nabla p. \tag{50}$$

Fourier expansion of the velocity field that will be used reads:

$$\begin{aligned} \boldsymbol{\mathcal{U}}(t) = \mathbf{u}_0 + \mathbf{u}_{\mathrm{S}_1} \sin(\omega t) + \mathbf{u}_{\mathrm{C}_1} \cos(\omega t) + \mathbf{u}_{\mathrm{S}_2} \sin(2\omega t) + \mathbf{u}_{\mathrm{C}_2} \cos(2\omega t) + \ldots + \\ \mathbf{u}_{\mathrm{S}_n} \sin(n\omega t) + \mathbf{u}_{\mathrm{C}_n} \cos(n\omega t). \end{aligned} \tag{51}$$

The expression for the expansion of $\boldsymbol{\mathcal{R}}$ is equivalent as for scalar transport, equation Eq. (12). After inserting Fourier expansions of velocity field and residual field into the momentum

equation, Eq. (49), we get the following expression:

$$\omega \mathbf{A}\mathbf{u} + \mathbf{R} = 0, \tag{52}$$

where matrices $\mathbf{u}$ and $\mathbf{R}$ read:

$$\mathbf{u} = \begin{bmatrix} \mathbf{u}_{S_1} \\ \mathbf{u}_{S_2} \\ \mathbf{u}_{S_3} \\ \vdots \\ \mathbf{u}_{S_n} \\ \mathbf{u}_0 \\ \mathbf{u}_{C_1} \\ \mathbf{u}_{C_2} \\ \mathbf{u}_{C_3} \\ \vdots \\ \mathbf{u}_{C_n} \end{bmatrix}, \qquad \mathbf{R} = \begin{bmatrix} \mathbf{R}_{S_1} \\ \mathbf{R}_{S_2} \\ \mathbf{R}_{S_3} \\ \vdots \\ \mathbf{R}_{Sn} \\ \mathbf{R}_0 \\ \mathbf{R}_{C_1} \\ \mathbf{R}_{C_2} \\ \mathbf{R}_{C_3} \\ \vdots \\ \mathbf{R}_{C_n} \end{bmatrix}. \tag{53}$$

Matrices $\mathbf{A}$, $\mathbf{E}$ and $\mathbf{E}^{-1}$ remain the same (see Eq. (16), (23) and (24)), hence the final expression of the momentum equation in time domain for Harmonic Balance Method reads:

$$\omega \mathbf{E}^{-1}\mathbf{A}\mathbf{E}\hat{\boldsymbol{\mathcal{U}}} + \hat{\boldsymbol{\mathcal{R}}} = 0, \tag{54}$$

where time-domain matrices $\boldsymbol{\mathcal{U}}$ and $\boldsymbol{\mathcal{R}}$ contain variables $\mathbf{u}$ in $2n+1$ time steps:

$$\hat{\boldsymbol{\mathcal{U}}} = \begin{bmatrix} \mathbf{u}_{t_1} \\ \mathbf{u}_{t_2} \\ \mathbf{u}_{t_3} \\ \vdots \\ \mathbf{u}_{t_{2n+1}} \end{bmatrix}, \quad \hat{\boldsymbol{\mathcal{R}}} = \begin{bmatrix} \mathbf{R}_{t_1} \\ \mathbf{R}_{t_2} \\ \mathbf{R}_{t_3} \\ \vdots \\ \mathbf{R}_{t_{2n+1}} \end{bmatrix}. \tag{55}$$

Following the procedure in section 3.3, coefficients P_i will be used as a substitute for the summation terms, as they are the same as in expression Eq. (33). The harmonic balance form of the momentum equation reads:

$$\nabla\bullet(\mathbf{u}_{t_j}\mathbf{u}_{t_j}) - \nabla\bullet(\gamma\nabla\mathbf{u}_{t_j}) = -\frac{2\omega}{2n+1}\left(\sum_{i=1}^{2n}\mathrm{P}_{(i-j)}\mathbf{u}_{t_i}\right). \tag{56}$$

Observing the Harmonic Balance Method for the Navier–Stokes equations, one can deduce that the Harmonic Balance Method transforms the time derivative in the transport equation into source terms: leaving convection, diffusion and additional source terms unchanged. Hence, it can be shown that the continuity equation remains the same, with $\mathbf{u}$ replaced with its discrete counterpart $\mathbf{u}_{t_j}$:

$$\nabla\bullet\mathbf{u}_{t_j} = 0. \tag{57}$$

Eq. (57) states that at each discrete time instant t_j, the incompressible continuity equation must hold.

3.4.4 The Finite Volume Implementation of Harmonic Balance for the Navier–Stokes System

As previously introduced in section 3.3.1 and using notation by Rusche [14], we use $[\cdot]$ to denote implicit FV discretisation. Discretised harmonic balance pressure–velocity system reads:

$$\left[\nabla\bullet(\mathbf{u}_{t_j}\mathbf{u}_{t_j})\right] - \left[\nabla\bullet\left(\nu\nabla\mathbf{u}_{t_j}\right)\right] = -\nabla p_{t_j} - \frac{2\omega}{2n+1}\left(\sum_{i=1}^{2n}P_{i-j}\mathbf{u}_{t_i}\right), \text{ for } j = 1\ldots 2n+1\,, \tag{58}$$

$$\left[\nabla\bullet\left(\frac{1}{a_{P t_j}}\nabla p\right)\right] = \nabla\bullet\left(\frac{\mathbf{H}(\mathbf{u}_{t_j})}{a_{P t_j}}\right), \text{ for } j = 1\ldots 2n+1\,, \tag{59}$$

where $a_{P t_j}$ is the diagonal coefficient of the momentum equation at time instant t_j, and $\mathbf{H}(\mathbf{u}_{t_j})$ is the flux operator as defined in [15]. Harmonic balance pressure equation, Eq. (59) is obtained from the harmonic balance continuity equation, using standard procedure for segregated solution algorithms. As discussed, harmonic balance variant of a transient transport equation yields $2n+1$ coupled steady-state problems. Hence, the SIMPLE [17] algorithm is employed to resolve the pressure–velocity coupling separately at each time instant t_j. In addition to pressure–velocity coupling at each time step, velocity fields at

different time instants are coupled due to harmonic balance source terms on the right hand side of Eq. (58). Each $\mathbf{u}_{t_j}$ and t_j are solved once per outer iteration and demand its own SIMPLE loop. However, only one SIMPLE iteration is sufficient for each t_j in order to simultaneously resolve $\mathbf{u}_{t_j} - p_{t_j}$ and $\mathbf{u}_{t_j} - \mathbf{u}_{t_k}$ coupling.

In contrast to the momentum equation, the pressure equations at different time instants are not coupled. The coupling in momentum equation is involved in source term which comes from the Fourier decomposition of the temporal derivative, equations Eq. (49)-Eq. (52). Temporal derivative is not present in the pressure equation.

Implementation of a fully coupled algorithm [18] will be the topic for future work, [19].

3.5 Example: Equation Set for 1 Harmonic

With the complete general derivation of the Harmonic Balance Method both for the scalar equation and for Navier–Stokes equations, an example for one harmonic will be given here. This example will give insight into the coupled set of equations that arises from the harmonic balance treatment.

For one harmonic, Eq. (34) reduces to:

$$\mathbf{E}^{-1}\mathbf{A}\mathbf{E} = \frac{2}{2n+1} \cdot \begin{bmatrix} 0 & P_1 & P_2 \\ -P_1 & 0 & P_1 \\ -P_2 & -P_1 & 0 \end{bmatrix} \tag{60}$$

In matrix form, Eq. (26) for passive scalar and Eq. (54) for momentum read:

$$\omega\mathbf{E}^{-1}\mathbf{A}\mathbf{E}\hat{\boldsymbol{\mathcal{Q}}} + \hat{\boldsymbol{\mathcal{R}}} = \frac{2\omega}{3} \begin{bmatrix} 0 & P_1 & P_2 \\ -P_1 & 0 & P_1 \\ -P_2 & -P_1 & 0 \end{bmatrix} \begin{bmatrix} \mathrm{Q}_{t_1} \\ \mathrm{Q}_{t_2} \\ \mathrm{Q}_{t_3} \end{bmatrix} + \begin{bmatrix} \mathrm{R}_{t_1} \\ \mathrm{R}_{t_2} \\ \mathrm{R}_{t_3} \end{bmatrix}, \tag{61}$$

$$\omega\mathbf{E}^{-1}\mathbf{A}\mathbf{E}\hat{\boldsymbol{\mathcal{U}}} + \hat{\boldsymbol{\mathcal{R}}} = \frac{2\omega}{3} \begin{bmatrix} 0 & P_1 & P_2 \\ -P_1 & 0 & P_1 \\ -P_2 & -P_1 & 0 \end{bmatrix} \begin{bmatrix} \mathbf{u}_{t_1} \\ \mathbf{u}_{t_2} \\ \mathbf{u}_{t_3} \end{bmatrix} + \begin{bmatrix} \mathbf{R}_{t_1} \\ \mathbf{R}_{t_2} \\ \mathbf{R}_{t_3} \end{bmatrix}. \tag{62}$$

Expanding Eq. (61) yields 3 scalar transport equations:

$$\begin{aligned}
\mathrm{Q}_{t_1}: \quad & \nabla\bullet(\mathbf{u}\mathrm{Q}_{t_1}) - \nabla\bullet(\gamma\nabla\mathrm{Q}_{t_1}) = -\frac{2\omega}{3}\left(\mathrm{Q}_{t_2}\mathrm{P}_1 + \mathrm{Q}_{t_3}\mathrm{P}_2\right), \\
\mathrm{Q}_{t_2}: \quad & \nabla\bullet(\mathbf{u}\mathrm{Q}_{t_2}) - \nabla\bullet(\gamma\nabla\mathrm{Q}_{t_2}) = -\frac{2\omega}{3}\left(\mathrm{Q}_{t_1}(-\mathrm{P}_1) + \mathrm{Q}_{t_3}\mathrm{P}_1\right), \\
\mathrm{Q}_{t_3}: \quad & \nabla\bullet(\mathbf{u}\mathrm{Q}_{t_3}) - \nabla\bullet(\gamma\nabla\mathrm{Q}_{t_3}) = -\frac{2\omega}{3}\left(\mathrm{Q}_{t_1}(-\mathrm{P}_2) + \mathrm{Q}_{t_2}(-\mathrm{P}_1)\right),
\end{aligned} \tag{63}$$

Scalar field Q at time instant t_1 depends on scalar fields from time steps t_2 and t_3: Q_{t_2} and Q_{t_3}. For calculation of the scalar field Q in time instant t_2, scalar fields from all the other time steps are needed. The same goes for the scalar field Q in time step t_3. Therefore, 3 resulting equations are coupled. Evaluating the coefficients P_1 and P_2 from equation Eq. (33), yields:

$$\begin{aligned}
P_1 &= 0.866025, \\
P_2 &= -0.866025.
\end{aligned} \tag{64}$$

In the case of one harmonic, P_1 and P_2 are the same in value, but opposite in sign. For calculation of Q_{t_1}, the coefficient P_2 multiplies the variable Q_{t_3} which is calculated at time instant $t_3 = \frac{3T}{2n+1} = \frac{3T}{3} = T$. Because of the assumed periodicity, t_3 represents both the end of the period as well as the beginning of the period. For number of harmonics $n > 1$, it can be shown that variables that appear closer in time to the variable currently calculated are multiplied with larger coefficients than those farther in time. For $n = 3$, coefficients P_i are:

$$\begin{aligned}
P_1 &= 4.03334, \\
P_2 &= -2.23833, \\
P_3 &= 1.795, \\
P_4 &= -1.795, \\
P_5 &= 2.23833, \\
P_6 &= -4.03334.
\end{aligned} \tag{65}$$

To summarise, the value of coefficient P depends on the relative location in time between the variable it multiplies and the variable currently calculated. In the case of one harmonic, time distance between all of the variables is the same and equals $t/3$, which explains why $|P_1| = |P_2|$. Relation between coefficients is shown in Figures 3 and 4.

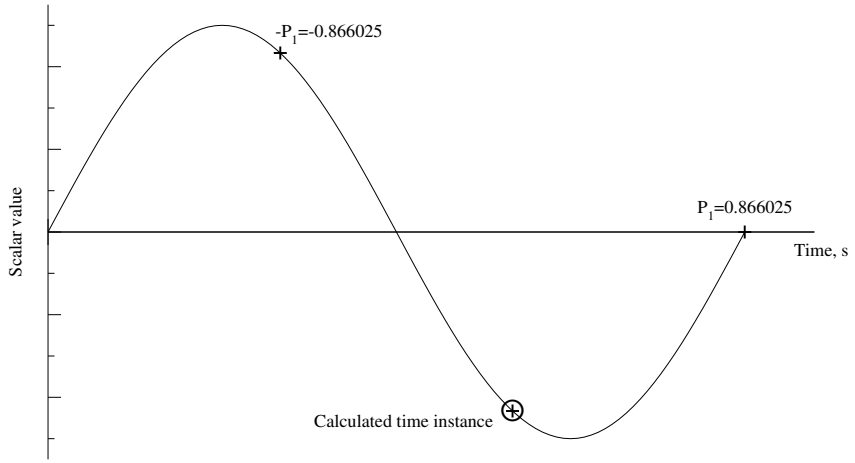

Figure 3: Coefficients related to calculation of solution in second time step for one harmonic.

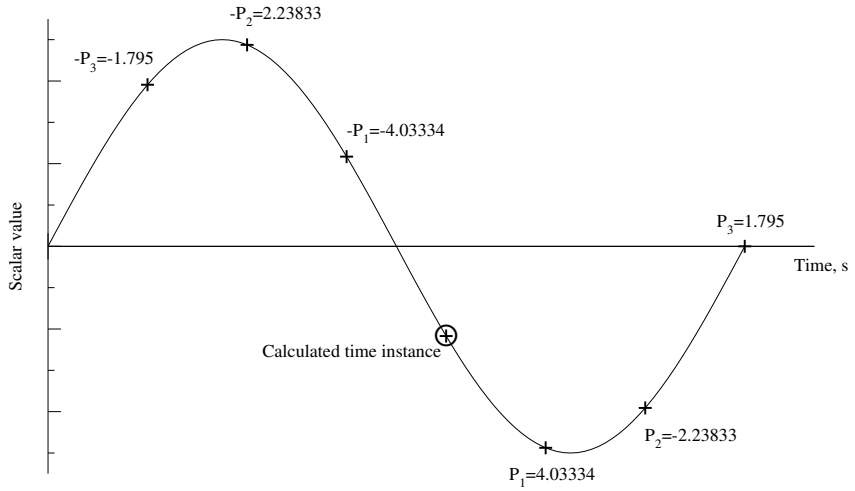

Figure 4: Coefficients related to calculation of solution in fourth time step for 3 harmonics.

The same is applicable for the momentum equation. The equations for 1 harmonic read:

$$\begin{aligned}
\mathbf{u}_{t_1}: \quad & \nabla_{\bullet}(\mathbf{u}_{t_1}\mathbf{u}_{t_1}) - \nabla_{\bullet}(\gamma\nabla\mathbf{u}_{t_1}) = -\frac{2\omega}{3}\left(\mathbf{u}_{t_2}\mathrm{P}_1 + \mathbf{u}_{t_3}\mathrm{P}_2\right), \\
\mathbf{u}_{t_2}: \quad & \nabla_{\bullet}(\mathbf{u}_{t_2}\mathbf{u}_{t_2}) - \nabla_{\bullet}(\gamma\nabla\mathbf{u}_{t_2}) = -\frac{2\omega}{3}\left(\mathbf{u}_{t_1}(-\mathrm{P}_1) + \mathbf{u}_{t_3}\mathrm{P}_1\right), \\
\mathbf{u}_{t_3}: \quad & \nabla_{\bullet}(\mathbf{u}_{t_3}\mathbf{u}_{t_3}) - \nabla_{\bullet}(\gamma\nabla\mathbf{u}_{t_3}) = -\frac{2\omega}{3}\left(\mathbf{u}_{t_1}(-\mathrm{P}_2) + \mathbf{u}_{t_2}(-\mathrm{P}_1)\right),
\end{aligned} \tag{66}$$

Pressure equations remain unchanged:

$$\begin{aligned} p_1: \quad & \nabla\bullet\left(\frac{1}{a_P}\nabla p_1\right) = \nabla\bullet\left(\frac{\mathbf{H}(\mathbf{u}_{t_1})}{a_P}\right), \\ p_2: \quad & \nabla\bullet\left(\frac{1}{a_P}\nabla p_2\right) = \nabla\bullet\left(\frac{\mathbf{H}(\mathbf{u}_{t_2})}{a_P}\right), \\ p_3: \quad & \nabla\bullet\left(\frac{1}{a_P}\nabla p_3\right) = \nabla\bullet\left(\frac{\mathbf{H}(\mathbf{u}_{t_2})}{a_P}\right). \end{aligned} \tag{67}$$

In case of specific problems, one harmonic might not be enough. If flow features that occur with frequency of order n want to be captured, then Fourier expansion at least of the order n should be used. This is achieved using more harmonics. If we assume for some flow field $n = 5$ harmonics should be used. At this point, the system of equations grows rapidly because $2n+1 = 11$ coupled equations are present. It slows down the simulation because more equations are to be calculated and the larger system of equations slows down the convergence. Even though higher number of harmonics slows down the simulation, the flow field is resolved more accurately and more time steps within a period are obtained.

3.6 Closure

The derivation of a general Harmonic Balance Method was presented in this section. As shown in the derivation of the Harmonic Balance Method for scalar transport and Navier–Stokes equations, equation set containing $2n+1$ coupled time instants is calculated. Calculating $2n+1$ velocity fields, $2n+1$ pressure fields, $2n+1$ scalar fields, etc. results in memory increase. While all scalar and velocity fields from all $2n+1$ time steps are coupled, pressure field is not coupled with other pressure fields because of its elliptic form. It is calculated subsequently the same way as it would be calculated if we weren't using Harmonic Balance Method. The main difference in pressure calculation is that in equations Eq. (47) and Eq. (48) the fluxes and the velocity field corresponding to the time step for which the pressure is calculated have to be used.

It should be noted that in the present derivation the non–linear term was not expanded using Fourier series. Two approaches are possible for this matter. The first approach is the one used in this work: linearisation of the non-linear term is assumed in advance, following the simple derivation of the Harmonic Balance Method. It can be shown that this approach is order-consistent. The second approach deals with Fourier expansion of both velocity fields in the convective term, yielding higher orders of frequency than the prescribed one, which is assumed inconsistent.

4 Scalar Transport Validation

Derivation of the Harmonic Balance Method was given in the previous section. In order to test validity of the proposed method, several test cases need to be considered. This section contains validation of the Harmonic Balance Method for scalar transport.

4.1 Introduction

Results obtained from present model will be compared with transient simulations. The Harmonic Balance Method for passive scalar transport will be validated on four test cases concerning forced periodic behaviour at the inlet. Two of the test cases will use harmonic waves, in the spirit of Fourier series expansion. The other two test cases will test both robustness and accuracy. The CPU time study is not performed for scalar transport validation cases, as these cases are not computationally demanding and the CPU time was too short to draw relevant conclusions. In section 5 CPU time comparison is given for validation cases considering Navier–Stokes equations.

4.2 Computational Domain

The domain for all of the test cases for scalar transport validation is a 2D rectangle, Figure 5. No walls or obstacles are present, leaving the domain open on all sides.

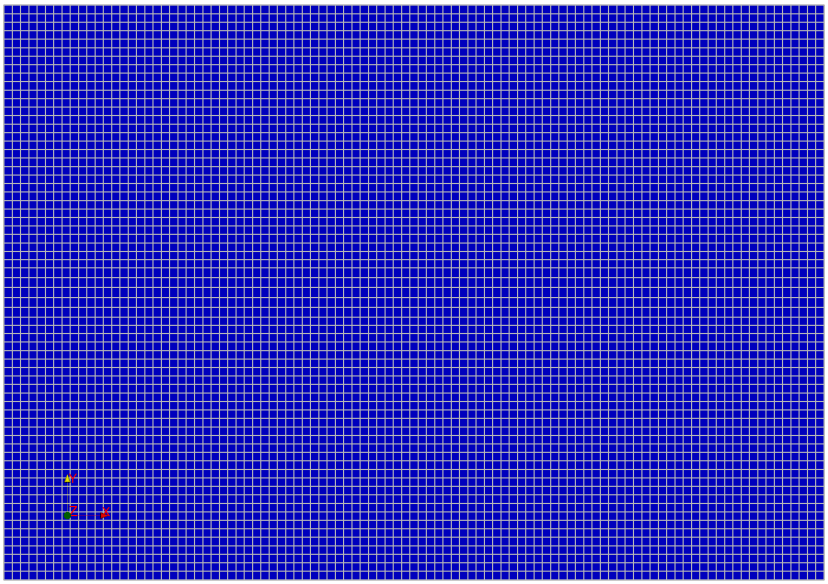

Figure 5: Domain used for scalar transport validation.

In order to obtain accurate results but also reduce the simulation time, the domain was meshed using 6633 hexahedral cells. The domain size is 10 m $\times$ 7 m.

4.3 Test Case 1 - Single Sine Wave

4.3.1 Boundary Conditions

In first test case a sine wave signal is imposed at the inlet:

$$T = A\sin(2\pi ft), \tag{68}$$

where A is the amplitude of the sine wave, f is the frequency, t is time and T is a scalar being transported. A is set to 5 and frequency of 2 Hz is used. With uniform velocity of 10 m/s in longitudinal direction and domain length 10 m, two complete waves will always be in the domain. Diffusion coefficient is set to $1.5\cdot 10^{-5}$ m^2/s.
For harmonic balance, boundary conditions need further comments. As it was described in section 3, by using harmonic balance we are not calculating the flow field continuously for the whole period. Instead, we are calculating the steady state flow field at $2n+1$ equally spaced time steps within a period, depending on the number of harmonics specified, n. Therefore, Eq. (68) is used for setting the boundary conditions on inlet: each time step will have different fixed value boundary condition for scalar T. Using n harmonics, we will have $2n+1$ boundary conditions and the scalar value on the inlet will be:

$$\text{For time step } j: \qquad T_j = A\sin(2\pi f t_j) \tag{69}$$

where:

$$t_j = \frac{P}{2n+1}\cdot j, \qquad j \in [1, 2n+1], \tag{70}$$

with P denoting the period.

Other boundary conditions for scalar T on all other boundaries are set to zero gradient. Velocity is uniform through the whole domain and it is not calculated, but only used for transporting the scalar T.

4.3.2 Results

Scalar field along the x axis is used for comparison at different time steps, Figure 6. Since a simple sine wave is imposed, only one harmonic is needed. Using one harmonic, $2n+1 = 3$ time steps are obtained and compared.

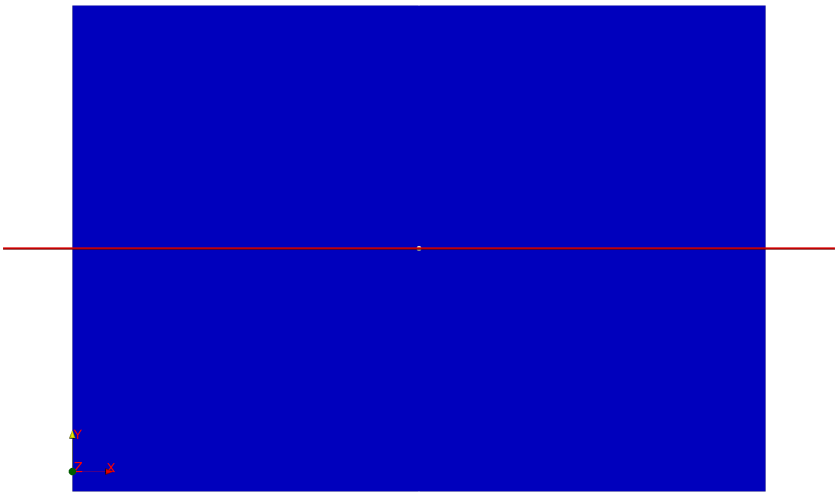

Figure 6: Line of data extraction for comparison.

The sine wave imposed at the inlet for scalar T is shown in Figure 7. Figure 8 shows the flow field in the domain at time $t = 1$ s.

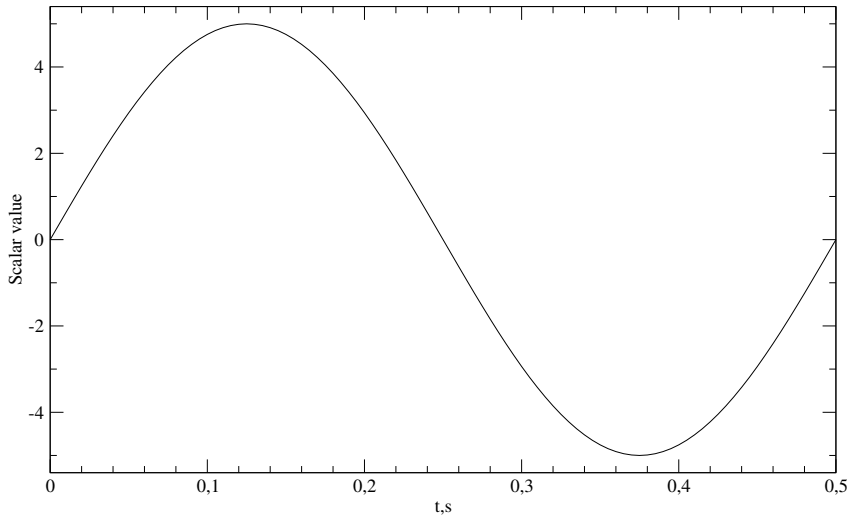

Figure 7: Sine wave imposed on inlet.

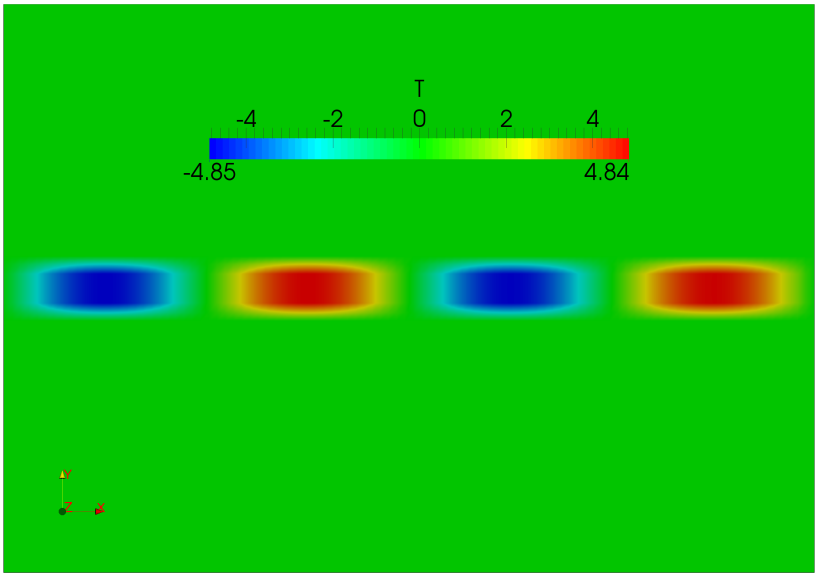

Figure 8: Scalar field at $t = 1$ s.

Figures 9, 10, 11 show the agreement between transient solver and Harmonic Balance Method for 1 harmonic. Figure 9 shows the agreement in the first third of the period. Figure 10 shows the agreement in the second third of the period and Figure 11 shows the agreement at the end of the period.

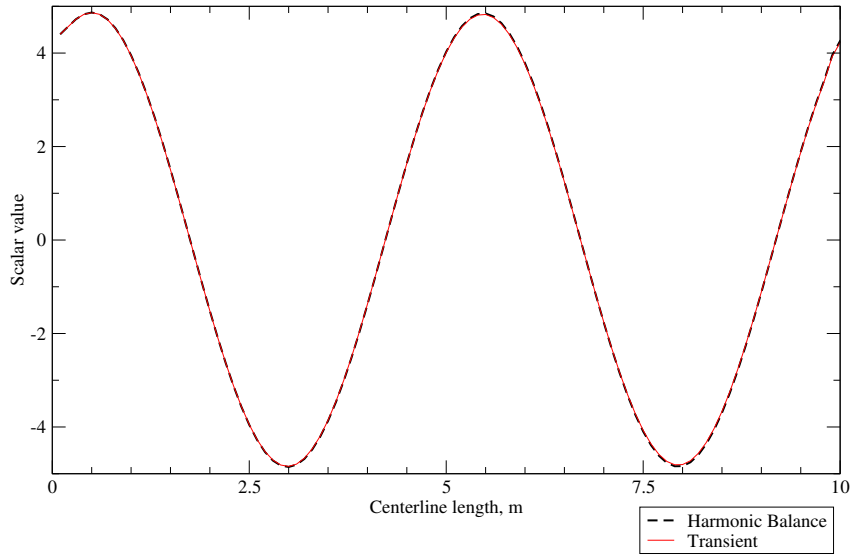

Figure 9: Transient solver and Harmonic Balance Method comparison at the first third of a period.

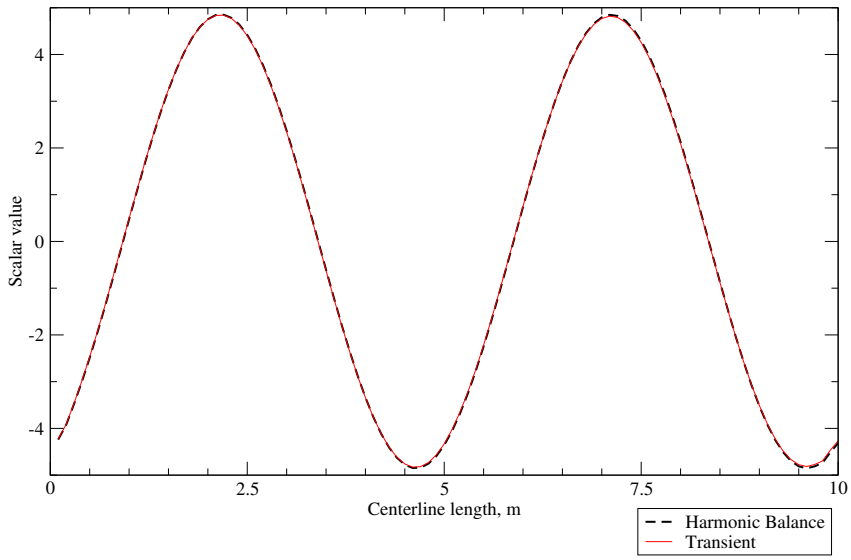

Figure 10: Transient solver and Harmonic Balance Method comparison at the second third of a period.

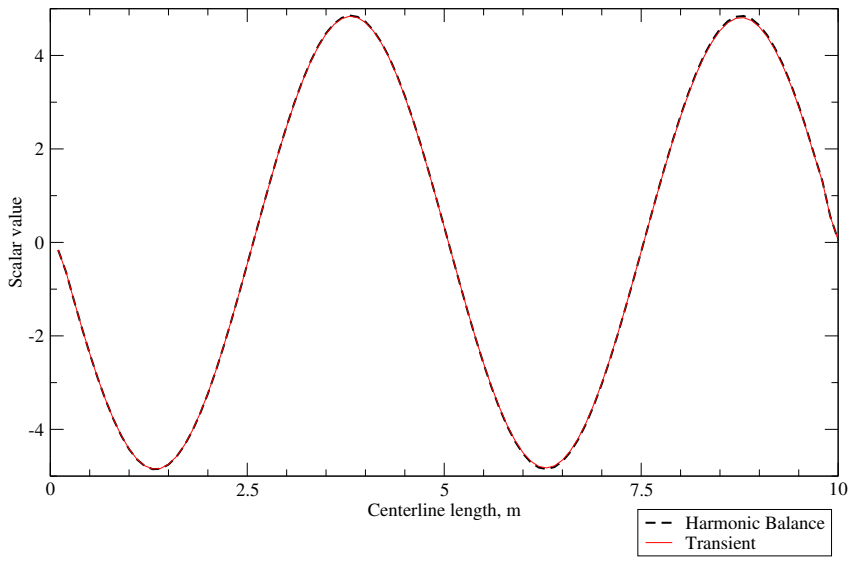

Figure 11: Transient solver and Harmonic Balance Method comparison at the end of a period.

Figures 9, 10, 11 show the expected result. One harmonic is sufficient to accurately describe a single harmonic sine wave. Using more than one harmonic in this case would not be useful as it would only prolong the simulation time without possible increase in accuracy.

4.4 Test Case 2 - Two Harmonic Waves

Test case 1 has shown the accuracy of Harmonic Balance Method with one harmonic on a sine wave excitation. Test case 2 will examine the accuracy of Harmonic Balance Method for 2 harmonic waves with second order behaviour.

4.4.1 Boundary Conditions

In this case, the wave imposed at the inlet is a linear combination of sine and cosine waves with different frequencies. To be fully compatible with Fourier series expansion, both waves frequencies should be a multiple of a base frequency:

$$T = A\sin(2\pi \cdot f_{\sin} \cdot (t-0.35)) + B\cos(2\pi \cdot f_{\cos} \cdot (t-0.35)). \tag{71}$$

A and B are coefficients representing amplitudes of sine (A) and cosine (B) waves. $f_{\sin}$ is the frequency used in sine wave while, $f_{\cos}$ is the frequency of a cosine wave. Coefficient 0.35 is used purely to position the period so that the wave at $t = 0$ has the value 0.
In this validation case coefficient values are chosen as follows:

$$A = 3 \tag{72}$$

$$B = 5 \tag{73}$$

$$f_{\sin} = 2\text{Hz} \tag{74}$$

$$f_{\cos} = 1\text{Hz}. \tag{75}$$

With this setup, the period is 1 second, hence only one wave is present in the domain. Figure 12 shows the described wave.

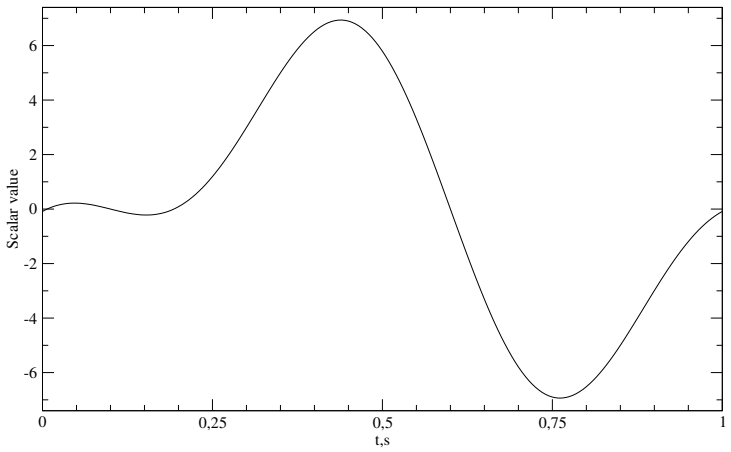

Figure 12: Wave imposed on inlet in second test case.

For harmonic balance simulation, 2 harmonics should be used. The inlet boundary conditions for scalar T in this case are:

$$T_j = A\sin(2\pi f_{\sin}(t_j - 0.35)) + B(2\pi f_{\cos}(t_j - 0.35)), \tag{76}$$

where:

$$t_j = \frac{P}{2n+1} \cdot j, \qquad j \in [1, 2n+1], \tag{77}$$

and P is the period.

4.4.2 Results

For two harmonics, $2n+1 = 5$ time steps are obtained, therefore 5 time steps are solved for.

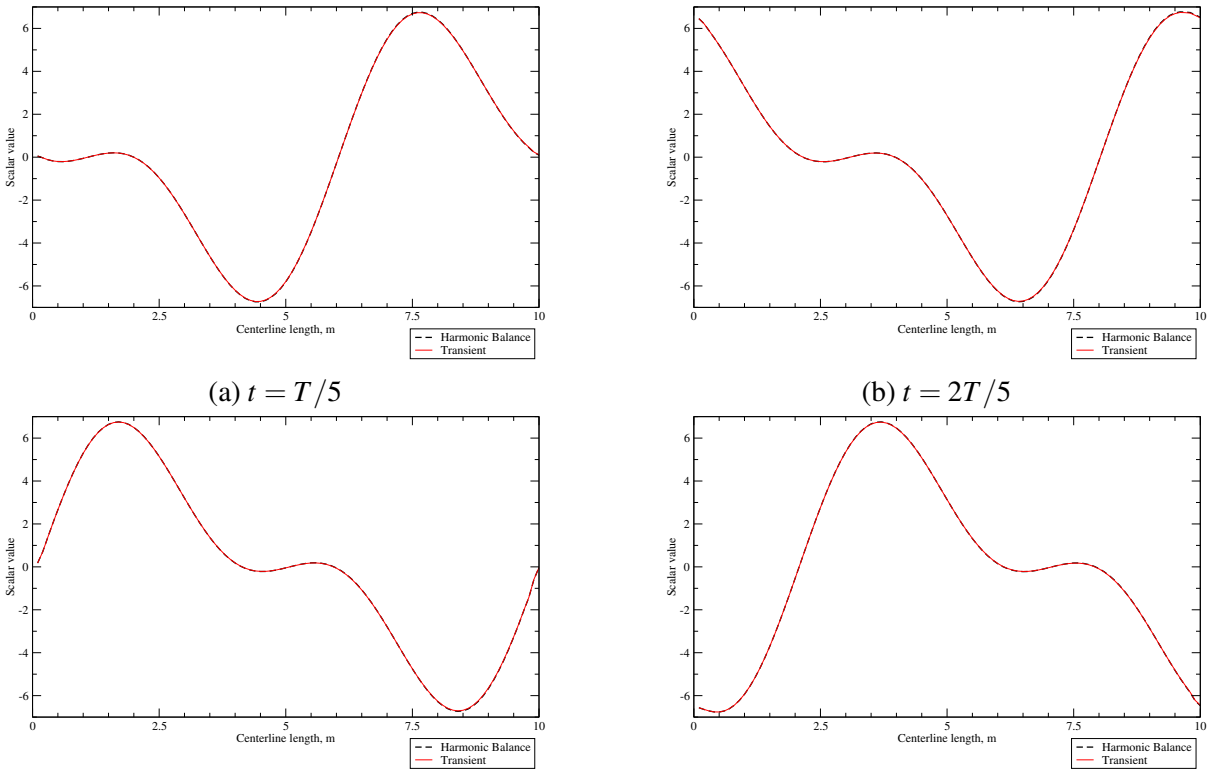

(a) $t = T/5$ (b) $t = 2T/5$

(c) $t = 3T/5$ (d) $t = 4T/5$

Figure 13: Scalar comparison in first four time steps for 2 harmonics used.

Figure 13 shows the comparison of the transient solver and the harmonic balance solver for two harmonics. First four time steps are compared. Figure 14 shows the comparison between the transient solver and the harmonic balance solver at the end of the period for both one harmonic and two harmonics.

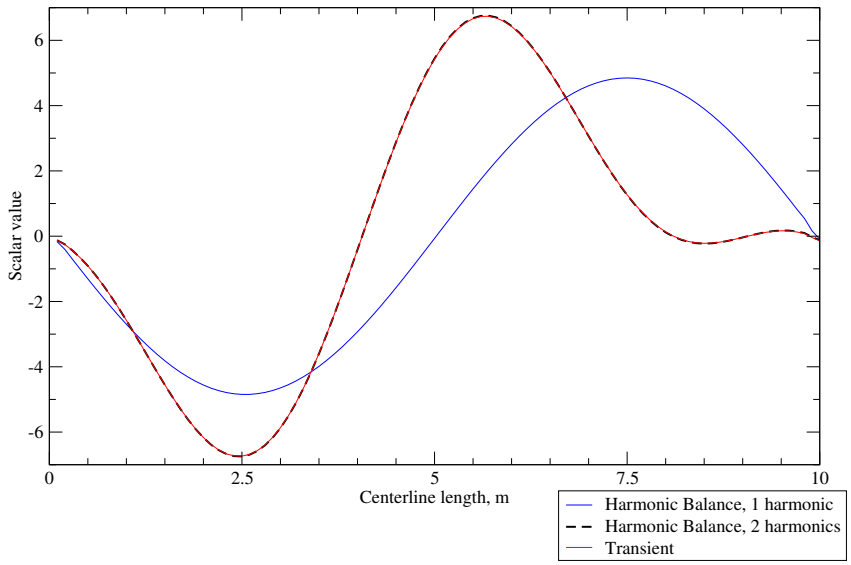

Figure 14: Comparison at the end of period for 1 and 2 harmonics.

Figure 14 demonstrates the accuracy of higher harmonic used. Only one harmonic is describing the sine or cosine wave with values prescribed. For more complex waves, higher number of harmonics should be used: for this case two harmonics are sufficient.

4.5 Test Case 3 - Ramped Square Wave

In Test cases 1 and 2, the behaviour of Harmonic Balance Method on simple harmonic waves is presented. In order to describe a more complex wave, higher number of harmonics should be used. Test cases 3 and 4 will show ramped square waves in order to test the accuracy and robustness of the method. The reason why square waves are chosen is because square waves are not continuous and present a challenge for numerical methods, since they theoretically require an infinite harmonic series.

4.5.1 Boundary Conditions

First square signal is a regular wave with steep, but ramped transition from one value to another. The signal amplitude is 3 and period is 1 s. The wave imposed on inlet is shown in Figure 15.

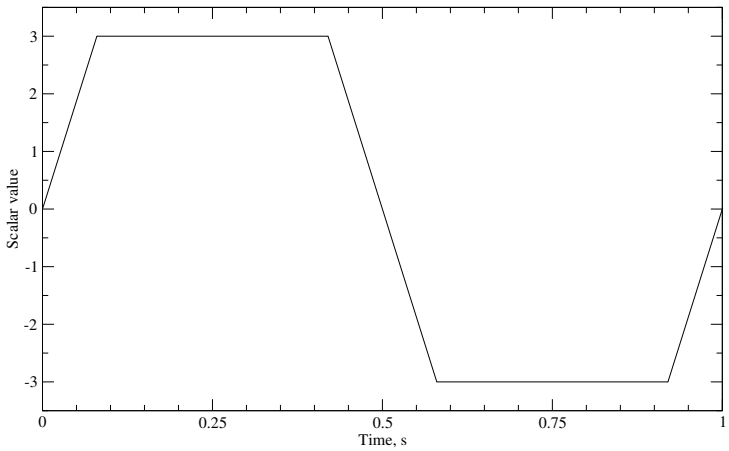

Figure 15: Wave imposed on the inlet in third test case.

4.5.2 Results

For square signal, results for a single time instant within the period are chosen and a convergence is compared using different number of harmonics. The square signal shown on Figure 15 is simulated using 3, 5 and 7 harmonics. With 7 harmonics satisfactory results are obtained, therefore no further testing with higher number of harmonics has been done.

Figure 16 shows the square wave obtained using transient simulation and compared with results obtained using Harmonic Balance Method with 3, 5 and 7 harmonics.

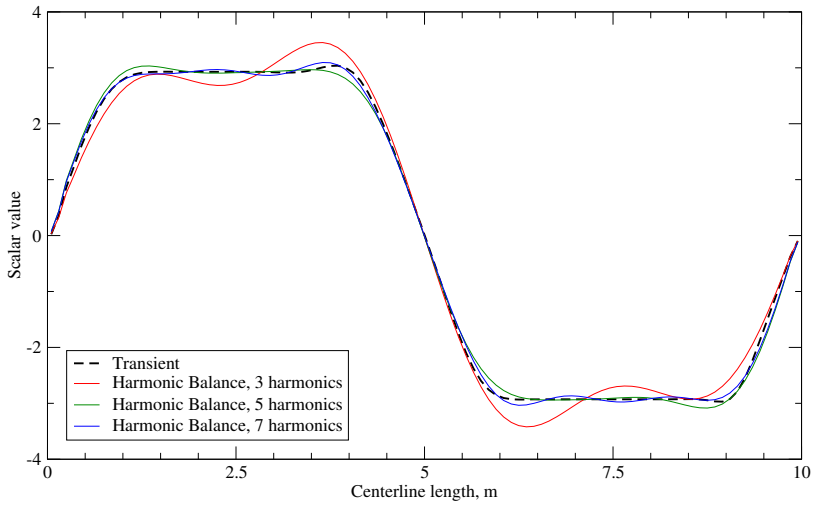

Figure 16: Square wave comparison between transient simulation and harmonic balance with 3, 5 and 7 harmonics.

Figures 17 and 18 show the domain at the and of the period for transient simulation and for harmonic balance with 3 harmonics. The difference between results obtained using 3 harmonics and a transient simulation is obvious from a slightly increased range (see scale on Figures 17 and 18). The harmonic nature can be observed in the middle of the wave crest and wave trough.

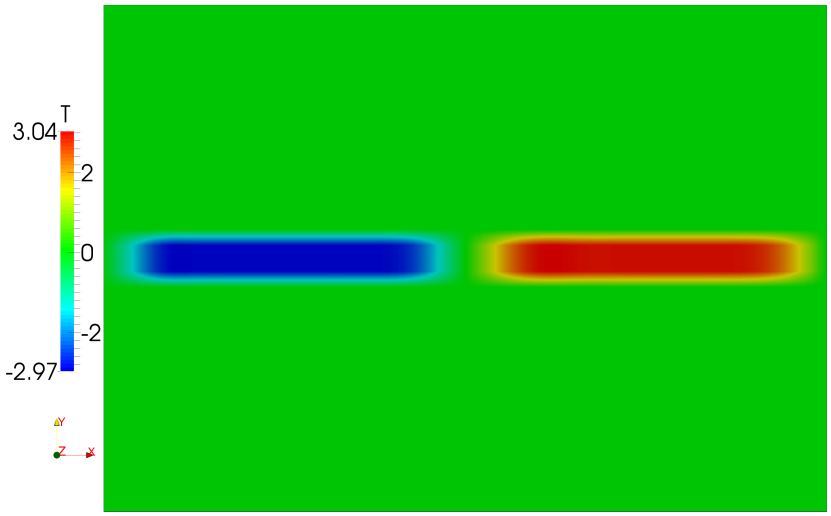

Figure 17: Scalar wave obtained using transient simulation.

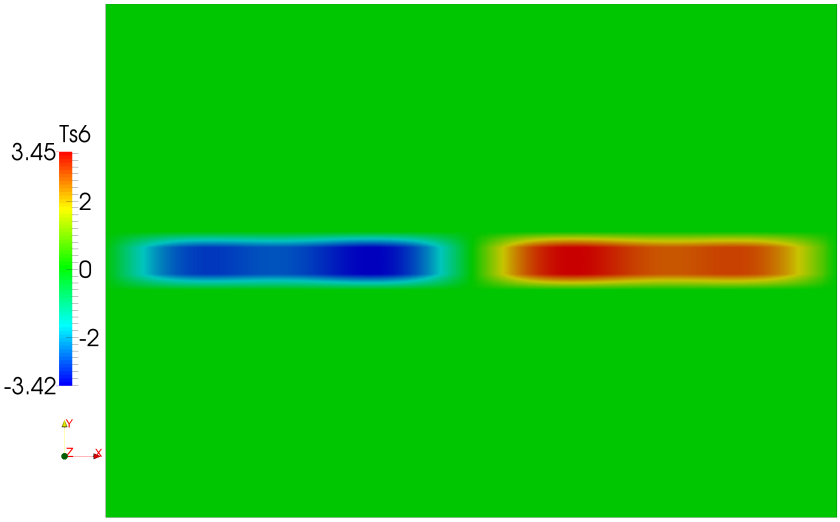

Figure 18: Scalar wave obtained using Harmonic Balance Method with 3 harmonics.

4.6 Test Case 4 - Complex Square Wave

4.6.1 Boundary Conditions

The final test case for passive scalar transport is a complex square signal depicted in Figure 19. Describing such wave is more demanding and up to 10 harmonics are used.

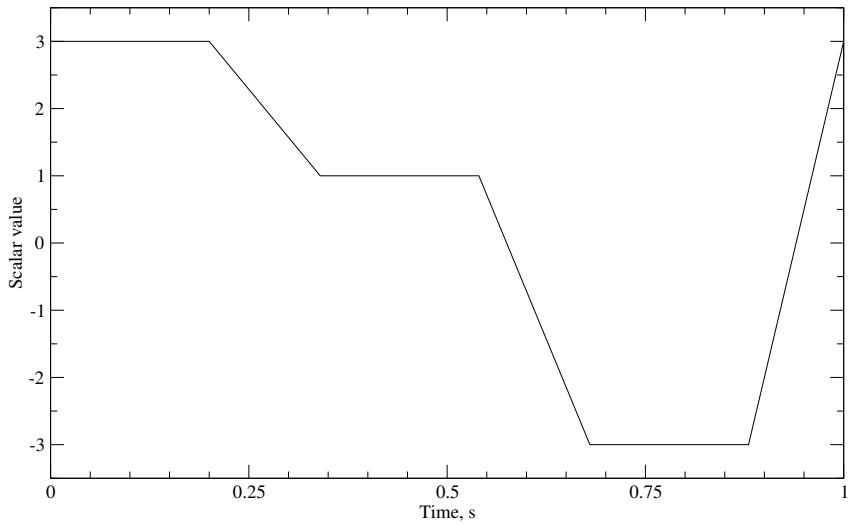

Figure 19: Wave imposed on the inlet in fourth test case.

4.6.2 Results

Results obtained using transient solver and harmonic balance with 3, 5, 7 and 10 harmonics are compared in Figure 20. As shown previously, solution converges to the transient one with increase in number of harmonics. It should be noted that even the transient solver distorts the solution due to spatial discretisation errors.

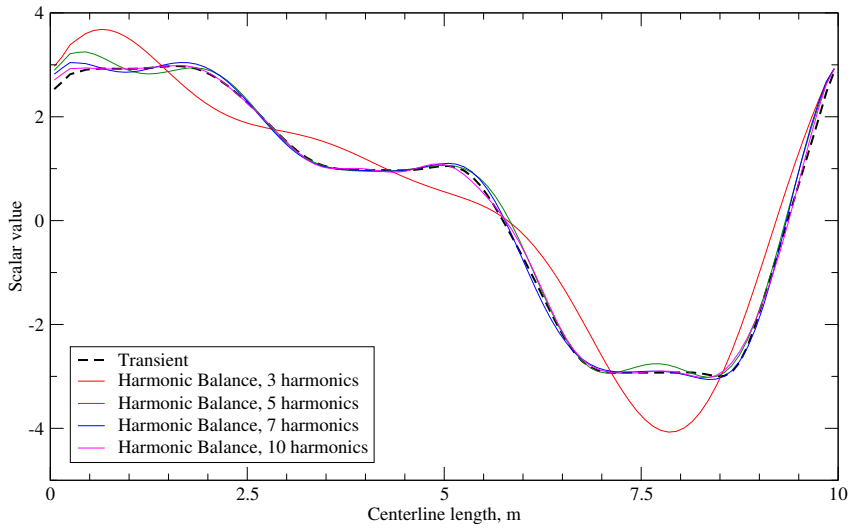

Figure 20: Solution comparison between transient solver and harmonic balance with 3, 5, 7 and 10 harmonics.

Figure 21 shows the error between the transient solution and solution obtained using 3, 5, 7 and 10 harmonics. Bars at the bottom of the graph represent the absolute value of error in logarithmic scale. Green bars stand for 10 harmonics, while red bars stand for 7 harmonics. Bars are included to show the difference between 7 and 10 harmonics and to demonstrate that

the difference is not significant, but involves solving 21 coupled equations (for 10 harmonics) rather than 15 (for 7 harmonics), thus increasing the computational time.

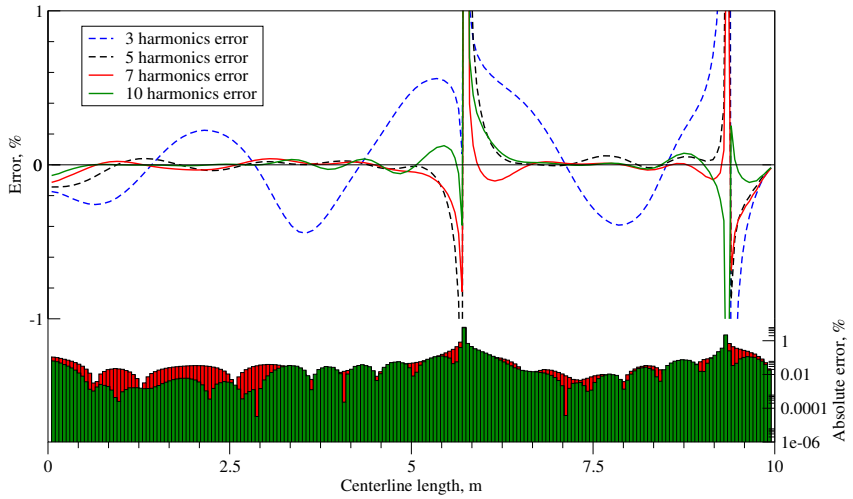

Figure 21: Absolute and relative error along centerline.

4.7 Closure

The validation of Harmonic Balance Method for passive scalar transport was presented in this section. Four cases were used to demonstrate the behaviour of the Harmonic Balance Method. For simple harmonic waves, small number of harmonics is needed, depending on the wave type. For square waves, higher number of harmonics is needed. The fourth test case has shown that at certain point increase in number of harmonics does not significantly improve the solution. It is an important engineering aspect because the engineer running the simulation should know in advance the nature of the flow to be simulated. Wrong assumptions about the flow field can lead to use of too few harmonics, causing inaccurate results. On the other hand, bad assumptions can also lead to use of too many harmonics, increasing the calculation time. As mentioned in [20], number of harmonics greater than 7 is rarely needed, which was also shown in test case 4 by comparing the error between solutions obtained using 7 and 10 harmonics.

5 Harmonic Balance Navier-Stokes Validation

Harmonic Balance Method for passive scalar transport was presented and validated in the previous section. This section deals with validation and test cases for Harmonic Balance Method for Navier–Stokes equations. Only laminar cases are considered as turbulence is not yet implemented in the harmonic balance solver at this stage.

5.1 Introduction

In engineering practice, two types of periodic problems are common and both types will be presented and discussed here. The first type is a periodic problem with a well-defined base frequency. In such cases, periodic oscillations are imposed as a boundary condition: therefore, frequency is known in advance. The first case presented here is the case from this category. It is a NACA 2412 pitching airfoil with a prescribed pitching angle and frequency. Other similar cases could include waves, rotating machinery, fluid-structure interaction problems, etc.

The second type is a periodic problem with frequency which is not known in advance. In such problems, there are no prescribed oscillating boundary conditions that make the problem periodic. Cases presented here are laminar vortex shedding behind a cylinder and edge tone noise. These cases are periodic because of the non-linear nature of convective terms in equation sets that may amplify initial instabilites. Even though boundary conditions are constant, periodic phenomena occurs, thus making it a periodic problem with unknown exact frequency in advance.

5.2 NACA 2412 Test Case

In order to validate the Harmonic Balance Method for Navier–Stokes equations, NACA 2412 test case is used. NACA 2412 is a standard airfoil for which pressure contours during periodic pitching are presented. Several test cases are simulated, varying the *Re* number and number of harmonics in order to show agreement between transient and harmonic balance solver.

5.2.1 Computational Domain

Domain used in NACA 2412 test case is a circular 2D domain with $d = 13$m, Figure 22. Computational mesh consists of 6060 hexahedral cells. Airfoil chord length is 1m. Harmonic Balance Method uses static mesh and therefore different boundary conditions are prescribed for each time step. In order to be fully consistent with the physics to be simulated, transient simulation uses a moving mesh to model airfoil pitching.

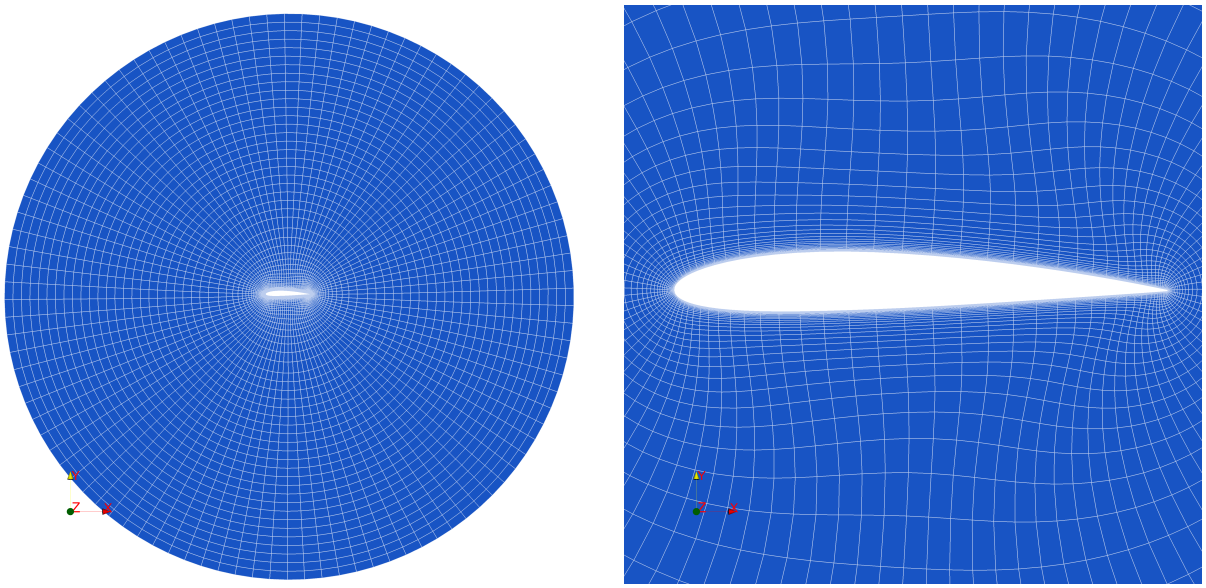

Figure 22: Computational domain for NACA 2412 test case.

5.2.2 Boundary Conditions

Since transient simulation and Harmonic Balance Method have different approaches to temporal periodicity, altered boundary conditions should be used. Transient boundary conditions will be discussed first. Transient simulation is intended to simulate the problem as close as possible as it is in reality. As a first simplification, because of the relative velocity between the airfoil and the air, the airfoil does not have to move in the simulation – air flow can be set in the opposite direction. That is the inlet boundary condition for velocity, fixed value, while zero gradient is set for pressure. In order for the flow to freely exit the domain, all the other boundary patches are set to zero gradient both for velocity and for pressure. To introduce pitching, mesh motion is prescribed as a rotation around the airfoil axis. The axis is set at the chord line at one third distance from the trailing edge. By including mesh motion in the transient simulation, simulation time increases. The Harmonic Balance Method, because of its steady-state concept, has $2n+1$ boundary conditions for n harmonics. As it was previously explained, Harmonic Balance Method solves $2n+1$ coupled steady-state problems and therefore each problem requires its own boundary condition. By alternating boundary conditions from one time step to another, periodic motion in the flow is created. In harmonic balance, static mesh is used which means that airfoil pitching has to be modelled by rotating the inlet flow. The flow is rotated in such manner that the angle between inlet air flow and airfoil in each time step matches the angle from the transient simulation at the same time instant. This relative rotation of the flow, rather than rotation of the airfoil, introduces a certain approximation error. This approach might not be fully consistent with the Space Conservation Law [21] and will further be investigated in future work.

Figure 23 depicts the difference between the approach used in the transient simulation and the one used in harmonic balance. Figure 23a shows the transient simulation in which the inlet flow is steady and undisturbed. The only disturbance caused is the one from the airfoil. Figure 23b shows the harmonic balance approach in which each time step has its own inlet boundary conditions, causing the flow to change. It means that by rotating the flow, different flow field is obtained even before reaching the airfoil.

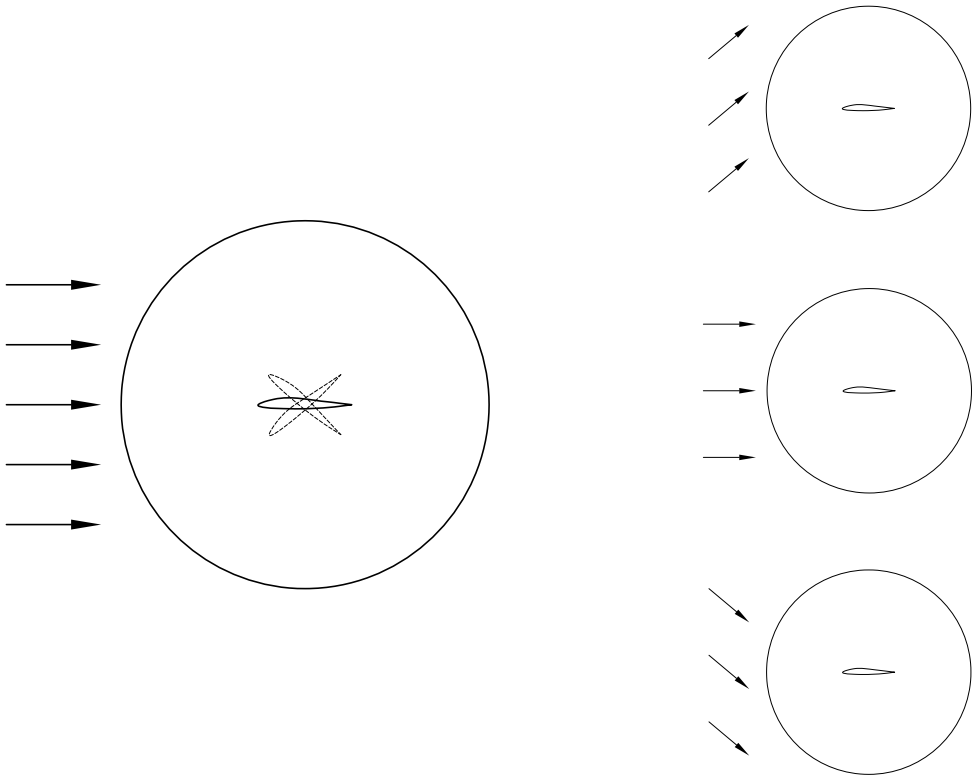

(a) Transient simulation mesh rotation,

(b) Inlet velocities at different time steps in harmonic balance.

Figure 23: Boundary condition treatment in the transient and the harmonic balance simulation.

8 test cases were run in order to compare transient simulation and Harmonic Balance Method. Two different setups were made, one for low *Re* number and the other for high *Re* number. For each setup a transient simulation and harmonic balance simulations with 1, 3 and 6 harmonics were made. Due to the numerical instabilities that occur at low speeds, the variation in *Re* numbers was achieved by changing the kinematic viscosity of fluid. First setup has inlet velocity set to 1 m/s with pitching angle of 6°. Kinematic viscosity is set to $\nu = 5.9 \cdot 10^{-4} \mathrm{m}^2/\mathrm{s}$ which gives $Re = 1\,695$ and stable laminar flow. Second setup has the same inlet velocity, 1 m/s with pitching angle of 6°, but the kinematic viscosity is set to $\nu = 1.5 \cdot 10^{-5} \mathrm{m}^2/\mathrm{s}$, yielding $Re = 66\,667$.

5.2.3 Results

Results presented here are given for airfoil pitching case with low and high *Re* number. Low *Re* number case is a laminar case without flow separation. Results of pressure contours obtained using 1, 3 and 6 harmonics are compared to transient simulation.

Figure 24 shows the results obtained using 1 harmonic and transient simulation. Figure 24a represents the pressure contour around the airfoil at $t = T/3$. Horizontal axis depicts the cells of the expanded airfoil, where pressure peak in the middle presents leading edge stagnation point, while values 0 and 100 stand for trailing edge. Values 0–50 represent the lower camber while 50–100 is upper camber. This representation is not length–authentic because some parts of the airfoil are meshed with finer mesh and some with coarser, meaning that 1 cell can have length of 1 mm as well as 100 mm. Such approach was chosen in order to be able to compare the obtained value in each cell. Figures 24b and 24c show the contours in $t = 2T/3$ and $t = T$, respectively.

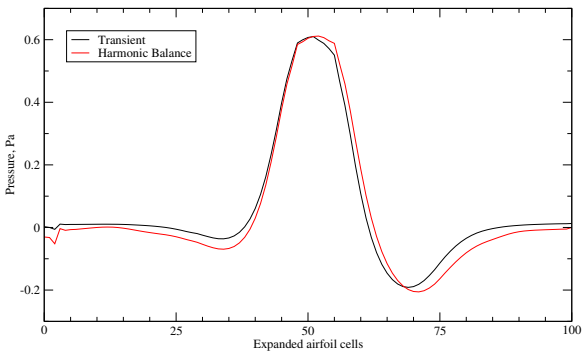

(a) Pressure contours at $t = T/3$

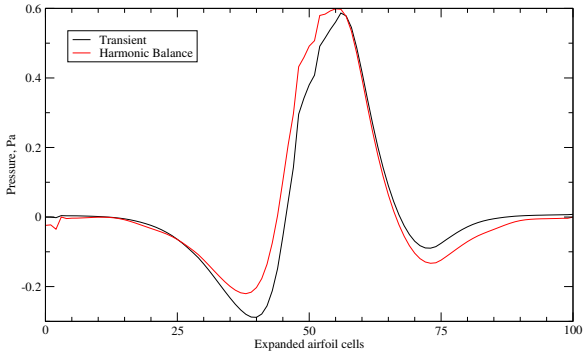

(b) Pressure contours at $t = 2T/3$

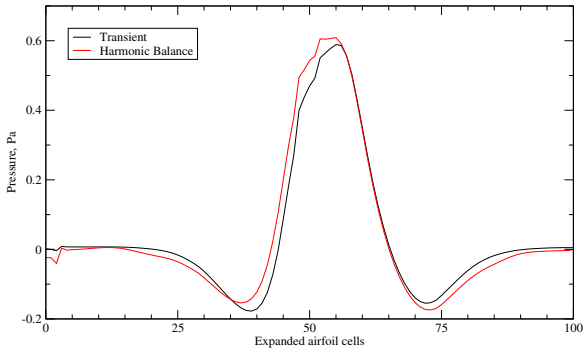

(c) Pressure contours at $t = T$

Figure 24: Pressure contours around the airfoil for 1 harmonic, 0–50 represents the lower camber while 50–100 the upper camber.

It can be seen that peak pressures show good agreement in all of the time steps. Pressure on lower camber sides show small deviations from transient case, while in second time step, there is a somewhat higher discrepancy around cell number 40 (horizontal axis).

Further results are shown for 3 harmonics. Figure 25 shows the comparison with transient simulation. It can be noticed that the deviation from transient results has been reduced. However, the discrepancy around cell number 40 which was observed in 1 harmonic case appears again and can be seen in Figures 25e and 25f.

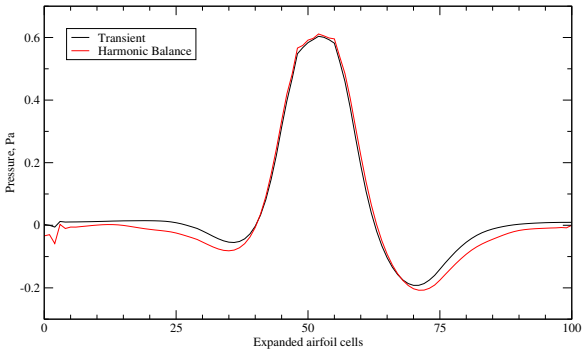

(a) Pressure contours at $t = T/7$,

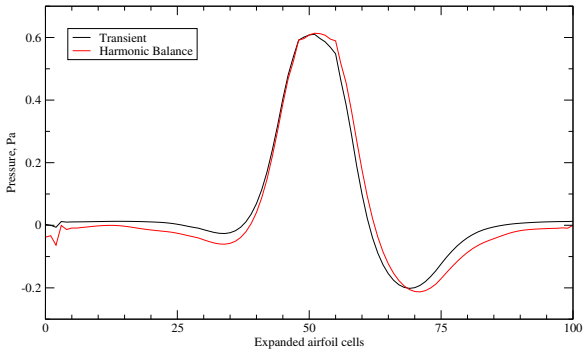

(b) Pressure contours at $t = 2T/7$,

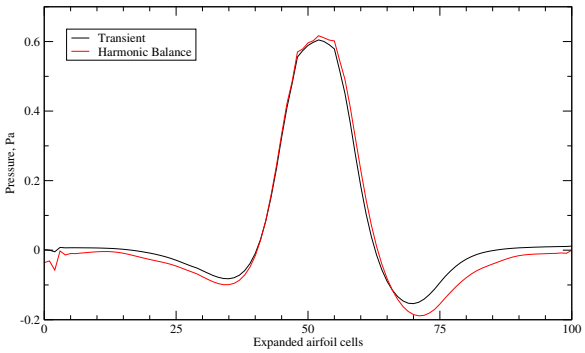

(c) Pressure contours at $t = 3T/7$,

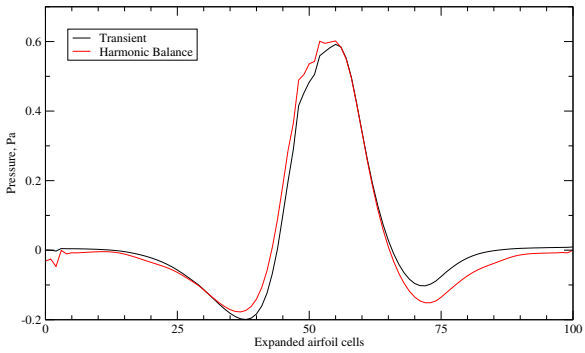

(d) Pressure contours at $t = 4T/7$,

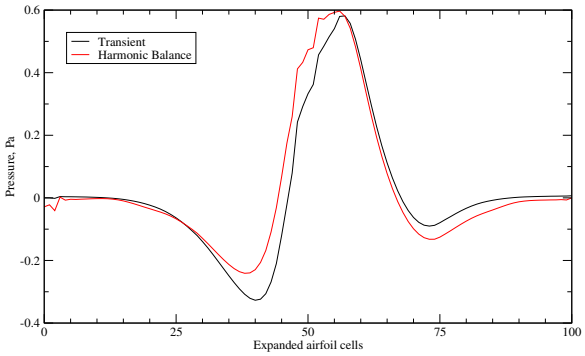

(e) Pressure contours at $t = 5T/7$,

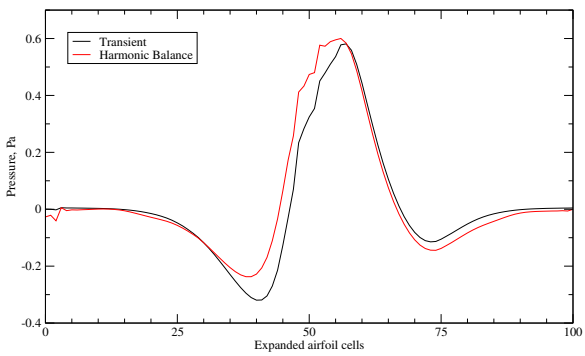

(f) Pressure contours at $t = 6T/7$,

Figure 25: Pressure contours around the airfoil for 3 harmonics.

The final set of results for setup with low *Re* number is obtained using 6 harmonics, offering good temporal resolution of 13 time steps. Although good temporal resolution is achieved, 6 harmonics slow down both the simulation time and convergence compared to 1 harmonic simulation. Comparison with transient simulation is shown in Figures 26 and 27 for all time steps.

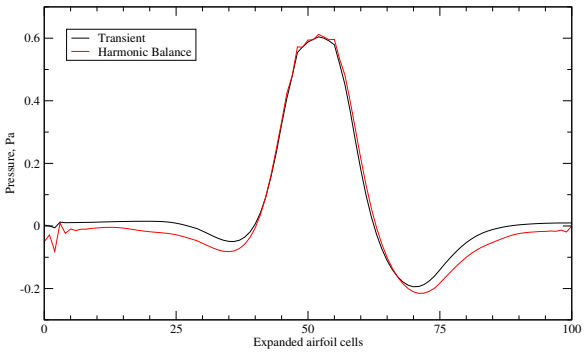

(a) Pressure contours at $t = T/13$,

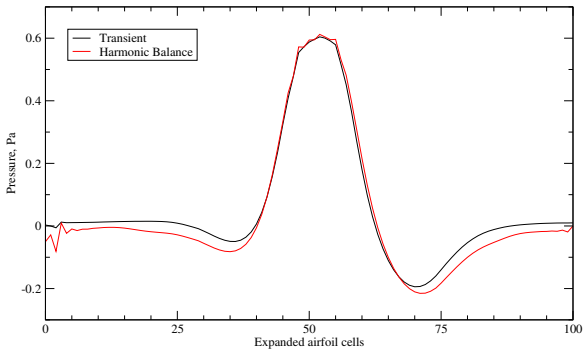

(b) Pressure contours at $t = 2T/13$,

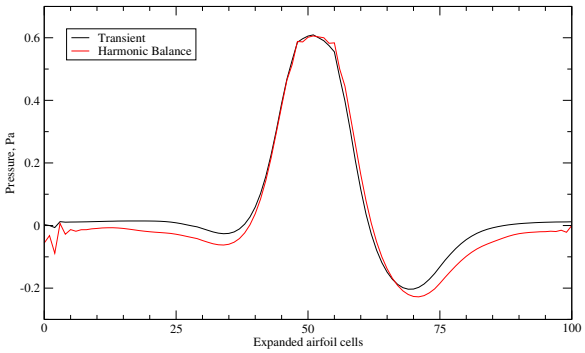

(c) Pressure contours at $t = 3T/13$,

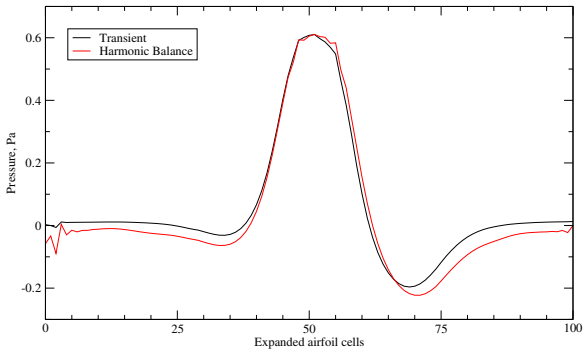

(d) Pressure contours at $t = 4T/13$,

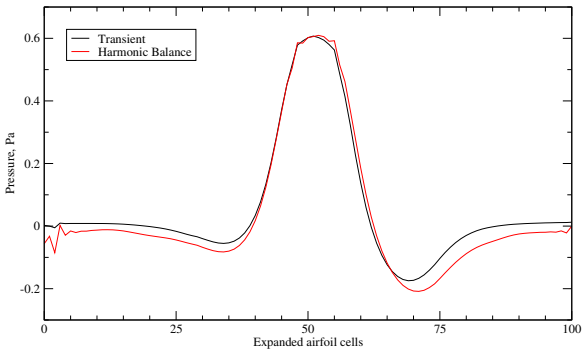

(e) Pressure contours at $t = 5T/13$,

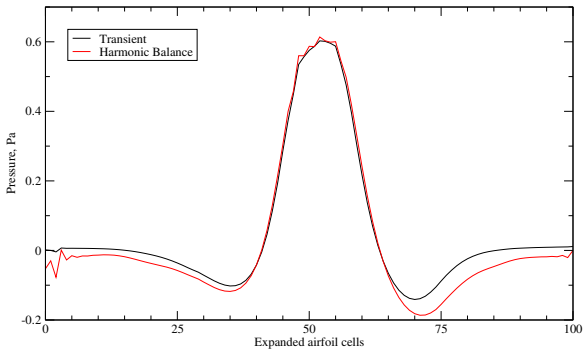

(f) Pressure contours at $t = 6T/13$.

Figure 26: Pressure contours around the airfoil for 6 harmonics.

It can be noticed once again, in Figures 27b to 27e, that harmonic balance is not accurately following the pressure contour of the transient simulation in the same areas as for 1 harmonic and 3 harmonics. There is still a discrepancy at the left trough around cell number 40. Apart from this discrepancy, the overall agreement is good. The causes for such behaviour will be discussed in section 5.2.4.

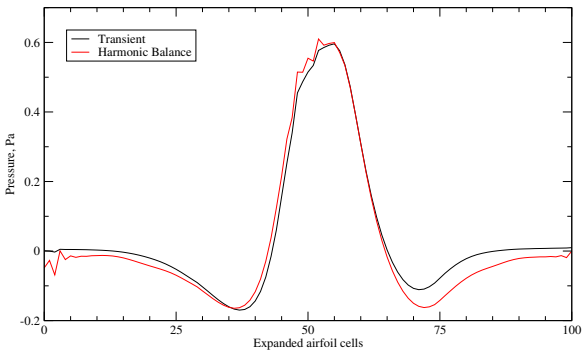

(a) Pressure contours at $t = 7T/13$,

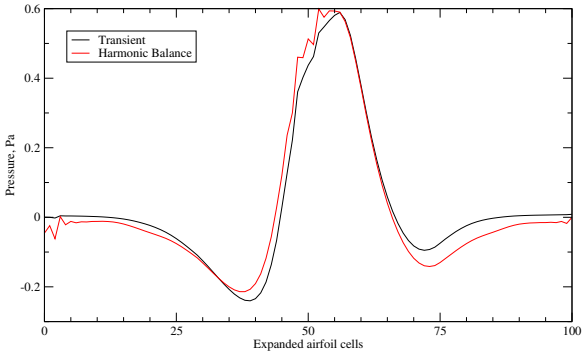

(b) Pressure contours at $t = 8T/13$,

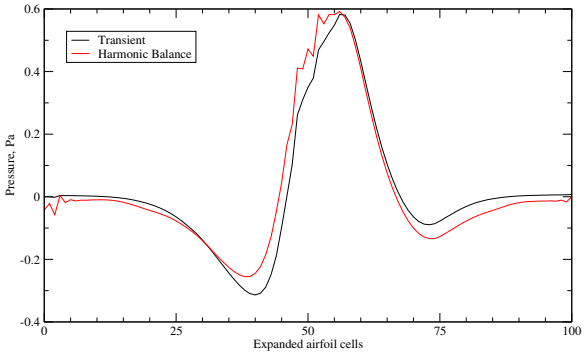

(c) Pressure contours at $t = 9T/13$,

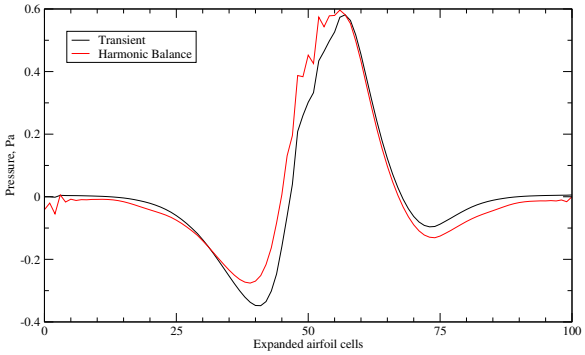

(d) Pressure contours at $t = 10T/13$,

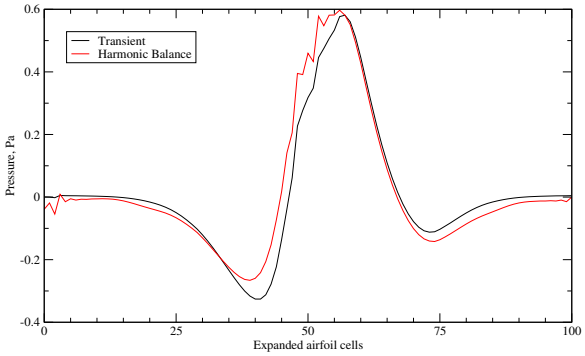

(e) Pressure contours at $t = 11T/13$,

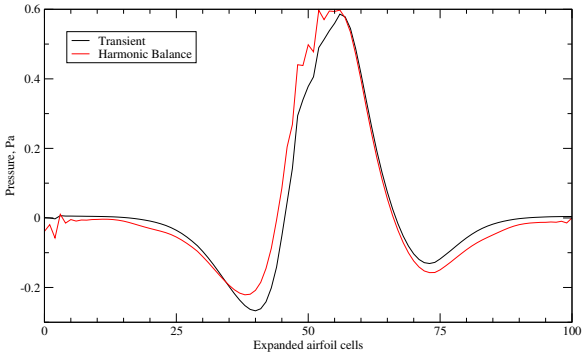

(f) Pressure contours at $t = 12T/13$,

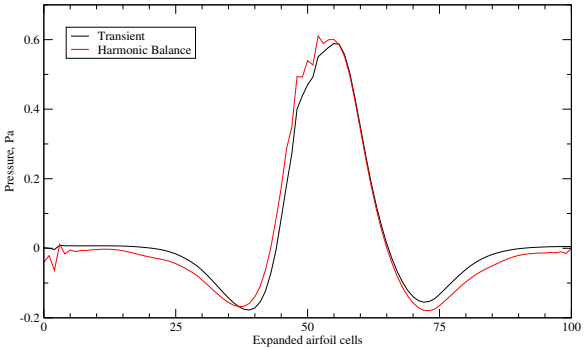

(g) Pressure contours at $t = T$.

Figure 27: Pressure contours around the airfoil for 6 harmonics.

In Figure 28, harmonic balance solution with 1, 3 and 6 harmonics is compared to transient solution at the end of a period With symbols representing each harmonic balance simulation overlapping, it can be noticed that the results are similar.

Results presented above suggest that for simulations where high temporal resolution is not needed, 1 or 3 harmonics are more than sufficient. As it was stated in the description of Fourier series in section 3.2 , in terms of energy, first harmonic has the largest influence on the solution, while every further harmonic has smaller and smaller influence. Also, higher number of harmonics contribute to the solution accuracy in terms of small disturbance frequencies. That explains why there is small difference between the solution with 1 and 3 harmonics, but results differ for 6 harmonics. It should also be noticed that an airfoil pitching case is not the case with many disturbances and complex flow phenomenon, therefore higher numbers of harmonics should not change the solution significantly.

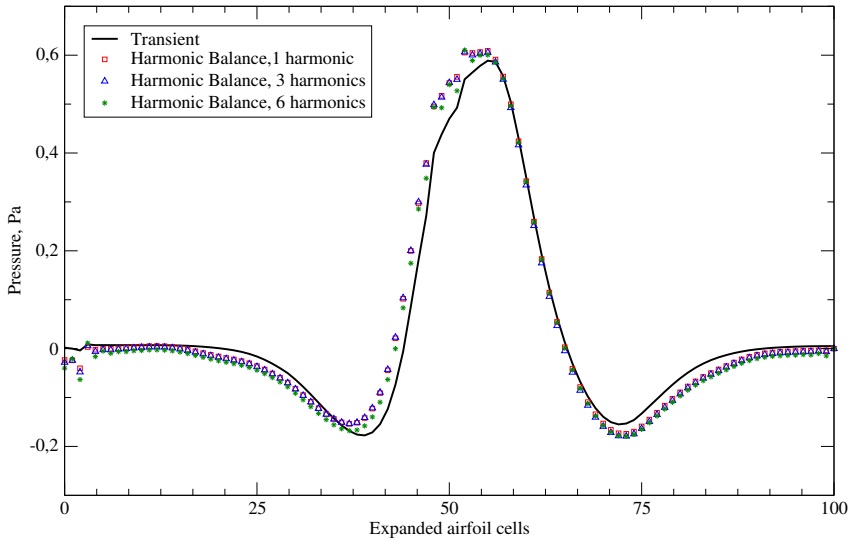

Figure 28: Comparison of transient simulation and harmonic balance with 1, 3 and 6 harmonics at $t = \mathrm{T}$.

For second example of a pitching airfoil, the same test case with high *Re* is simulated. This test case is carried out to show that transient interaction of vortices cannot be accurately captured using harmonic balance. Pressure contour on the airfoil at the point where flow separation occurs does not match the pressure contour in the harmonic balance solution. Transient pressure contour is curved with jumps, while harmonic balance pressure contour is smooth. Some of the previously introduced approximations may be the cause of such behaviour and it will be discussed more thoroughly later.

Four simulations are compared: a conventional transient simulation with three harmonic balance simulations, using 1, 3 and 6 harmonics. Because of turbulent flow at $Re = 66\,667$, pressure contours are not completely identical at certain time instants within every period. Therefore, in a transient simulation, 10 periods were simulated and only the last five were

compared in order to neglect the start–up unsteadiness. At certain time instants, where there were variations in pressure contours, average of 5 periods is made and compared to harmonic balance. In time instants where transient pressure contours matched each other closely in all of the periods, no averaging is done. Higher *Re* than in previous case was achieved by reducing the kinematic viscosity to $\nu = 1.5 \cdot 10^{-5}$ m^2/s and setting the inlet velocity to u = 1 m/s.

The comparison of results is shown in Figure 29 for one harmonic case. It can be observed that both upper and lower camber side exhibit lack of disturbances in harmonic balance simulation. These disturbances cause pressure fluctuations which are also the cause of differences in other regions of airfoil where flow separation does not occur.

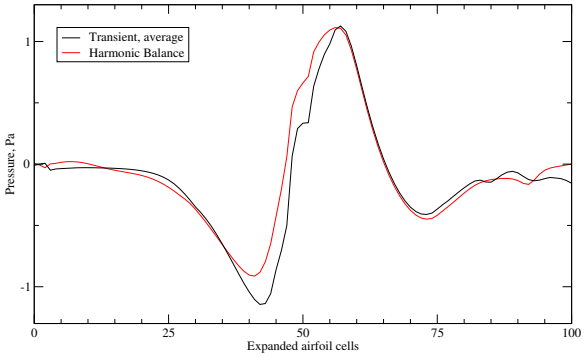

(a) Pressure contours at $t = T/3$,

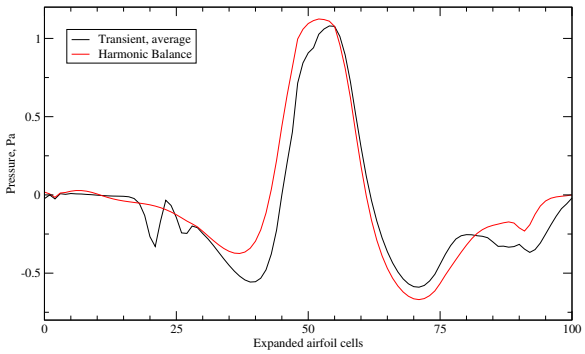

(b) Pressure contours at $t = 2T/3$,

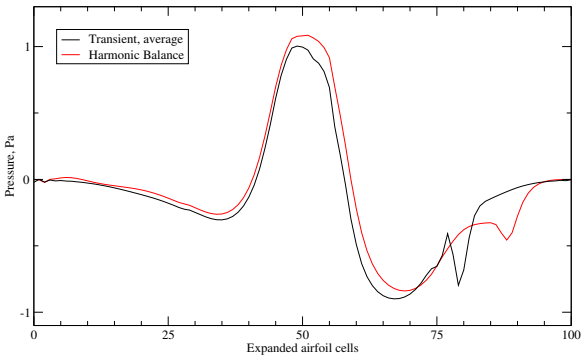

(c) Pressure contours at $t = T$.

Figure 29: Pressure contours around the airfoil for 1 harmonic for high *Re*.

Transient results compared in Figures 29a and 29c are averaged over 5 periods. Figure 30 shows the transient contours and the resulting averaged contour. Dashed lines present the pressure contours, while black line presents the averaged profile.

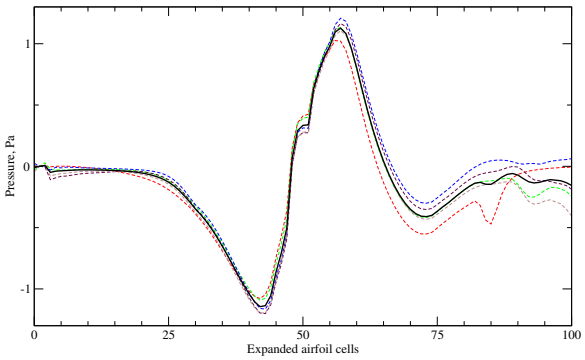

(a) Averaged pressure contour at $t = T/3$

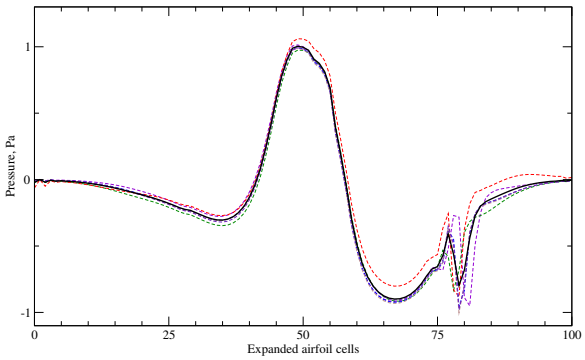

(b) Average pressure contour at $t = T$.

Figure 30: Averaged pressure contours, dashed lines present the contours in different periods.

The results for 3 harmonics are shown in Figure 31. Similar to the low *Re* number case, discrepancy around cell number 40 can be seen both in Figures 31a, 31d, but also in the 1 harmonic case in Figure 29a. Even though higher number of harmonics is used compared to previous case, flow separation and turbulence is not resolved. Results are only shown at some of the time steps because other time steps exhibit similar behaviour and are therefore not presented.

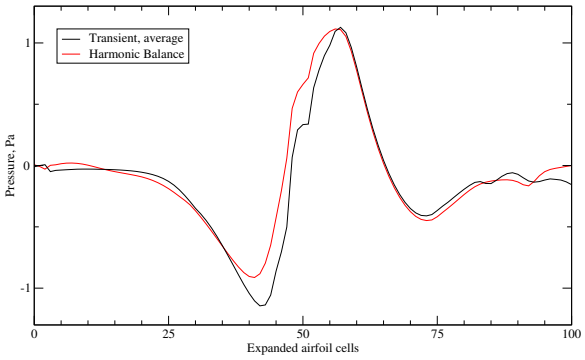

(a) Pressure contours at $t = T/7$,

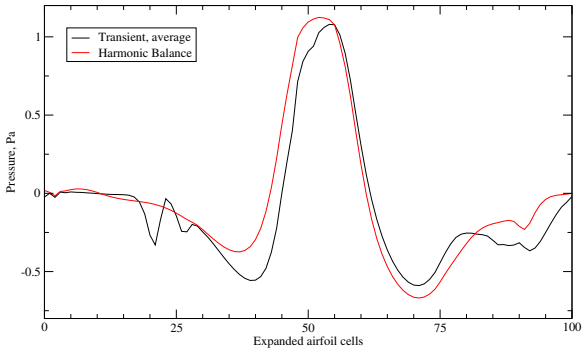

(b) Pressure contours at $t = 3T/7$,

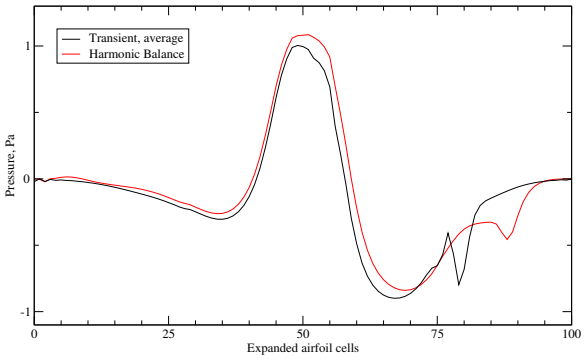

(c) Pressure contours at $t = 5T/7$,

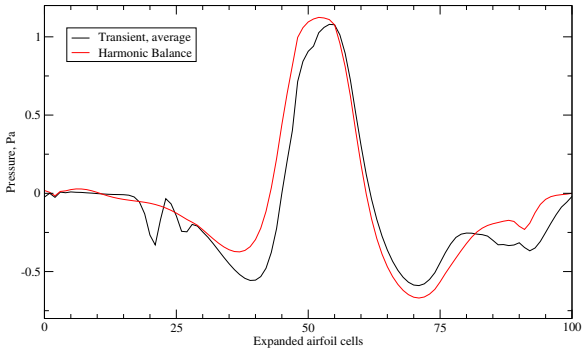

(d) Pressure contours at $t = T$.

Figure 31: Pressure contours around the airfoil for 3 harmonics used at high *Re*.

The 6 harmonics case is presented in Figure 32. It can be observed that results are similar

to ones shown previously for 1 and 3 harmonics. As stated in case with low *Re* number, airfoil pitching case is not a complex case which could easily demonstrate the behaviour of results by including higher number of harmonics. Even though accuracy of higher harmonics is not presented here, effects of higher number of harmonics are demonstrated in section 4, dealing with scalar transport, and behaviour is analogous. The results for other time instants exhibit similar behaviour and are not presented.

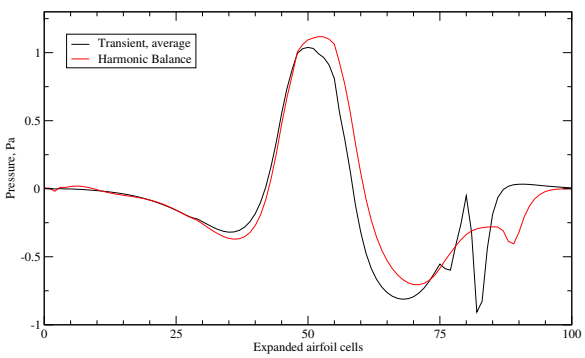

(a) Pressure contours at $t = T/13$,

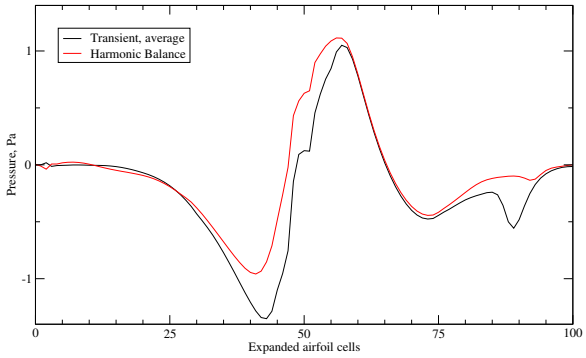

(b) Pressure contours at $t = 5T/13$,

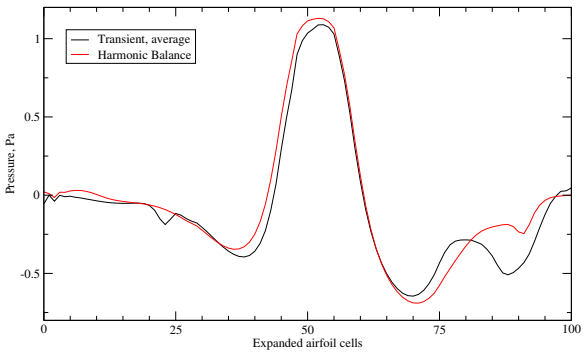

(c) Pressure contours at $t = 9T/13$.

Figure 32: Pressure contours around the airfoil for 6 harmonics at high *Re*.

In Figure 32b, discrepancy around cell number 40 is still not present, irrespective of 6 harmonics used.

Flow field visualisation is presented in Figures 33 and 35. Flow field is from fifth time step, $t = 5T/13$, or in Figures it is labeled as UTime4 and pTime4, counting from zero. Overall velocity fields are quite similar with both trailing wakes going slightly downwards. Disturbance present in graphs of pressure contours can also be noticed in Figure 33b, and it does not appear in Figure 33a of the harmonic balance flow field. More detailed view is depicted in Figure 34. Stagnation point and areas of high and low velocities appear in same locations for the transient simulation and harmonic balance cases.

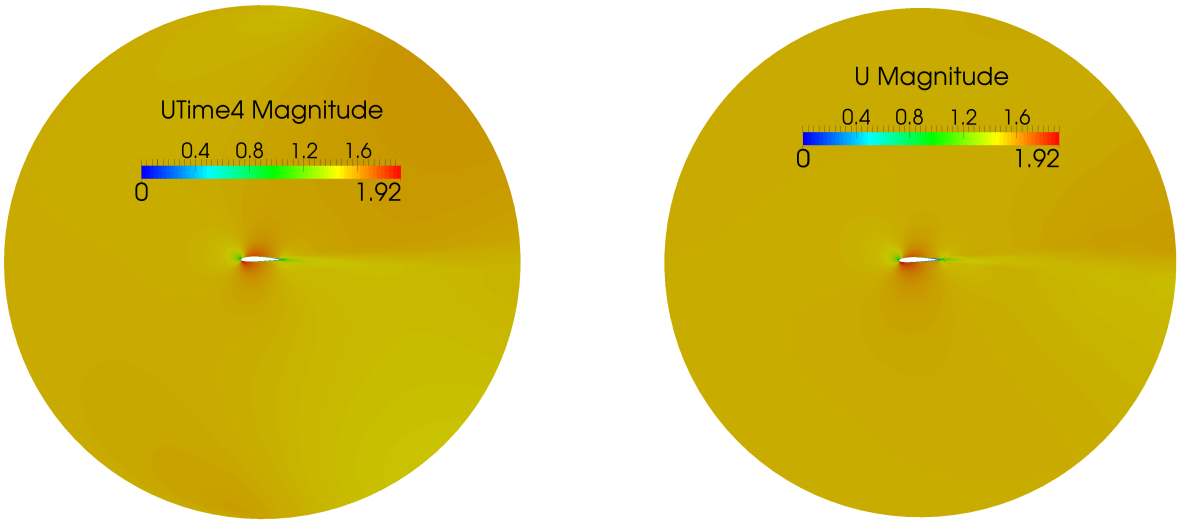

(a) Harmonic balance, 6 harmonics, (b) Transient simulation.

Figure 33: Velocity field visualisation at $t = 5T/13$.

Figure 34 shows flow fluctuation that occurs at the trailing edge. In the transient simulation, larger flow separation appears compared to the harmonic balance, both at the trailing edge and lower camber side.

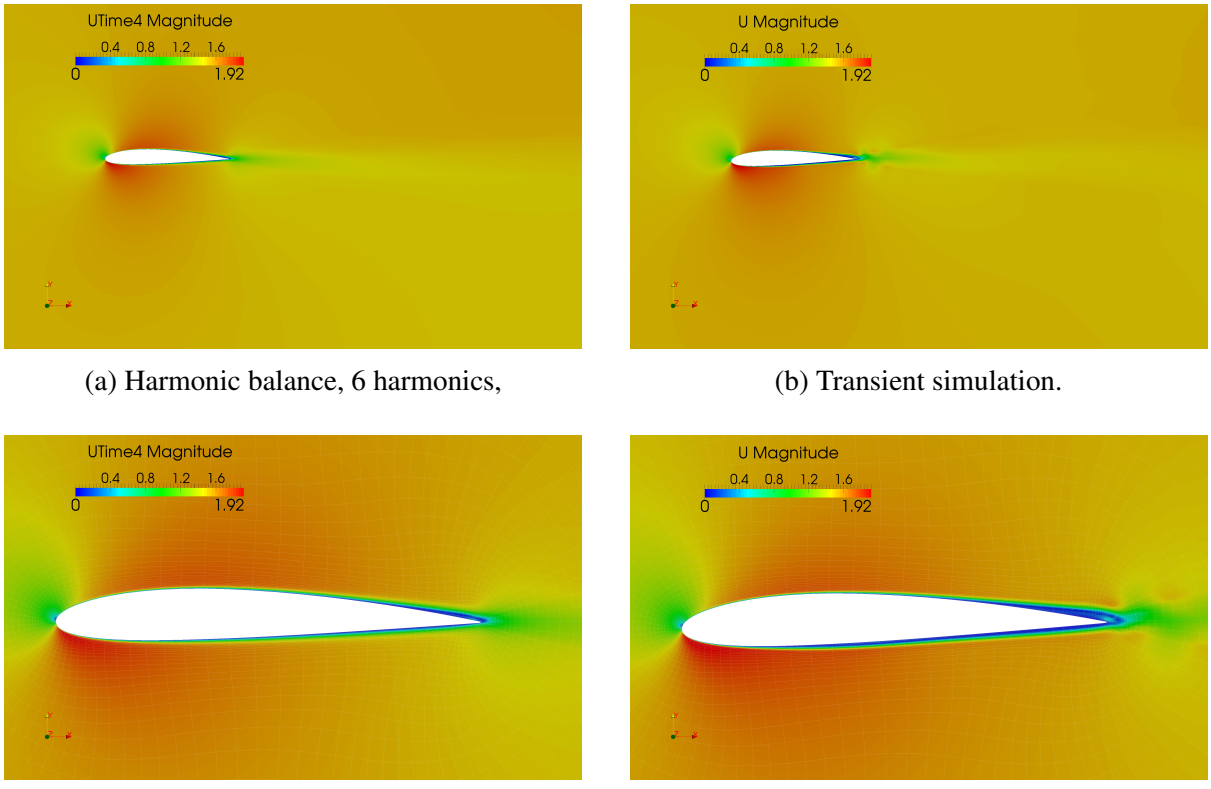

(a) Harmonic balance, 6 harmonics, (b) Transient simulation.

(c) Harmonic balance, 6 harmonics, (d) Transient simulation.

Figure 34: Detailed look at velocity field at $t = 5T/13$.

Figure 35 shows the visualization of the pressure field within the domain. The pressure

field is similar with a slightly different distribution at the upper camber side. Stagnation point appears at the same place in both simulations with larger pressure diffusion around the stagnation point in transient simulation. For the trailing edge, the difference was already noted: the transient simulation has flow separation while the harmonic balance resolves the flow as if it is smooth and undisturbed.

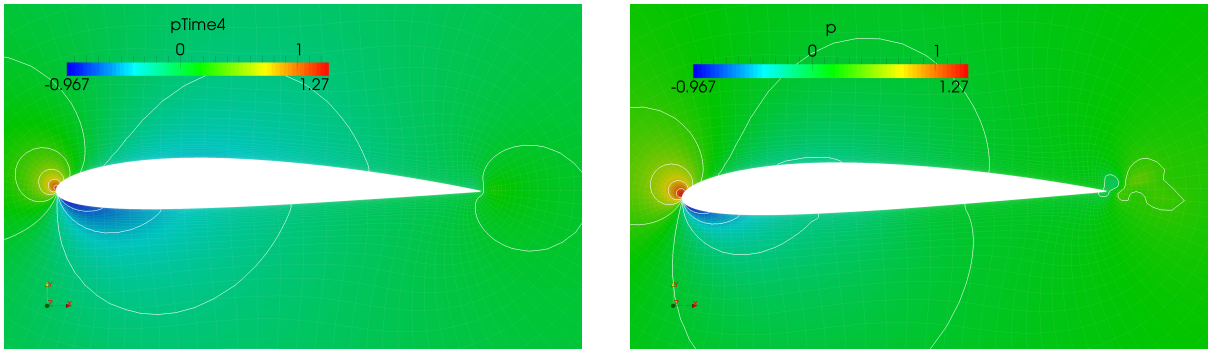

(a) Harmonic balance, 6 harmonics, (b) Transient simulation.

Figure 35: Detailed look at velocity field at $t = 5T/13$.

5.2.4 Approximations Introduced

In order to use the Harmonic Balance Method and to be able to present its current progress and development, some simplifications and approximations are present in the NACA 2412 test case. Simplifying the physics of the flow is necessary, but introduces a certain error into the calculation. This section deals with errors introduced only by the case setup.

Differences that arise from the Harmonic Balance Method are caused by three main approximations. These approximations are believed to cause most problems visible in NACA 2412 test case and introduce significant errors. The first cause arises from the relative flow direction. In contrast to real situation (and the transient simulation) where flow is unidirectional and the airfoil is pitching, in NACA 2412 test case for the Harmonic Balance Method a single and static mesh is used. By doing this, we have accepted that the flow direction is changing rather than the airfoil is pitching, which is not an accurate approximation. This will be clarified by referencing the hypothetical transient case with variable inlet velocity which is changing direction. When inlet flow changes direction, it has to change the direction of the surrounding flow too before it reaches the airfoil. It means that the flow reaching the airfoil, in the relative coordinate system, is not the same as in transient simulation. Other than disturbed flow, in the transient simulation when the pitch angle changes, the angle of attack is changed instantly and the stagnation point moves instantly. In approximation used here, changing the inlet direction changes only the inlet direction instantly while airfoil is reached after some time. Only then will stagnation point move and

pressure and velocity field correspond to the pitching angle. These are the remarks concerning the hypothetical transient case with a variable velocity direction, but the same boundary condition setup will cause the same effects in the harmonic balance too. In order to improve this effect, a rotating mesh should be used. Every time step would have a static mesh corresponding to its pitch angle, while the inlet velocity would stay unchanged.

The second cause is closely related to the one just mentioned and it concerns the way harmonic balance works. In the Harmonic Balance Method velocity fields from all the time steps are coupled together. In order to calculate the solution in time step $t = T/13$, all other 12 velocity fields are used as the source terms. This type of velocity coupling, together with the case setup as shown in Figure 23 causes the flow field to flatten out in the x–direction. Therefore, what was intended to be a unidirectional flow at α degrees, is the inlet flow at α degrees which eventually tends to flatten. As it was shown, such approximation produces sufficiently good results compared to the level of simplicity that this approach offers – no moving mesh, only one mesh used, memory reduction, etc. On the other hand, the multiple mesh approach is believed to converge more quickly because velocity fields in all of the time steps are similar and results would be more accurate.

The third cause of errors in the NACA 2412 test case could not be resolved by using a multiple mesh approach, but it is also the result of moving mesh. In transient simulation, by pitching the airfoil not only the relative angle between the flow and the airfoil changes, but also the relative velocity. This acceleration causes an increase of velocity on one side of the airfoil and reduction of velocity on the other, and opposite for the pressure. This effect caused by airfoil movement is not captured by the Harmonic Balance Method and cannot be captured using steady-state approach, unless some of the methods similar to MRF are used, as described in [22]. This could explain why in some graphs contours were slighly offset in the y direction.

5.3 CPU Time Comparison

For the presented NACA 2412 cases, a CPU time comparison study is carried out. Harmonic balance is a quasi-steady technique depending on the number of iterations and residuals. The residual noted in tables 1 and 2 is the initial residual for velocity and pressure fields, obtained using L_1 norm. Conventional transient simulation is directed using time step size. Maximum Courant–Friedrichs–Lewy number was used to determine the suitable time step size. In order to neglect the start-up instabilities and produce a perfectly periodic results, simulation was run for 10 periods. Table 1 shows comparison of case setup and time required to satisfy the residual criterion for the NACA 2412 low *Re* case.

Transient		Δt=0.005 s	Max Co = 1	1 period = 116 s
HB	1h	520 iter	residual = 10^{-6}	18 s
	3h	1000 iter	residual = 10^{-6}	90 s
	6h	2700 iter	residual = 10^{-6}	350 s

Table 1: CPU time comparison for low *Re* NACA 2412 test case.

In transient simulation, simulating one period took 116 s and is consistent through all the periods. On the other hand, the harmonic balance simulation took substantially less time for the simulation with one harmonic, 18 s. Three harmonics simulation took nearly as one period of transient simulation, while six harmonics took three times more. It should be noted here that one period of transient simulation is not representative. In terms of low *Re* case, at least 4 periods should be run for the results to become consistent. Hence, transient simulation time of at least 464 s should be used for comparison.

Transient		Δt=0.001 s	Max Co = 0.5	1 period = 431 s
HB	1h	850 iter	residual = 10^{-6}	26 s
	3h	3200 iter	residual = 10^{-6}	250 s
	6h	2800 iter	residual = 10^{-6}	352 s

Table 2: CPU time comparison for high *Re* NACA 2412 test case.

Table 2 presents the CPU time comparison for the NACA 2412 high *Re* case. Transient simulation was run with time step $\Delta t = 0.001$ s, at lower Courant-Friedrichs-Lewy number than in low *Re* case, yielding the period time of 431 s. The harmonic balance simulation for one and three harmonics took considerably more time than in the previous case, while for six

harmonics the same CPU time was required. In validation section it was shown that transient simulation was not completely periodic after ten periods: CPU time of at least 4310 s should be used for comparison.

CPU time tables 1 and 2 present the harmonic balance efficiency in terms of computational resources. For the low *Re* case, simulation with one harmonic is 25 times faster, while three and six harmonic simulations are 5 and 1.3 times faster, respectively. High *Re* case took more time both for the transient and harmonic balance simulation. Hence, harmonic balance simulation with one harmonic being 165 times faster, with three harmonics 17 times faster and with six harmonics 12 times faster, compared to 10 periods of transient simulation. Presented savings in CPU time justify the error introduced in the harmonic balance simulations.

5.4 Test Cases with Unknown Frequency

Previous test cases dealt with prescribed motion of an airfoil with a known dominant frequency. In this section, cases with unknown frequency will be presented. Such cases present special problems for the Harmonic Balance Method for two reasons. The first reason is already mentioned: frequency which is an input parameter for the harmonic balance is unknown. Therefore, frequency should be either guessed or a transient simulation should be performed and a frequency spectrum could be obtained using FFT (Fast Fourier Transform). The second problem is the problem of non–linearity. In cases where periodicity doesn't come from enforced motion or prescribed periodic boundary condition, periodicity is the result of the nature of the flow. Because of unsteadiness, convergence is hard to reach. Both of the mentioned problems are presented in the following two cases.

5.4.1 Laminar Cylinder Vortex Shedding Test Case

First test case deals with laminar vortex shedding behind the cylinder. Following [23] where vortex shedding behind a cylinder with enforced motion is simulated using the Harmonic Balance Method, a similar case without enforced motion is reconstructed. The computational domain is a 2D structured mesh with 25 920 hexahedral cells, shown in Figure 36.

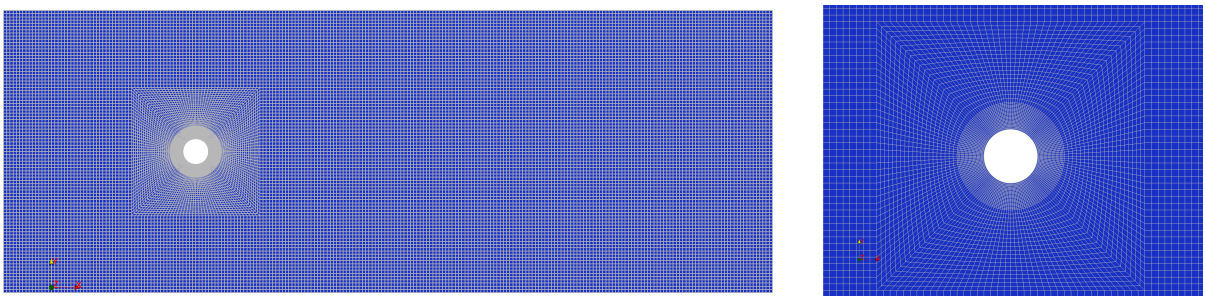

Figure 36: Domain for laminar vortex shedding case.

The domain size is 30 m $\times$ 11 m with cylinder diameter of 1 m. Inlet velocity is 0.333 m/s and the kinematic viscosity $\nu = 1.44715 \cdot 10^{-5}$ m^2/s. This setup, with $D = 1$ m, yields Reynolds number of 23 010. Due to unknown dominant frequency, a transient simulation is performed first and frequency spectrum is obtained. The frequency spectrum depicted in Figure 37 shows the base frequency of $f = 0.09677$ Hz which is an input parameter for the harmonic balance simulation.

Figure 38 shows the periodical behaviour of residuals of velocity in x direction. Lack of convergence is caused by the convective term that involves non–linearity in Navier–Stokes equations which is still present in the Harmonic Balance Method. Therefore, the periodicity arising from convective term will also be present in the harmonic balance, despite the Fourier

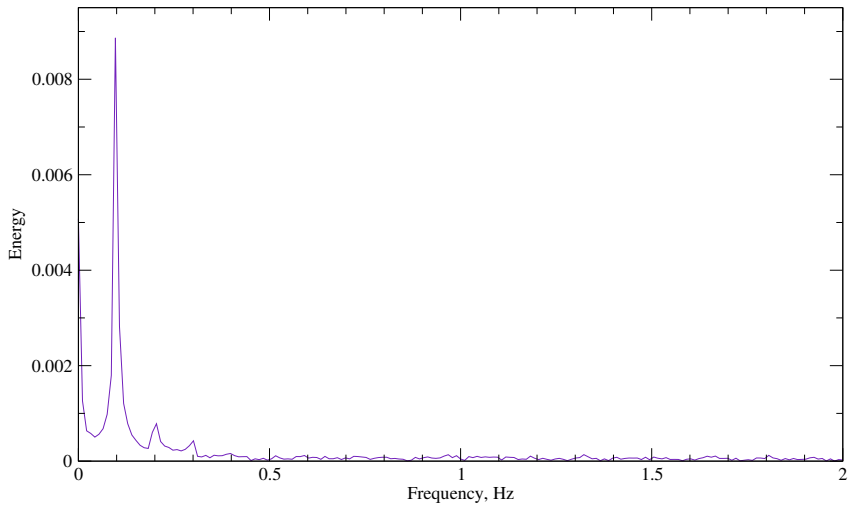

Figure 37: Frequency spectrum of shedding of vortices.

decomposition. It is the reason why satisfactory convergence is not possible.

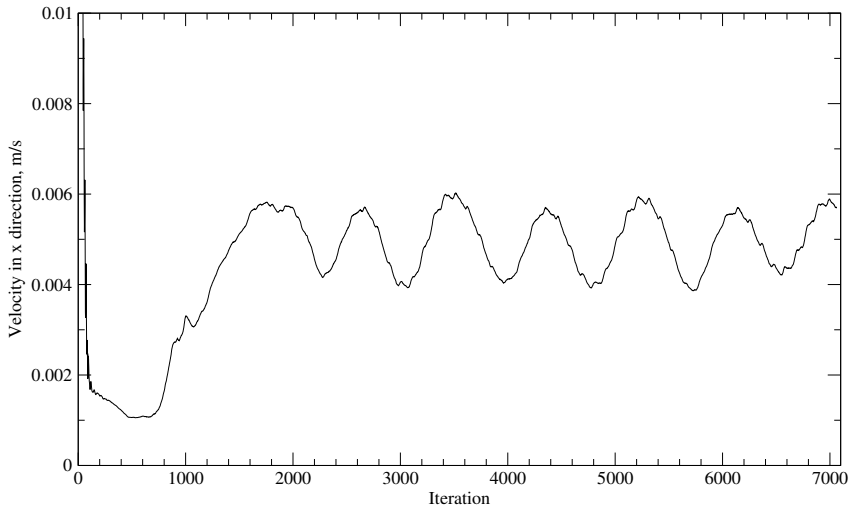

Figure 38: Residuals of velocity in x direction for the Harmonic Balance Method in $t = T/3$ for one harmonic.

In Figures 39a and 39b the transient and the harmonic balance flow fields are compared. Although some resemblance can be noticed, the harmonic balance solution is not converged and representative.

The results shown here are for case with one harmonic and only first time step. Other results exhibit the same behaviour and therefore are not presented. For cases with higher number of harmonics, satisfactory convergence is still not reached.

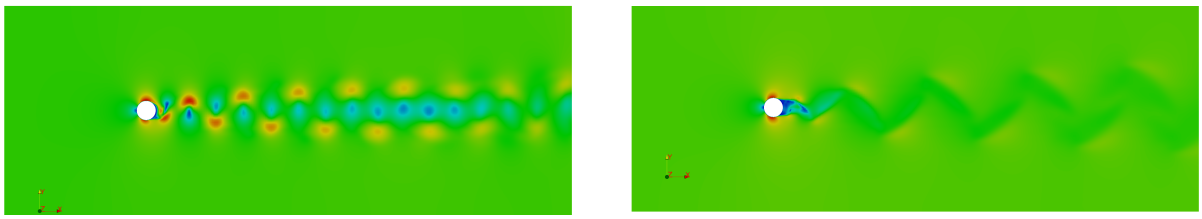

(a) Transient simulation velocity field, (b) Harmonic balance velocity field.

Figure 39: Velocity field comparison between transient solution and the harmonic balance solution.

5.4.2 Edge Tone Noise Test Case

The second test case with frequency which is unknown in advance is the edge tone noise test case. In this test case the phenomena described in [24] is reconstructed. The computational domain is a 2D domain consisting of 35 500 hexahedral cells. The domain size is 0.0975 m $\times$ 0.151 m and it is depicted in Figure 40.

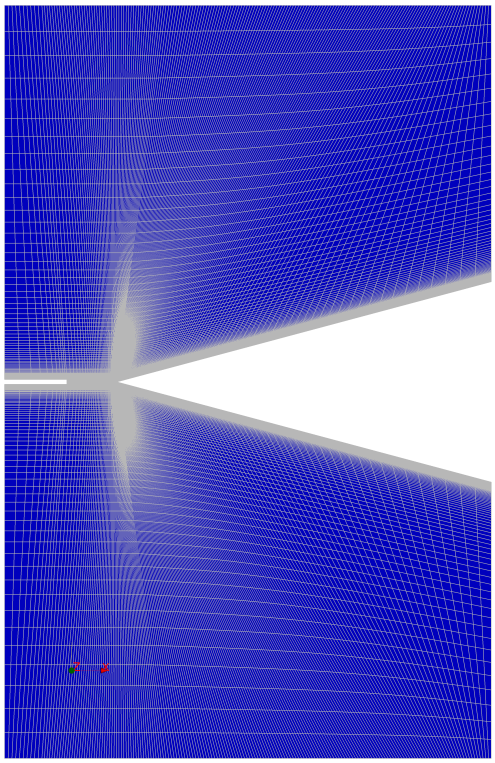

Figure 40: Edge tone test case domain.

Fluid properties and boundary conditions are the same as in [24], hence the frequency is also the same. Inlet velocity is set to 0.0309 m/s with kinematic viscosity $\nu = 1.54515 \cdot 10^{-5}$ m^2/s. Frequency spectrum is obtained running a transient simulation, Figure 41. Dominant frequency is $f = 117$ Hz.

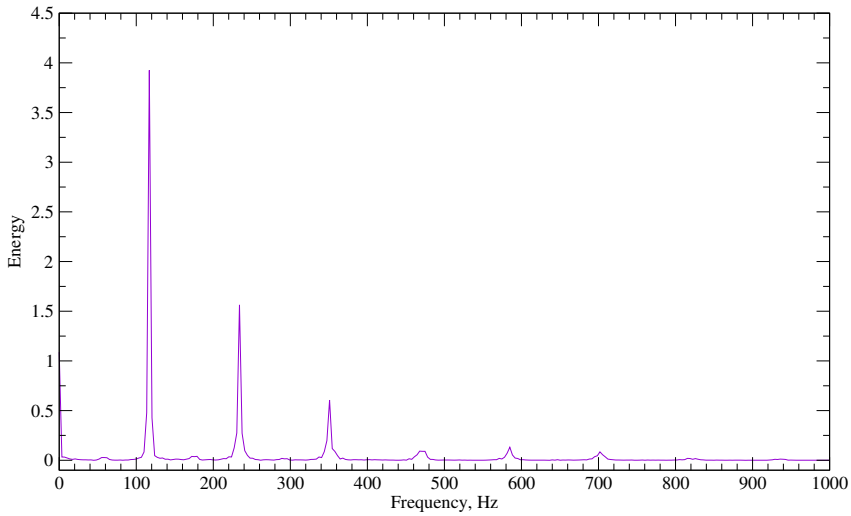

Figure 41: Edge tone frequency spectrum.

Although convergence is not reached using the Harmonic Balance Method approach, Figures 42, 43 and 44 show that flow phenomena has been captured and the flow is qualitatively similar to one obtained using transient simulation.

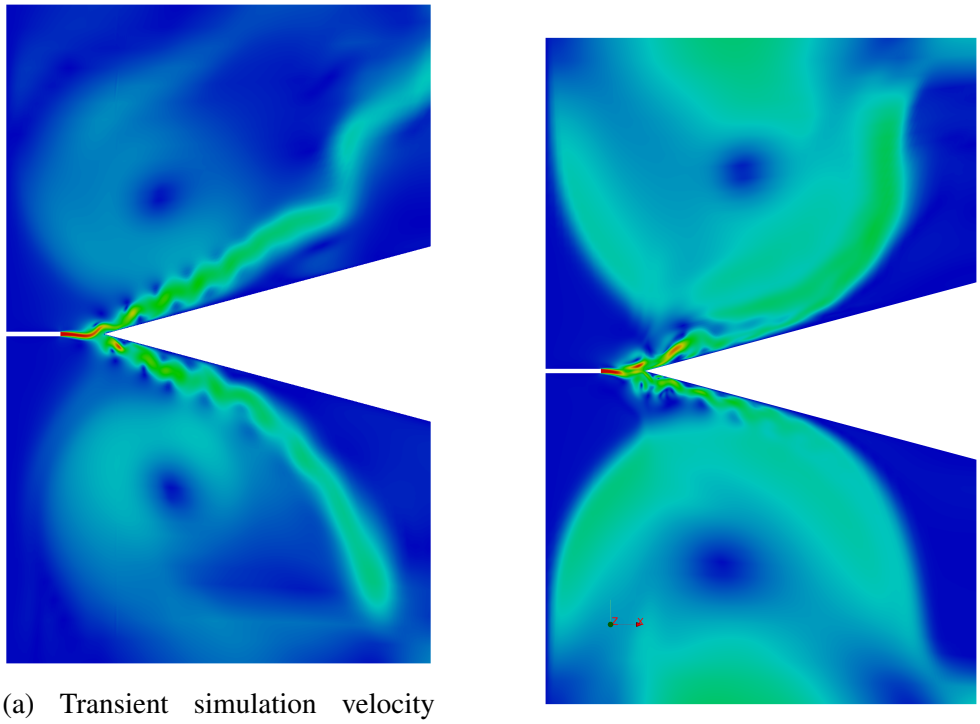

(a) Transient simulation velocity field,

(b) Harmonic balance velocity field.

Figure 42: Transient solution and the Harmonic balance solution at $t = T/3$.

Figures 42, 43 and 44 are obtained using the harmonic balance with one harmonic and depict solution in time instants $t = T/3$, $t = 2T/3$ and $t = T$, respectively. Results using higher number of harmonics do not exhibit improved convergence, therefore are not presented here.

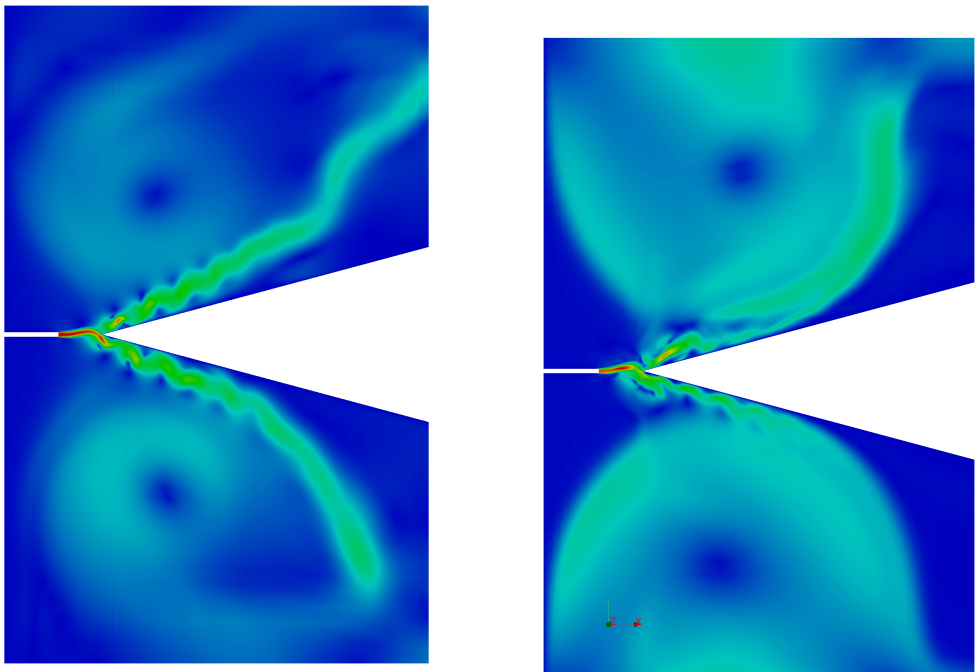

(a) Transient simulation velocity field,

(b) Harmonic balance velocity field.

Figure 43: Transient solution and the harmonic balance solution at $t = 2T/3$.

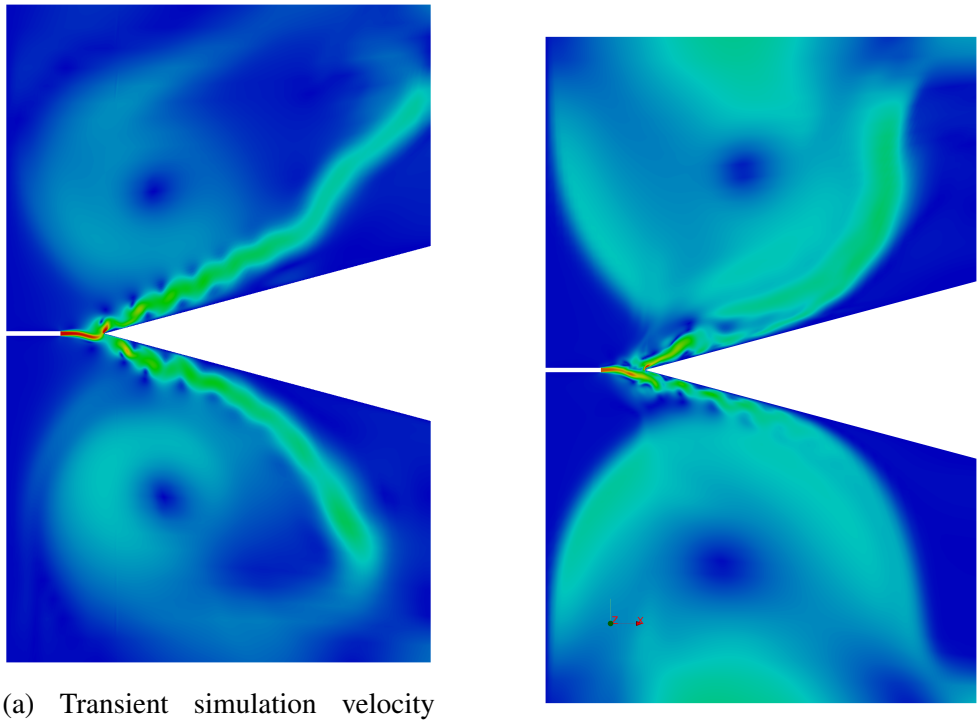

(a) Transient simulation velocity field,

(b) Harmonic balance velocity field.

Figure 44: Transient solution and the harmonic balance solution at $t = T$.

Results presented here show that the Harmonic Balance Method could offer an efficient tool not only for problems with prescribed motion, but also with phenomena where dominant

frequency is not precisely known in advance. Even though the frequency problem persists, further development of the Harmonic Balance Method could lead to better results and convergence.

5.5 Closure

This section presented the validation of the Harmonic Balance Method. First, passive scalar transport was tested and validated. Presented test cases have shown the accuracy of the Harmonic Balance Method in various problems. Scalar transport was validated using four types of periodic impulses resembling sine wave, complex wave consisting of sine and cosine waves and two square waves. Harmonic waves are described perfectly, while square wave test cases have demonstrated convergence and robustness of the Harmonic Balance Method.

The Harmonic Balance Method for Navier–Stokes equations was validated using NACA 2412 test case with low and high *Re* number. Although simulations with different numbers of harmonics were performed, the convergence study is not satisfactory. Further development in area of mesh motion should be taken into consideration, as it is believed to be the main cause of discrepancies compared to transient simulation.

Finally, two cases where frequency is not known in advance were presented. In these cases, the instabilities arise from the convective term rather than prescribed harmonic behaviour. As derived in section 3, in the Harmonic Balance Method the convective term is also present, therefore, instabilities occur regardless of Fourier decomposition of the temporal term.

6 Conclusion and Future Work

The thesis describes derivation and validation of the Harmonic Balance Method in computational fluid dynamics and its implementation in OpenFOAM. Harmonic Balance Method is a method for non–linear temporally periodic flows in which variables are represented by a Fourier series with spatially varying coefficients. Harmonic or non–linear transient equations are converted into a set of coupled steady-state equations which yield flow fields at discrete instants of time throughout a representative harmonic period. The method is implemented in OpenFOAM, using second–order accurate, polyhedral Finite Volume Method, developed for a general transport equation and generalised to coupled non–linear sets including incompressible Navier–Stokes equations.

The results obtained using the Harmonic Balance Method demonstrate that the method is capable to successfully capture the periodic flow field. Comparison of passive scalar transport given in Section 4 shows the nature of the Harmonic Balance Method presented on harmonic waves. For the square waves imposed, a convergence resulting from with the increase in number of harmonics is presented, showing that closer approximation is achieved with higher number of harmonics. Square waves were found to be a challenge in numerical terms, but, on the other hand, it allows testing of the robustness and accuracy of the Harmonic Balance method.

Successful validation of the harmonic balance solver for passive scalar transport led to development of the harmonic balance for Navier-Stokes equations. The Harmonic Balance Method for Navier-Stokes equation was validated using NACA 2412 airfoil in two flow regimes: at low and high *Re* number. Comparison is presented in Section 5 using four setups for each *Re* number. Harmonic balance results with 1, 3 and 7 harmonics were compared to transient results. As NACA 2412 at low *Re* number is a simple case, results obtained with 1, 3 and 7 harmonics were close. For the high *Re* test case, the results of the Harmonic Balance Method differ more from the transient results due to flow separation near the trailing edge. Even though the flow separation is not resolved using the harmonic balance, the flow trend is successfully captured. Overall, comparison carried out on NACA 2412 airfoil shows good agreement of the harmonic balance solver with conventional transient solver.

The CPU time comparison, presented for the NACA 2412 test case, shows the efficiency and computational accuracy of the Harmonic Balance Method; in some cases it was up to 165 times faster than the conventional transient solver. While in transient simulation a perfect periodical state could be reached provided that the adequate number of periods was used, in the Harmonic Balance Method the accuracy was defined by the number of harmonics. Therefore, the results obtained in the thesis demonstrate that the Harmonic Balance Method is a useful and reliable tool for solving periodic problems and that it offers a great potential for further

development.

In addition to application presented in the thesis, versatile Harmonic Balance features indicate that the method could be used in a wide variety of technology and industrial domains. Other than current areas of interest (turbomachinery, airfoil simulation, etc.), naval hydrodynamics involves periodic phenomena that corresponds to the one presented in the thesis and, therefore, it is an important topic crucial for future progress. Whatever is the area of application and intended use, the results obtained in the thesis point to the importance of implementation of mesh motion for further developments in both theoretical and practical knowledge.

References

[1] Hall, K. C., Thomas, J. P., and Clark, W. S., "Computation of Unsteady Nonlinear Flows in Cascades Using a Harmonic Balance Technique," *AIAA Journal*, Vol. 50, No. 5, 2002, pp. 879–886.

[2] Weller, H. G., Tabor, G., Jasak, H., and Fureby, C., "A tensorial approach to computational continuum mechanics using object oriented techniques," *Comput. Phys.*, Vol. 12, No. 6, 1998, pp. 620–631.

[3] Jain, P. C. and Goel, B. S., "Shedding of vortices behind a circular cylinder," *Comput. Fluids*, Vol. 4, 1976, pp. 137–142.

[4] Paál, G. and Vaik, I., "Unsteady phenomena in the edge tone," *Int. J. Heat Fluid Fl.*, Vol. 28, No. 4, 2007, pp. 575–586.

[5] Jasak, H., "Numeričke metode u mehanici montinuuma (Numerical Methods in Continuum Mechanics)," *Material for lectures, in Croatian*, 2007.

[6] Šavar, M., Džijan, I., and Virag, Z., "Mehanika fluida II (Fluid Mechanics II)," *Material for lectures, in Croatian*, 2013.

[7] Hall, K., Ekici, K., Thomas, J., and Dowell, E., "Harmonic balance methods applied to computational fluid dynamics problems," *International Journal of Computational Fluid Dynamics*, Vol. 27, No. 2, 2013, pp. 52–67.

[8] Chen, T., Vasanthakumar, P., and He, L., "Analysis of Unsteady Blade Row Interaction Using Nonlinear Harmonic Approach," *Journal of propulsion and power*, Vol. 17, No. 3, 2001, pp. 651–658.

[9] Sanliturk, K., Imregun, M., and Ewins, D., "Harmonic Balance Vibration Analysis of Turbine Blades With Friction Dampers," *Journal of Vibration and Acoustics*, Vol. 119, 1997.

[10] Dufour, G., Sicot, F., and Puigt, G., "Contrasting the Harmonic Balance and Linearized Methods for Oscillating-Flap Simulations," *AIAA Journal*, Vol. 48, No. 4, 2010, pp. 788–797.

[11] Thomas, J., Dowell, E., Hall, K., and Denegri Jr., C., "Further Investigation of Modeling Limit Cycle Oscillation Behavior of the F-16 Fighter Using a Harmonic Balance Approach," *American Institute of Aeronautics and Astronautics Paper*, 2005.

[12] Stewart, J., *Calculus Early Transcedentals, 6e*, Thomson Brooks/Cole, 2008.

[13] Da Ronch, A., Ghoreyshi, M., Badcock, K., Görtz, S., Widhalm, M., and Dwight, R.P.and Campobasso, M., "Linear Frequency Domain and Harmonic Balance Predictions of Dynamic Derivatives," *Journal of Aircraft*, Vol. 50, No. 3, 2013, pp. 694–707.

[14] Rusche, H., *Computational Fluid Dynamics of Dispersed Two - Phase Flows at High Phase Fractions*, Ph.D. thesis, Imperial College of Science, Technology & Medicine, London, 2002.

[15] Jasak, H., *Error Analysis and Estimation for the Finite Volume Method with Applications to Fluid Flows*, Ph.D. thesis, Imperial College of Science, Technology & Medicine, London, 1996.

[16] Saad, Y., *Iterative Methods for Sparse Linear Systems*, Society for Industrial and Applied Mathematics, SIAM, 2003.

[17] Patankar, S. V. and Spalding, D. B., "A calculation procedure for heat, mass and momentum transfer in three-dimensional parabolic flows," *Int. J. Heat Mass Transf.*, Vol. 15, No. 10, 1972, pp. 1787–1806.

[18] Darwish, M., Sraj, I., and Moukalled, F., "A coupled finite volume solver for the solution of incompressible flows on unstructured grids," *J. Comput. Phys.*, Vol. 228, No. 1, 2009, pp. 180–201.

[19] Cvijetić, G., Jasak, H., and Vukčević, V., "Finite Volume Implementation of Harmonic Balance Method for Periodic Non-Linear Flows," *AIAA*, 2015.

[20] Hall, K. C., Thomas, J. P., Ekici, K., and Voytovych, D., "Frequency Domain Techniques for Complex and Nonlinear Flows in Turbomachinery," *33rd AIAA Fluid Dynamics Conference and Exhibit*, 2003.

[21] Demiridžić, I. and Perić, M., "Space conservation law in finite volume calculations of fluid flow," *Int. J. Numer. Meth. Fluids*, Vol. 8, 1998, pp. 1037–1050.

[22] Jasak, H. and Beaudoin, M., "OpenFOAM turbo tools: from general purpose CFD to turbomachinery simulations," *Proceedings of ASME-JSME-KSME Joint Fluids Engineering Conference*, 2011.

[23] Verma, H., *Aerodynamic and structural modeling for vortex-excited vibrations in bundled conductors*, Ph.D. thesis, Dem Fachbereich Maschinenbau an der Technischen Universität Darmstadt, Darmstadt, 2008.

[24] Azenić, A., *Numerical simulation of acoustic response coupled with flow*, Master's thesis, Faculty of Mechanical Engineering and Naval Architecture, Zagreb, 2014.